Virgo: a laser interferometer to detect gravitational waves

T. Accadia[11], F. Acernese[5ac], M. Alshourbagy[7ab], P. Amico[6ab], F. Antonucci[8a], S. Aoudia[15a], N. Arnaud[10a], C. Arnault[10a], K. G. Arun[10a], P. Astone[8a], S. Avino[5a], D. Babusci[19], G. Ballardin[2], F. Barone[5ac], G. Barrand[10a], L. Barsotti[7ab], M. Barsuglia[1], A. Basti[7ab], Th. S. Bauer[14a], F. Beauville[11], M. Bebronne[11], M. Bejger[17c], M.G. Beker[14a], F. Bellachia[11], A. Belletoile[11], J. L. Beney[10a] ‡, M. Bernardini[7a], S. Bigotta[7ab], R. Bilhaut[10a], S. Birindelli[15a], M. Bitossi[7a], M. A. Bizouard[10a], M. Blom[14a], C. Boccara[10b], D. Boget[11], F. Bondu[15b], L. Bonelli[7ab], R. Bonnand[13], V. Boschi[7a], L. Bosi[6a], T. Bouedo[11], B. Bouhou[1], A. Bozzi[2], L. Bracci[3ac], S. Braccini[7a]†, C. Bradaschia[7a], M. Branchesi[3ab], T. Briant[12], A. Brillet[15a], V. Brisson[10a], L. Brocco[8a], T. Bulik[17bc], H. J. Bulten[14ab], D. Buskulic[11], C. Buy[1], G. Cagnoli[3a], G. Calamai[3ad], E. Calloni[5ab], E. Campagna[3ab], B. Canuel[2], F. Carbognani[2], L. Carbone[6a], F. Cavalier[10a], R. Cavalieri[2], R. Cecchi[7a] §, G. Cella[7a], E. Cesarini[3b], E. Chassande-Mottin[1], S. Chatterji[8a], R. Chiche[10a], A. Chincarini[4], A. Chiummo[2], N. Christensen[2], A.C. Clapson[10], F. Cleva[15a], E. Coccia[9ab], P.-F. Cohadon[12], C. N. Colacino[7ab], J. Colas[2], A. Colla[8ab], M. Colombini[8b], G. Conforto[3ab], A. Corsi[8a], S. Cortese[2], F. Cottone[6ab], J.-P. Coulon[15a], E. Cuoco[2], S. D'Antonio[9a], G. Daguin[11], A. Dari[6ab], V. Dattilo[2], P.Y, David[11], M. Davier[10a], R. Day[2], R. De Rosa[5ab], R. DeSalvo[k], G. Debreczeni[18], G. De Carolis[7a], M. Dehamme[10a], R. Del Fabbro[7a], W. Del Pozzo[14a], M. del Prete[16b], L. Derome[11], R. De Salvo[7a], M. Dialinas[10a] ‡, L. Di Fiore[5a], A. Di Lieto[7ab], M. Di Paolo Emilio[9ac], A. Di Virgilio[7a], A. Dietz[11], M. Doets[14a], P. Dominici[3ab], A. Dominjon[11], M. Drago[16ab], C. Drezen[11], B. Dujardin[15], B. Dulach[19], C. Eder[10a], A. Eleuteri[5a] α, D. Enard[2]†, M. Evans[2], L. Fabbroni[3ac], V. Fafone[9ab], H. Fang[19], I. Ferrante[7ab], F. Fidecaro[7ab], I. Fiori[2], R. Flaminio[13], D. Forest[13], L. A. Forte[5a], J.-D. Fournier[15a], L. Fournier[11], J. Franc[13], O. Francois[2], S. Frasca[8ab], F. Frasconi[7a], A. Freise[2+], A. Gaddi[7a]*, M. Galimberti[13], L. Gammaitoni[6ab], P. Ganau[13], C. Garnier[10a], F. Garufi[5ab], M. E. Gáspár[18], G. Gemme[4], E. Genin[2], A. Gennai[7a], G. Gennaro[7a], L. Giacobone[11], A. Giazotto[7a], G. Giordano[19] β, L. Giordano[5a], C. Girard[11], R. Gouaty[11], A. Grado[5a] ††, M. Granata[1], V. Granata[11], X. Grave[11], C. Greverie[15a], H. Groenstege[14a], G. M. Guidi[3ab], S. Hamdani[2], J.-F. Hayau[15b], S. Hebri[2], A. Heidmann[12], H. Heitmann[15], P. Hello[10a], G. Hemming[2], H. Hennes[14a], R. Hermel[11], P. Heusse[10a], L. Holloway[2], D. Huet[2], M. Iannarelli[19], P. Jaranowski[17d], D. Jehanno[10a], L. Journet[11], S. Karkar[11], T. Ketel[14ab], H. Voet[14b], J. Kovalik[6a], I. Kowalska[17b], S. Kreckelbergh[10a], A. Krolak[17ae], J.C. Lacotte[11], B. Lagrange[13], P. La Penna[2], M. Laval[15], J.C. Le Marec[11], N. Leroy[10a], N. Letendre[11], T. G. F. Li[14a], B. Lieunard[11], N. Liguori[16ab], O. Lodygensky[10a], B. Lopez[2], M. Lorenzini[3a], V. Loriette[10b], G. Losurdo[3a], M. Loupias[2], J. M. Mackowski[13], T. Maiani[7a]†, E. Majorana[8a], C. Magazzù[7a], I. Maksimovic[10b], V. Malvezzi[9a], N. Man[15a], S. Mancini[7a], B. Mansoux[10a], M. Mantovani[7ac], F. Marchesoni[6a], F. Marion[11], P. Marin[10a]†, J. Marque[2], F. Martelli[3ab], A. Masserot[11], L. Massonnet[11], G. Matone[19]†, L. Matone[10a] μ, M. Mazzoni[3], F. Menzinger[2], C. Michel[13], L. Milano[5ab], Y. Minenkov[9a], S. Mitra[15],

M. Mohan[2], J.-L. Montorio[13], R. Morand[11] †, F. Moreau[11], J. Moreau[10b] §§, N. Morgado[13], A. Morgia[9ab], S. Mosca[5ab], V. Moscatelli[8a], B. Mours[11], P. Mugnier[11], F.-A. Mul[14b], L. Naticchioni[8ab], I. Neri[6ab], F. Nocera[2], E. Pacaud[11], G. Pagliaroli[9ac], A. Pai[8a], L. Palladino[9ac], C. Palomba[8a], F. Paoletti[7a,2], R. Paoletti[7a], A. Paoli[2], S. Pardi[5a], G. Parguez[2], M. Parisi[5ab], A. Pasqualetti[2], R. Passaquieti[7ab], D. Passuello[7a], M. Perciballi[8a], B. Perniola[3], G. Persichetti[5ab], S. Petit[11], M. Pichot[15a], F. Piergiovanni[3ab], M. Pietka[17d], R. Pignard[13], L. Pinard[13], R. Poggiani[7ab], P. Popolizio[2], T. Pradier[10a] λ, M. Prato[4], G. A. Prodi[16ab], M. Punturo[6a], P. Puppo[8a], K. Qipiani[5a] π, O. Rabaste[1], D. S. Rabeling[14ab], I. Rácz[18], F. Raffaelli[7a], P. Rapagnani[8ab], S. Rapisarda[7a], V. Re[9ab], A. Reboux[10a], T. Regimbau[15a], V. Reita[10b] δ, A. Remilleux[13], F. Ricci[8ab], I. Ricciardi[5a] φ, F. Richard[2], M. Ripepe[3ac], F. Robinet[10a], A. Rocchi[9a], L. Rolland[11], R. Romano[5ac], D. Rosińska[17cf], P. Roudier[10a], P. Ruggi[2], G. Russo[5a], L. Salconi[2], V. Sannibale[11], B. Sassolas[13], D. Sentenac[2], S. Solimeno[5a], R. Sottile[11], L. Sperandio[9ab], R. Stanga[3], R. Sturani[3ab], B. Swinkels[2], M. Tacca[2], R. Taddei[2], L. Taffarello[16c], M. Tarallo[7ab], S. Tissot[11], A. Toncelli[7ab], M. Tonelli[7ab], O. Torre[7ac], E. Tournefier[11], F. Travasso[6ab], C. Tremola[7ab], E. Turri[19], G. Vajente[7ab], J. F. J. van den Brand[14ab], C. Van Den Broeck[14a], S. van der Putten[14a], M. Vasuth[18], M. Vavoulidis[10a], G. Vedovato[16c], D. Verkindt[11], F. Vetrano[3ab], O. Véziant[11], A. Viceré[3ab], J.-Y. Vinet[15a], S. Vilalte[11], S. Vitale[14a], H. Vocca[6a], R. L. Ward[1], M. Was[10a], K. Yamamoto[16bd], M. Yvert[11], J.-P. Zendri[16c], Z. Zhang[2].

‡ Present address: SUBATECH 4 Rue Alfred Kastler BP 20722 44307 NANTES CEDEX 3 FRANCE
† Deceased
§ Present address: Dipartimento di Ingegneria dell'Informazione, Universitá degli Studi di Siena, Via Roma, 56 53100 Siena ITALY
k Present address: LIGO - California Institute of Technology, Pasadena, CA 91125, USA
α Present address: Royal Liverpool Univ Hosp, Dept Med Phys & Clin Engn, Liverpool, Merseyside England
+ Present address: School of Physics and Astronomy, University of Birmingham, Edgbaston Birmingham, B15 2TT, UK
* Present address: CERN, European Organization for Nuclear Research, Geneva, Switzerland
β Present address: Selex Sistemi Integrati, Roma, Italy
†† Present address: INAF, Osservatorio Astronomico di Capodimonte, via Moiariello 16, 8013 1 Napoli, Italy
μ Present address: Columbia University 1236 Pupin Hall MC 5247 Box 47 New York NY 10027 USA
§§ Present address: Laboratoire Charles Fabry, Institut d'optique, 91127 Palaiseau Cedex FRANCE
λ Present address: IPHC 23 rue du Loess BP 28 67037 STRASBOURG CEDEX 2 FRANCE
π Present address: E.Andronikashvili Institut of Physics, Tbilisi, Georgia
δ Present address: Institut Neel 25 rue des Martyrs BP 166 38042 GRENOBLE CEDEX 9 FRANCE
φ Present address: CNR–INOA, Istituto Nazionale di Ottica Applicata, Sezione di Napoli, Via Campi Flegrei 34, I-80078 Pozzuoli (NA), Italy

[1] Laboratoire AstroParticule et Cosmologie (APC) Université Paris Diderot, CNRS: IN2P3, CEA: DSM/IRFU, Observatoire de Paris, 10 rue A.Domon et L.Duquet,
75013 Paris - France
[2] European Gravitational Observatory (EGO), I-56021 Cascina (PI), Italy
[3] INFN, Sezione di Firenze, I-50019 Sesto Fiorentino[a]; Università degli Studi di

Urbino 'Carlo Bo', I-61029 Urbino[b] ; Università degli Studi di Firenze, I-50121
Firenze[c] , Osservatorio Astrofisico di Arcetri, I-50125 Firenze[d] , Italy

[4] INFN, Sezione di Genova; I-16146 Genova, Italy

[5] INFN, Sezione di Napoli [a] ; Università di Napoli 'Federico II'[b] Complesso Universitario di Monte S.Angelo, I-80126 Napoli; Università di Salerno, Fisciano, I-84084 Salerno[c] , Italy

[6] INFN, Sezione di Perugia[a]; Università di Perugia[b], I-06123 Perugia,Italy

[7] INFN, Sezione di Pisa[a]; Università di Pisa[b] ; I-56127 Pisa; Università di Siena, I-53100 Siena[c] , Italy

[8] INFN, Sezione di Roma[a]; Università 'La Sapienza'[b] , I-00185 Roma, Italy

[9] INFN, Sezione di Roma Tor Vergata[a]; Università di Roma Tor Vergata, I-00133 Roma[b] ; Università dell'Aquila, I-67100 L'Aquila[c] , Italy

[10] LAL, Université Paris-Sud, IN2P3/CNRS, F-91898 Orsay[a]; ESPCI, CNRS, F-75005 Paris[b], France

[11] Laboratoire d'Annecy-le-Vieux de Physique des Particules (LAPP), Université de Savoie, CNRS/IN2P3, F-74941 Annecy-Le-Vieux, France

[12] Laboratoire Kastler Brossel, ENS, CNRS, UPMC, Université Pierre et Marie Curie, 4 Place Jussieu F-75005 Paris, France

[13] Laboratoire des Matériaux Avancés (LMA), IN2P3/CNRS, F-69622 Villeurbanne, Lyon, France

[14] Nikhef, Science Park, Amsterdam, the Netherlands[a]; VU University Amsterdam, De Boelelaan 1081, 1081 HV Amsterdam, the Netherlands[b]

[15] Université Nice-Sophia-Antipolis, CNRS, Observatoire de la Cote d'Azur, F-06304 Nice[a]; Institut de Physique de Rennes, CNRS, Université de Rennes 1, 35042 Rennes[b] , France

[16] INFN, Gruppo Collegato di Trento[a] and Università di Trento[b] , I-38050 Povo, Trento, Italy; INFN, Sezione di Padova[c] and Università di Padova[d], I-35131 Padova, Italy

[17] IM-PAN 00-956 Warsaw[a]; Astronomical Observatory Warsaw University 00-478 Warsaw[b] ; CAMK-PAN 00-716 Warsaw[c]; Bialystok University 15-424 Bialystok[d]; IPJ 05-400 Świerk-Otwock[e]; Institute of Astronomy 65-265 Zielona Gora[f], Poland

[18] RMKI, H-1121 Budapest, Konkoly Thege Miklós út 29-33, Hungary

[19] INFN, Laboratori nazionali di Frascati, I-00044 Frascati, Italy

Corresponding author: Carlo Bradaschia
e-mail: carlo.bradaschia@pi.infn.it

Abstract

This paper presents a complete description of the French Italian detector of gravitational waves Virgo. This detector, built at Cascina near Pisa (Italy), is a very large Michelson interferometer, with 3 km long arms. After a presentation of the physics requirements, leading to the specifications for the detector construction, a detailed description of all the different parts is given. They include civil engineering infrastructures, a huge Ultra High Vacuum chamber (about 6000 cubic meters), all the optical components including high quality mirrors and their seismic isolating suspensions, all the electronics for controlling the interferometer and for signal detection. The expected performances of these different parts are given, leading to an overall sensitivity curve as a function of the incoming gravitational wave frequency.

This description represents the detector as built and used in the first data taking runs. Improvements in different parts have been and continue to be performed, giving better sensitivities. They will be detailed in a forthcoming paper.

1. Introduction

Gravitational waves were predicted by Einstein [1] as a consequence of the theory of General Relativity; its geometrical interpretation states that gravitation is the result of the curvature of space-time caused by mass (or energy) density. In this geometrical view gravitational waves are thus deformations of space-time which are predicted to travel at the speed of light: by considering small deviations of the metric tensor $g_{\mu\nu}$ from Minkowski metric $\eta_{\mu\nu}$, Einstein's equations can be linearized giving a wave equation for the quantity $h_{\mu\nu} = g_{\mu\nu} - \eta_{\mu\nu}$ with propagation speed equal to c.

GW emission has been indirectly demonstrated through the radiative energy loss of PSR1913+16 [2], allowing high precision tests of the predictions of General Relativity. A direct detection would allow to study their properties and would initiate a new kind of photonless astroparticlephysics.

The process of detecting gravitational waves consists in measuring directly or indirectly time variations of h, that is variations in the geometry of local space-time. The order of magnitude of the change of distance δL between two free falling test masses located L meters apart caused by $h_{\mu\nu}$ is

$$\delta L \propto \frac{h}{2} L$$

where h is the typical magnitude of $h_{\mu\nu}$ components.

The main mechanism for generating gravitational waves is acceleration of a mass, in analogy with electromagnetism. Due to the very small value of the gravitational constant G the amplitude of the generated wave is such that only astrophysical compact objects in violent motion can generate waves with significant amplitude. This amplitude decreases as *1/R* where *R* is the distance from the source. Nearby events may have higher amplitude but are rare while far away events have lower amplitude but come from a much larger portion of the Universe and are more frequent. Considering catastrophic (burst) events in nearby galaxies at a distance of the order of 20 Mpc an amplitude of h of the order of 10^{-21} is expected. For such events the above formula indicates that a precision on the δL measurement of the order of 10^{-18} m for $L = 1$ km is required.

The detection of gravitational waves has been attempted using mainly two approaches. The first consists in measuring the amplitude of oscillations of a resonant bar originated by gravitational waves: following the pioneering work of Weber [3], the Allegro, Auriga, Explorer, Nautilus and Niobe detectors [4] were built and have been operating in a network for several years. The second method measures spacetime geometry variations detected by free falling masses using interferometry. Since the eighties of the past century this seems to be the most promising technique for detecting gravitational waves. Several detectors based on a Michelson scheme with km long arms have been built, where the mirrors of the interferometer act as "free falling" test masses. Virgo, the French Italian detector [5], the US LIGO [6], as well as the British German GEO600 [7] are now taking data. A smaller interferometer TAMA is operating in Japan where there are also plans for a cryogenic 3 km interferometer (LCGT) [8]. In Australia the interferometer AIGO [9] is being developed. In addition the LISA project [10] for a space interferometer is currently being developed.

This paper is meant to be a reference for the French Italian Virgo interferometer located in Cascina, near Pisa. A comprehensive description of the detector as built will be presented here while its detailed performance will be the subject of separated papers.

Section 2 will present the general description and resulting specifications for detector performance. Sections 3, 4 and 5 describe the site and infrastructures, the vacuum chamber as well as the baffle system that absorbs scattered light. Section 6 describes the suspensions for seismic isolation of mirrors and optical benches and their position control. Section 7 is about the interferometer optical scheme including the high quality mirrors used in Virgo. Section 8 describes the elements used for interferometer feedback control. The details of the control scheme for longitudinal mirror position and mirror alignment is beyond the scope of this paper. Section 9 describes the system that monitors environmental conditions that may influence the interferometer. Section 10 describes the data acquisition and online data processing systems. Section 11 summarizes the expected performance of the Virgo detector, presenting the design sensitivity curve in the

form of linear spectral density in the frequency domain. Conclusions and perspectives are presented in Section 12.

2. Description and requirements

2.1 General description

The Virgo interferometer is based on the Michelson scheme which foresees two perpendicular arms of equal length to cancel wavelength fluctuations of the light source. The passage of gravitational waves changes the geometry of space time resulting in a different apparent length of each arm. The resulting length difference δL between the two arms gives the gravitational wave signal. In terms of h

$$\delta L = h\,L$$

showing that the sensitivity in h is proportional to L. The measurement of δL is obtained from the phase difference of the returning beams, which is deduced from the intensity of the interference figure. The best sensitivity is achieved setting the interferometer at almost complete destructive interference (dark fringe).

Sensitivity is improved by introducing Fabry-Perot resonant cavities in the arms that multiply the optical path, resulting in a larger phase variation for a given arm length change. However the resulting gain is reduced at high frequency. For practical reasons the Virgo arm length was limited to 3 km while the optical path increase was chosen to be around 30 giving an effective optical length of 90 km. The sensitivity of the phase measurement is limited by photon counting statistics and can be improved by increasing the light intensity in the interferometer. By working on the dark fringe most of the light power goes back to the light source. This light can be usefully sent back to the interferometer, increasing the total circulating intensity by a factor of the order of 50. This is achieved by installing an additional semireflective mirror at the entrance of the interferometer that sends back the outgoing light in phase with the incoming beam, forming an overall resonant cavity or "recycling cavity" [11]. The resulting principle scheme is shown in figure 1.
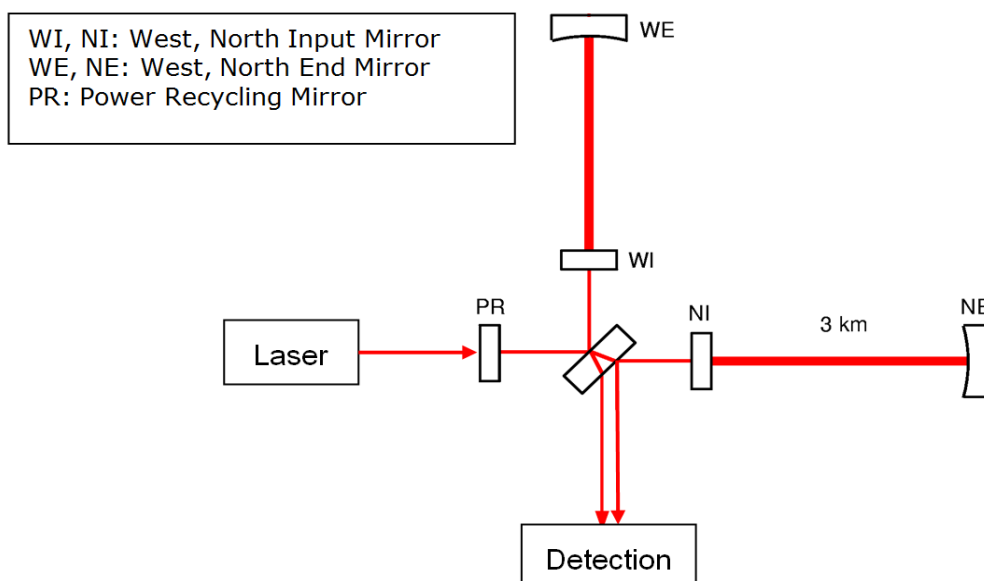
Figure 1. Virgo optical scheme principle.

2.2 Required sensitivity

Due to local gravity fluctuations ground based interferometers are sensitive to gravitational waves with frequency higher than a few Hz. At lower frequency a gravitational wave detector has to operate in space. On the high side of the frequency band the gravitational wave signal strongly decreases due to source dynamics. The Virgo interferometer has been designed to cover a frequency band starting from 10 Hz up to a few kHz. Expected sources in this range are coalescing binary systems like neutron star or black hole pairs, stellar collapses, rotating neutron stars, and possibly cosmological background radiation. Estimations for gravitational wave amplitude on Earth from these sources are at the level of $h = 10^{-21}$. This figure was used

as a guideline to set a requirement on the spectral sensitivity $\tilde{h} \sim 10^{-22}$ to $10^{-23}/\sqrt{\text{Hz}}$.

The Virgo sensitivity is limited by noise sources that can be grouped in different categories. The position of the test masses can fluctuate due to local perturbations like residual seismic noise, local gravity fluctuations and thermal motion. Other noise sources affect the detected signal without a real mirror displacement, the main one being photon shot noise. This is illustrated in figure 2 which shows the Virgo expected sensitivity as a function of frequency (here sensitivity is meant to represent the amplitude of a gravitational wave giving

a signal level equal to the one of detector noise). Typical values are $\tilde{h} = 5 \ 10^{-23}/\sqrt{\text{Hz}}$ at 100 Hz., and $\tilde{h} = 3 \ 10^{-21}/\sqrt{\text{Hz}}$ at 10 Hz where large efforts have been made to reduce the seismic noise through the use of superattenuators and so improve the sensitivity at very low frequency, where many interesting sources can be found.

Figure 2. Design sensitivity of Virgo, as a function of frequency. The coloured curves show the main limiting noises.

2.3 General requirements

The construction of a detector of such a size is resource and time consuming in particular for what concerns the infrastructures and the vacuum tank. These items have been designed to have a lifetime of the order of 20 years. It is expected that progress in sensitivity can be achieved with improvements in optics and mirror materials, which can be done more rapidly using the same infrastructure.
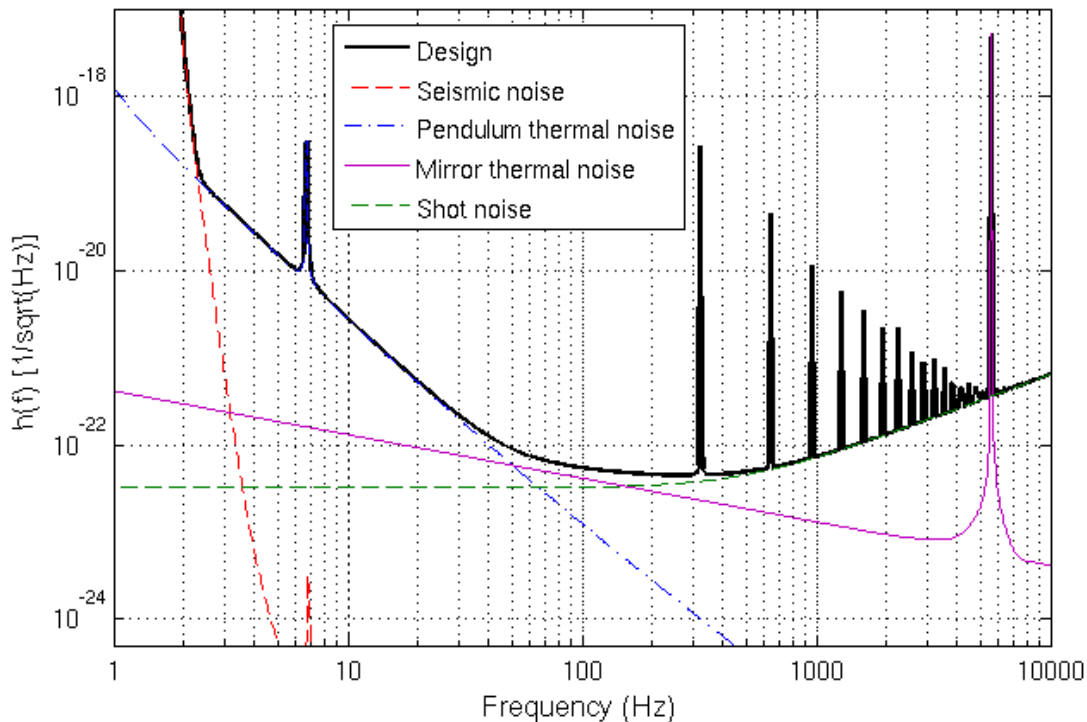The aimed sensitivity induces stringent specifications in the following domains:

2.3.1 Seismic isolation

At the Virgo site the seismic noise must be strongly reduced in the detection frequency range (10 to 10000 Hz) up to a factor of $\sim 10^{12}$ at low frequency (10–100 Hz), where it is dominant.

2.3.2 Vacuum

The arm optical length depends on the refraction index along the light beam path. That can change with pressure fluctuations of the medium. To minimize them the whole interferometer has to be located in ultra high vacuum. Moreover vacuum isolates the test masses from external acoustic noise, air turbulence and temperature fluctuations. The most stringent requirement comes from the statistical fluctuations of the molecule number along the beam path. Anticipating a factor of 10 in sensitivity improvement during the detector lifetime and keeping another factor of 10 as safety margin gives an upper limit for the contribution to the detector noise from this source of $10^{-25}/\sqrt{Hz}$ in $\tilde{h}$. With Hydrogen as main residual gas this translates into a pressure limit of 10^{-7} Pa (10^{-9} mbar).

2.3.3 Interferometer specifications

In a resonant optical cavity, the minimum detectable signal is proportional to $1/Q\sqrt{N}$, Q being the "quality factor" of the cavity, and N the number of photons entering the cavity. So both values have to be as high as possible. However the gain introduced by a high value of Q is effective only for signals that have a period longer than the storage time of the cavity. The laser power arriving on the beam splitter mirror of the Michelson interferometer has to be at least 1 kW with a power fluctuation $\delta P/P \leq 10^{-8}/\sqrt{Hz}$. The laser frequency fluctuations due to coupling to the expected interferometer asymmetries (1%) have to be mastered in order to get a laser frequency noise spectral density not larger than 4.10^{-4} Hz/$\sqrt{Hz}$ at 60 Hz and 3.10^{-4} Hz/$\sqrt{Hz}$ at 10 Hz.

2.3.4 Mirrors

Each mirror has to meet very stringent specifications: the total losses at the Virgo laser beam wavelength (1064 nm) must be less than 100 ppm. The maximum allowed absorption is 5 ppm to reduce thermal effects, giving constraints on the substrate choice, and the scattering level has to be less than 5 ppm, requiring very high quality coatings.
        The mechanical dissipation of the substrate and coatings determines the level of thermal noise from the mirrors. An overall mechanical quality factor of more than 10^6 is needed.
        The wires suspending the mirror are also source of thermal noise coming from mechanical dissipation. There too low dissipation materials like carbon steel or silica have to be used. A mechanical quality factor for the pendulum of more than 10^6 is required.

2.3.5 Mirror position control

During the whole data taking operation the interferometer has to remain at its working point, with the two Fabry-Perot and the recycling cavities in a resonant state and the Michelson output on a dark fringe. To get and keep this situation, suspended optical components need to have their position and angles continuously controlled. The constraints are about 10^{-10} meter RMS for the length control (locking), and 10^{-9} rad. RMS for the angular degrees of freedom of mirrors (alignment).

3. The Infrastructure

3.1 Infrastructure function and requirements

The infrastructure for the Virgo interferometer consists of the buildings and the tunnels necessary for the interferometer installation and of all the technological equipments needed for the interferometer operation.

The general requirements used for the realization of the Virgo infrastructure are:

- o detector and infrastructure capable of a 20 years lifetime
- o detector performances at the limits of present technologies
- o locate the interferometer on a flat, controlled area, as far as possible away from mechanical vibration sources (like roads, trains, industries), within a reasonably short distance from one of the collaborating laboratories
- o keep to a minimum the perturbation to the geological, biological and economical equilibrium of the surrounding region.

The following stability requirements have been also established:

- o the foundations of the buildings have to guarantee that the mirror suspension points will not move more than 1 mm per day
- o the overall displacement of the suspension points in 20 years will be within the design adjustment range of a few centimeters
- o the foundations of the tunnel have to guarantee that the center of any cross-section of the vacuum tube stays inside a straight cylinder of 50 mm radius
- o in order to keep the previous limit, only a limited number of tube supports will have to be realized, not more frequently than once per year.

The most peculiar Virgo buildings are the long and narrow halls, called tunnels, protecting the 3 km long vacuum tubes. The two orthogonal tunnels are laid down approximately in the South-North direction and in the East-West direction, starting from an almost cubical Central Building, containing a large majority of the electronic and optical equipments, including the laser source (Figures 3, 4).
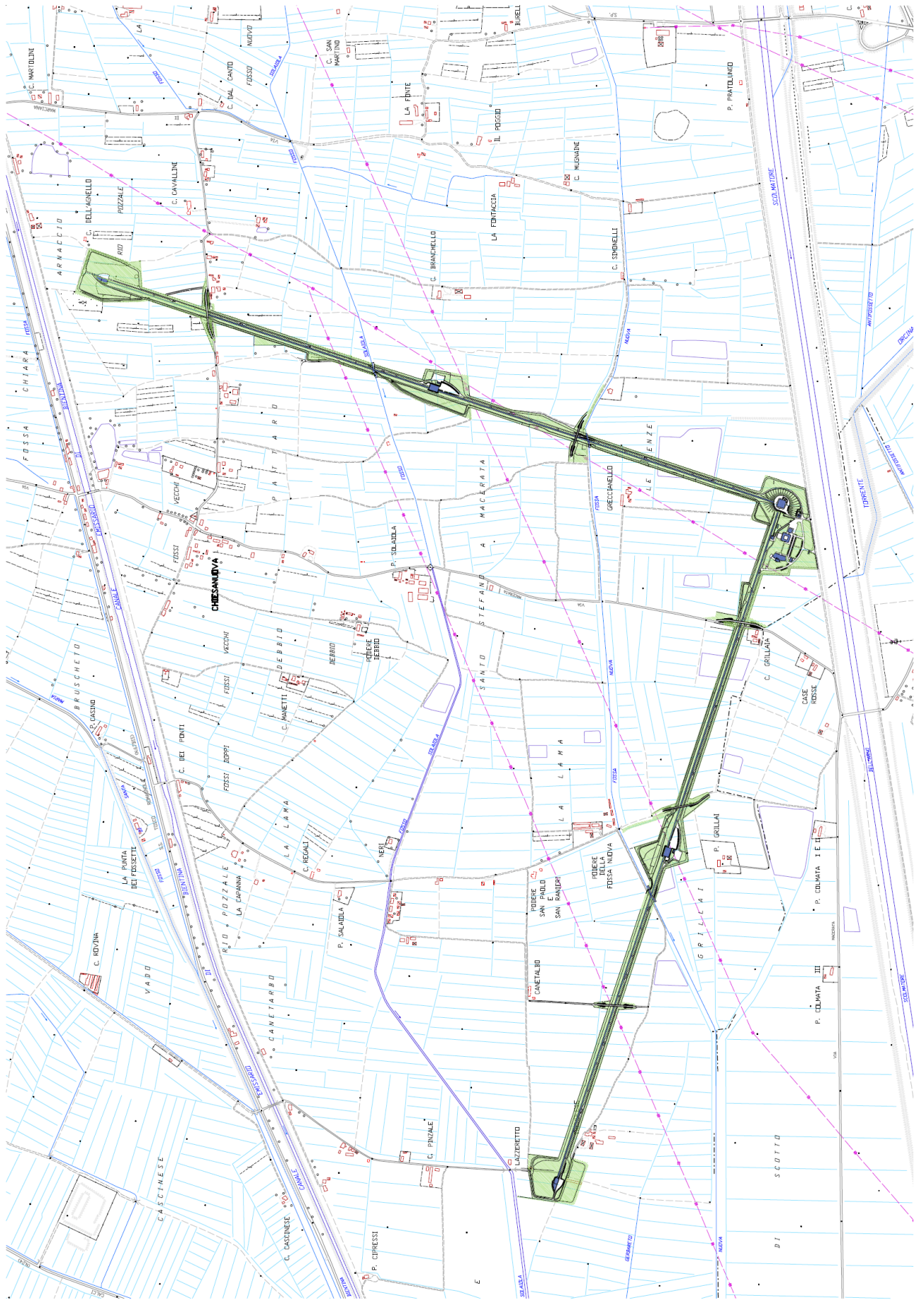
Figure 3. General Plan.
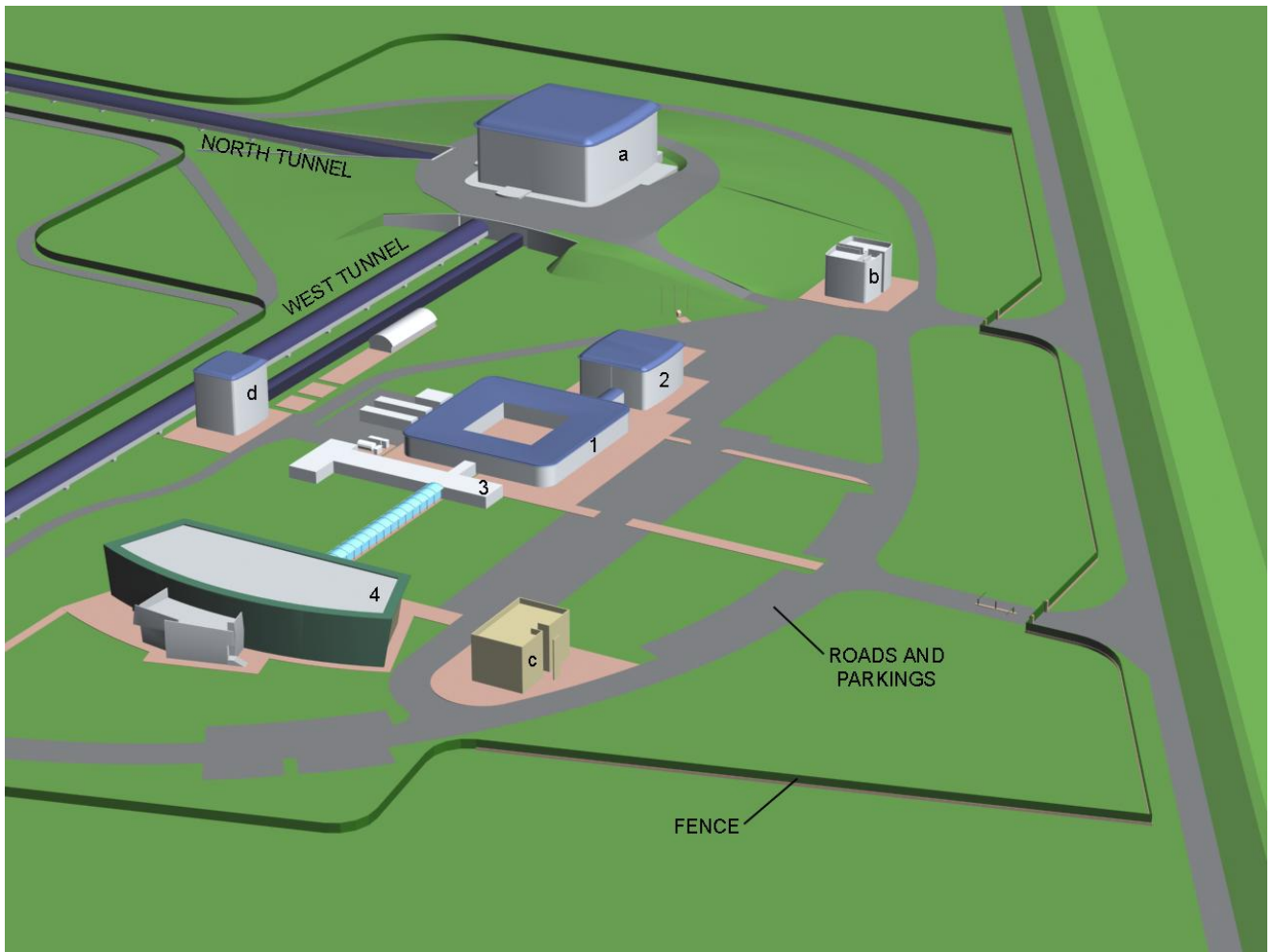
Figure 4. The central site. Building numbering and nomenclature: a- Central Building, b- old Technical B., c- new Technical B., d- Mode Cleaner B., 1- Office B., 2- Control B., 3- Office Trailers, 4- Main B.

At the far ends of the tunnels there are the Terminal Buildings, containing the interferometer end mirrors. At mid length of each tunnel there is a large technical hall, used as assembly hall for the tubes and, later, as laboratory and workshop space. From the Central Building starts also the Mode Cleaner Tunnel, ending in the Mode Cleaner Building; they contain the 144 m long Mode Cleaner (MC) resonant cavity.

Close to the Central Building there are also:

the Technical Building, containing the main electricity connections, transformers, uninterrupted power supply, diesel generators, hot and chilled water generators;

the Control Building, containing the interferometer Control Room, the main computers and offices;

the Office Building, added in 2002, containing offices, the seminar room and two smaller meeting rooms;

the Main Building, completed in 2007, containing offices, laboratories, the auditorium, two meeting rooms and a cafeteria.

Along the arms, on the outside of the 90° angle, there is a service paved road, running on the East side of the North tunnel, turning around the Central buildings and running on the South side of the West tunnel. The road and the overcrossing bridges are large enough to allow the passage of full size trucks and buses.

3.2 The Site

The land necessary for the interferometer consists of two orthogonal strips, 48 m wide and 3 km long, converging in a central area of about 80,000 m^2 and four areas of about 40,000 m^2 each, at the far ends and at mid length of the strips. The total surface is about 480,000 m^2. The width of the strips and the dimensions of the five areas have been chosen in order to keep external noise sources at a reasonable distance from the interferometer.

3.2.1 Site Choice

The Cascina site has been preferred for the following reasons:
- o the previously listed requirements can be easily met
- o along the arms it is flat at the level of $\pm$ 0.5 m
- o it has a relatively low density of population and farmhouses
- o there are a few small roads, no highways, no railways.

On this site it has been possible to find an interferometer lay-out crossing only two secondary roads and keeping Central and Terminal buildings, containing the mirrors (the test masses), at least at 200 m from existing farms and from electrical power lines, and at least at 500 m from main roads. The access turned out to be very comfortable through an existing paved road. The whole Virgo area is enclosed by a fence, with several access gates; only one of them, close to the central area, is normally operative.

In addition to the two bridges needed for road crossings, three more bridges have been built above the tunnels, to allow circulation of agricultural machines and sheep herds.

The site geology is not ideal, from the point of view of stability. In fact the area is an alluvial plane, made of a clay pack several hundred meters deep, interlaid with a few gravel and sand layers. To proof the suitability of the site for Virgo, a detailed geological survey has been performed, including penetrometric tests, core borings, water-table height measurements. Undisturbed core samples have been collected down to a depth of 60 m; in some locations 180 m have been reached.

A computer simulation of the soil subsidence in 20 years has been developed by a specialized company, using also a few measurements at large distance from the site, all the available historical data and the existing plans for water pumping.

The results of the study showed an average ground lowering of 15 cm, with a time constant of the order of 5-10 years; the calculated differential subsidence turned out to be below 5 cm, hence within the straightness requirements of the vacuum tubes.

From the seismic point of view, the site turned out to be acceptable, showing a linear power spectrum, as a function of the frequency ν, below the curve $10^{-6}/\nu^2$ m Hz$^{-1/2}$. This condition holds in any weather condition and during the peak working hours (Figure 5).
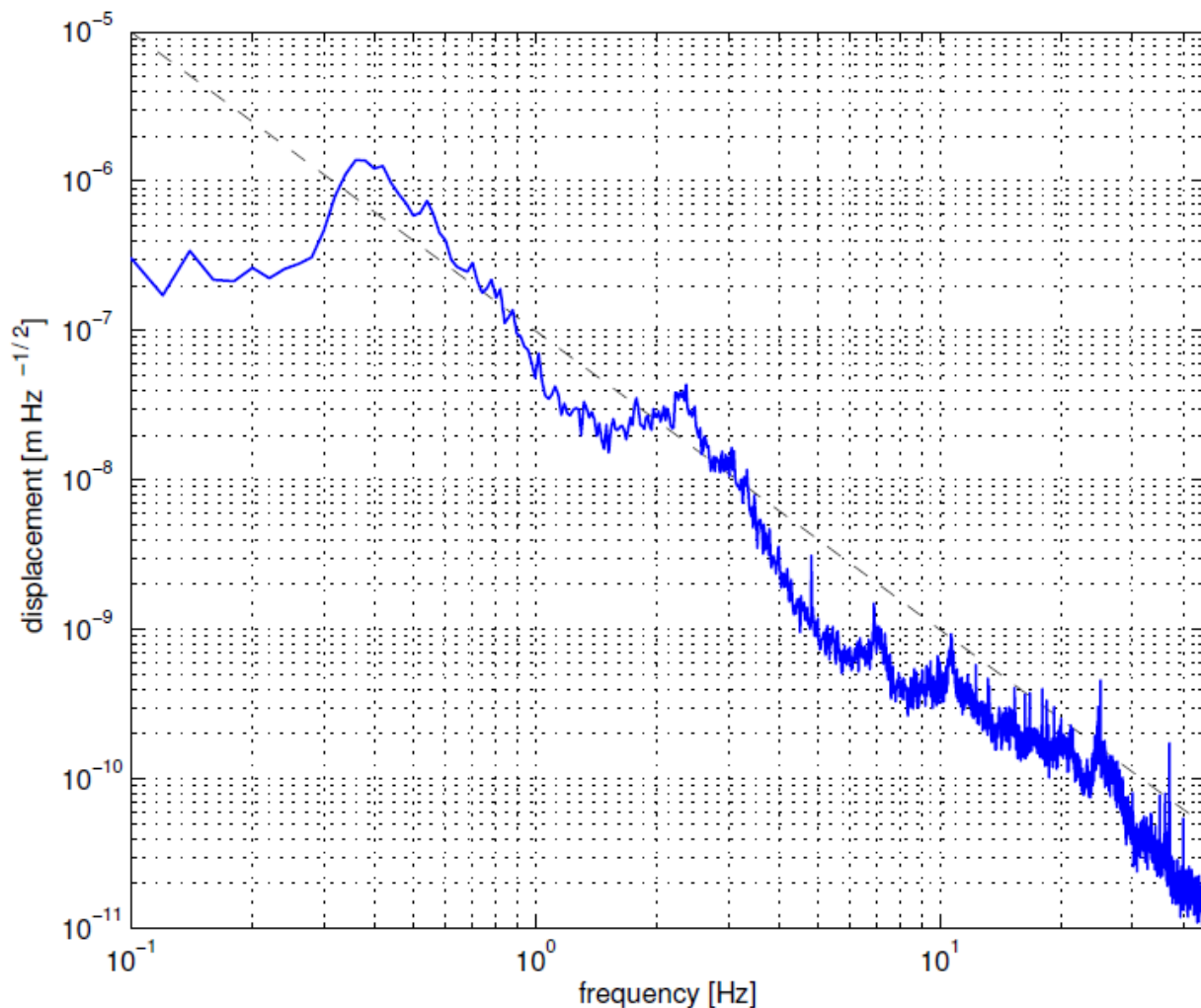
Figure 5. Seism linear power spectral density.

In the Cascina region temperature ranges between -5°C, during cold winter nights, and 35 $^{\circ}$C, in summer sunny days. These data have been considered in order to specify the mechanical characteristics of the bellows inserted in the tubes to accommodate thermal expansion.

3.2.2 Site Acquisition

Besides the physical characteristics, the Cascina site (via Edoardo Amaldi, Santo Stefano a Macerata, 56021 Cascina, Italia) has been chosen thanks to the administrative help of the Mayor and of the County Council of Cascina, of Provincia di Pisa, of Regione Toscana and of Pisa University.

The site has been acquired and made ready to build for Virgo by INFN. The acquisition procedure was a classical "esproprio", that is a forced acquisition for national interest. Due to the number of owners (about fifty), the operation required a few years to be completed.

3.3 The Central Buildings

3.3.1 Central Building

The Central Building (Figure 6), at the common starting point of the interferometer arms, contains the main optical components, suspended to six independent Superattenuator (SA) chains, inside six vacuum towers. The bottom part of a seventh tower has been installed, ready for the future installation of a "Signal Recycling" mirror and its SA. This is planned in the transition from Virgo+ to Advanced Virgo (see the Conclusion paragraph). The installation at a later time of a further tower basement, 17 tons heavy, would be impossible. The seven towers are installed in one single room, about 34 m by 34 m, 18 m high, equipped with a bridge crane, needed to assemble the SA and the upper parts of the towers. The interferometer beams run 1,100 mm above the floor supporting the towers.

Inside the building, at the South-East corner, there are three floors of laboratories and offices.
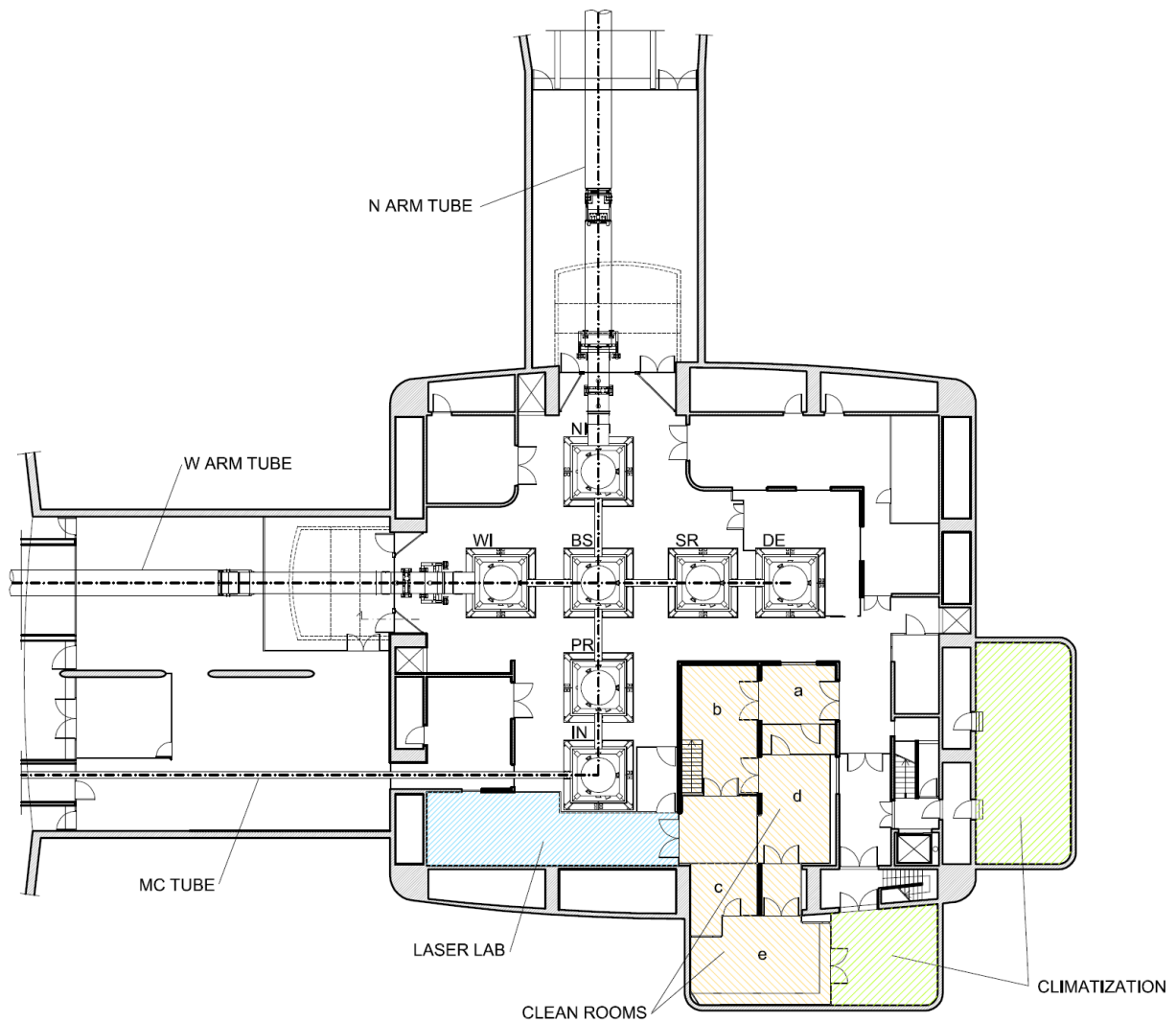
Figure 6. The Central Building ground floor plan. Clean room detail: a- entrance, b- central room, passage to clean basement (trap door for materials, staircase for personnel), c- class 10 cabin, d- payload assembly, e- washing facilities.

At the ground floor, that is the same level where the towers are installed, there is a large area of clean rooms down to class 10. In one clean laboratory there is the laser source; the other clean rooms are used to assemble the optical payloads and for any other operation on optical components. At the first floor there are: a room for control and acquisition electronics and two electronic laboratories. At the second floor optics laboratories and offices. The third floor is open and, being served by the bridge crane, is used as storage area.

In order to preserve cleanliness, the clean rooms are kept at a pressure slightly higher than the rest of the building, which is, in turn, at higher pressure with respect to the external atmosphere.

On the South and East sides, there are two underground rooms, external to the building, hosting heat exchangers and air treatment units for the clean rooms and for the general air conditioning system, respectively; hot and chilled water are supplied from the Technical Building.

The Central building (Figure 7) has been built, with one floor underground, at the top of an existing small hill, about 4 m high.
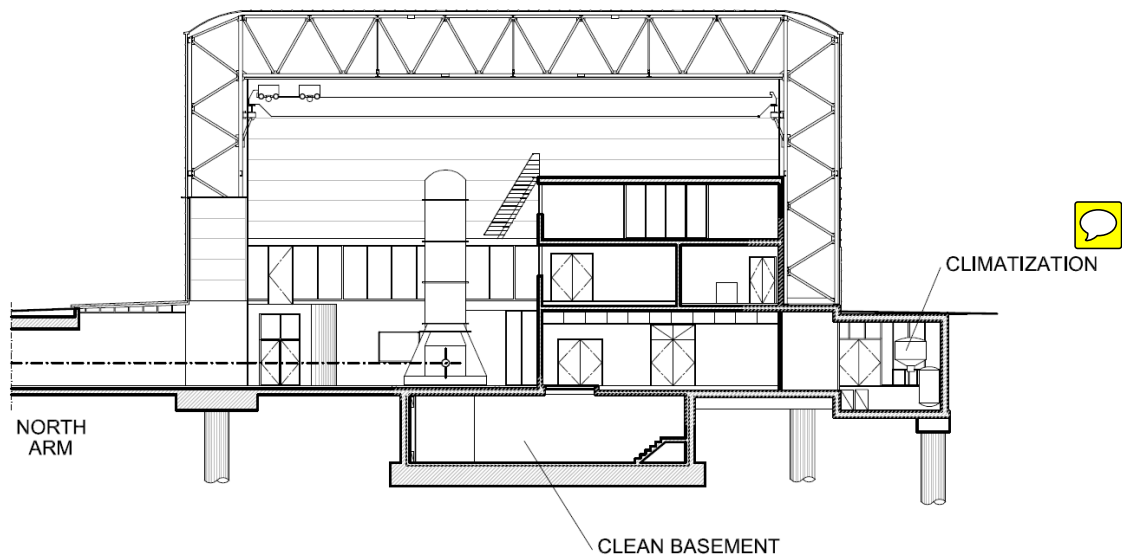
Figure 7. A Central Building elevation cross-section.

In this way the "ground" floor of the building is at the same level as the floor in the arm tunnels, which come out from under the hill, towards North and West. The top of the hill gives the access to the building, at first floor level, and allows crossing the tunnels as on natural bridges. On the South wall there are a door for the personnel and a door for trucks. Two much larger trap doors, on North and West sides, allowed the introduction of the 17 tons tower basements by a large mobile crane. After this operation, those apertures have been permanently sealed.

Under the ground floor there is a basement, running under all the towers, and accessible through the clean rooms; the basement itself is equipped with filtered air circulation, and has a cleanliness class between 10,000 and 100,000. The assembled payloads, wrapped in clean foil, are brought from the clean rooms down to the basement, then they are raised into the towers, through suitable trap doors; more details on this operation are given in the tower section.

The ground floor and the basement floor have been built as a very rigid double wall concrete box, supported by 25 piles running in the clay ground and reaching a gravel layer, at a depth of about 35 m. In this way the building has a very good long term stability. The upper walls and the roof of the building are made of a light and stiff steel structure, 2 m thick, enclosed between two walls of metal sheet and thermal insulation sandwich. This design allowed to push any mechanical resonance of the building above 7.5 Hz, since the SA's would have not been able to properly damp vibrations at lower frequencies. The upper layer of the armoring steel embedded in the concrete structure has been completely welded and electrically connected to the upper metal walls, in order to constitute a large Faraday cage, with a good ground connection.

3.3.2 Mode Cleaner Building and Tunnel

The MC Building (Figure 8) has structure and all main features very similar to the Central Building, but on a smaller scale, since it contains only one short tower. It has a surface of 11 m by 12 m and it is 12 m high; it has one single room, equipped with a bridge crane, and a clean room basement under the tower, for payload installation.
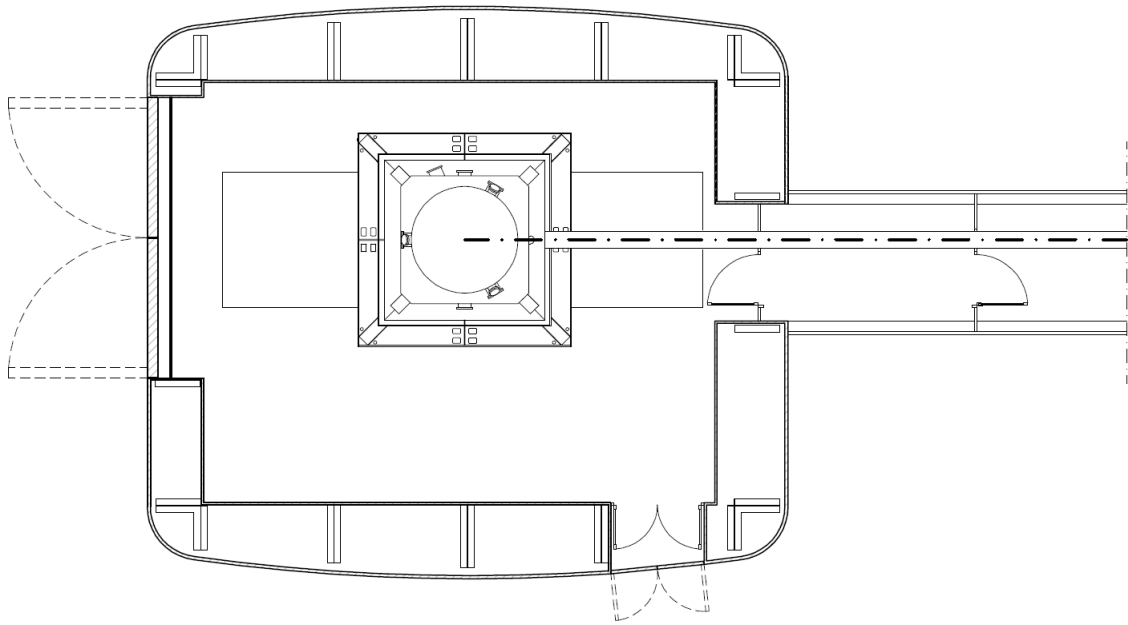
Figure 8. Mode Cleaner Building plan; the M.C. tower is shown, at the end of the M.C. vacuum tube.

The MC tunnel, about 130 m long, runs from the Central Building to the MC Building, protecting the MC vacuum tube. The tunnel is 2.7 m wide and 2.7 m high, the lower part is a "U" shaped concrete beam, supported by 24 m deep pairs of piles, every 15 m; the upper part of the walls and the roof are made of metal/insulation/metal sandwich.

3.3.3 Control Building

This building (Figure 9) hosts, at ground floor, the control room of the interferometer. There displays and projection screens present data and video images coming from the Detector while consoles allow to fully control the interferometer remotely.
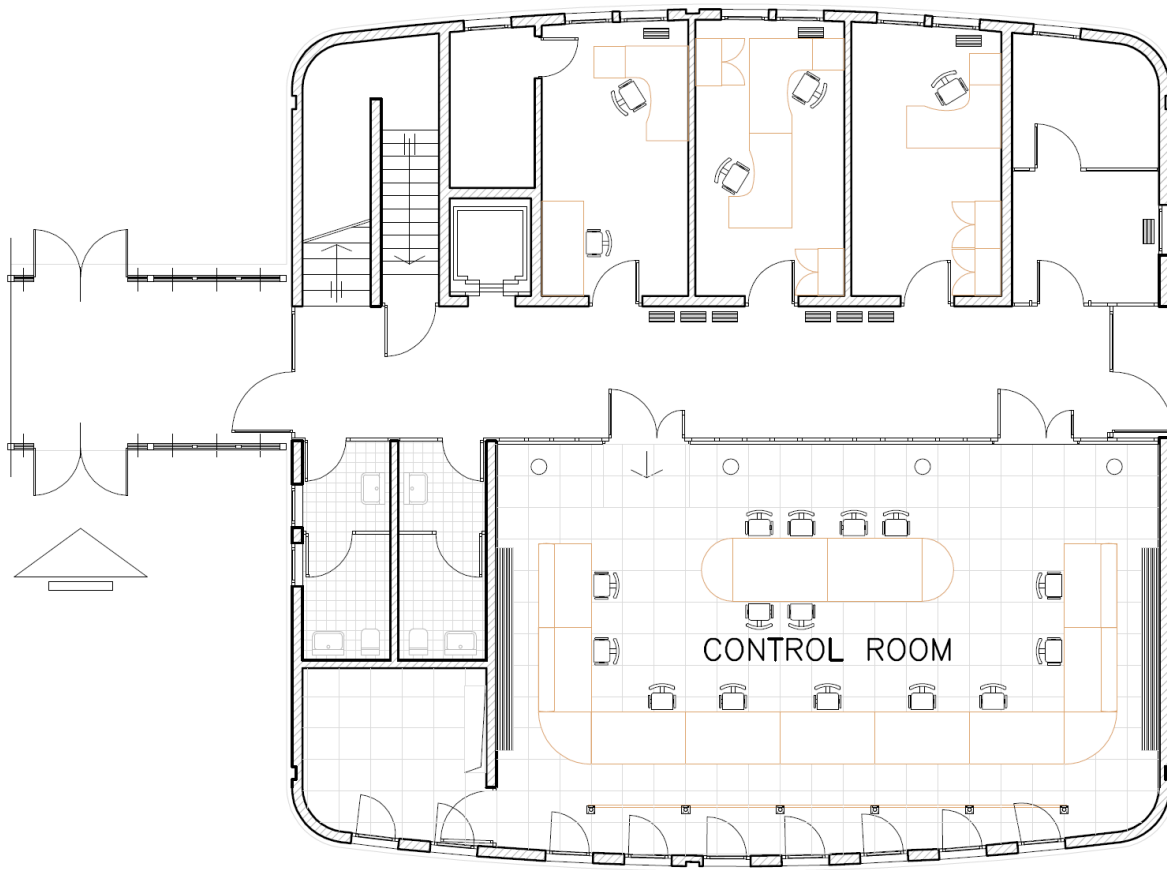
Figure 9. Control Building ground floor plan.

At the upper floor, besides some more office space, there is the main computing center for data storage and processing, with about 400 CPU and 250TB of disk. The Network room hosts the network infrastructure, that covers the whole site, with a total of 180 km cabling and 130 switches and the internet connection at 1Gb/s.

The building is connected to the Office Building through a covered passage.

3.3.4 Main Building

It is a two floor building, inaugurated at the end of 2007, to host more comfortably personnel and laboratories previously located in prefabricated barracks. There is also a 99 seat auditorium, two meeting rooms and a cafeteria.

3.3.5 Office Building

The Office Building has the square lay out of a classical roman villa, with a central "impluvium" with a large olive tree. In the four sides of the building there are two rows of offices, a 50 seat seminar room and two smaller meeting rooms.

3.3.6 Technical Buildings

In the two floor Technical Building close to the Central Building (Figure 4) arrives the main underground connection to the 15 kV, 1 MW power line. This building contains all main services for the

central zone: transformers, diesel generators, uninterrupted power supplies, hot water generators and, on the roof, chilled water generators.

From the Technical Building, electricity is distributed by underground 15 kV cables to each Assembly Building and to each Terminal Building. At each of the five connection points to the 15 kV line, there are transformers to low voltage (400 V, three-phase). Low voltage available power is: 800 kW in the central zone, 200 kW in each-one of the four other supply points. From each point power is distributed along the tunnels, up to a distance of 750 m.

Low voltage mono-phase (240 V) and three-phase (400 V) power is distributed to users and plugs at three levels of reliability:

- o as from the external company (any interruption time)
- o assisted by diesel generators (1 minute maximum interruption time)
- o assisted by battery uninterrupted power supplies (0 interruption time)

Diesel generators can run indefinitely, if supplied with fuel; uninterrupted power supplies can last 30 minutes, but, being assisted by the diesel generators, can last indefinitely.

Respective available powers at the three reliability levels are: 800 kW, 400 kW, 300 kW at the central buildings, 250 kW, 200 kW, 24 kW at Terminal Buildings and 160 kW, 30 kW, no uninterrupted power, at mid arm Assembly Buildings.

A second similar technical building has been built to serve the new Main building. Its structure allows to increasing the capabilities, in case of possible larger demands.

3.4 The Terminal Buildings

They are located at the far ends of the interferometer arms, each hosting only one tower, containing the terminal mirror (Figure 10).
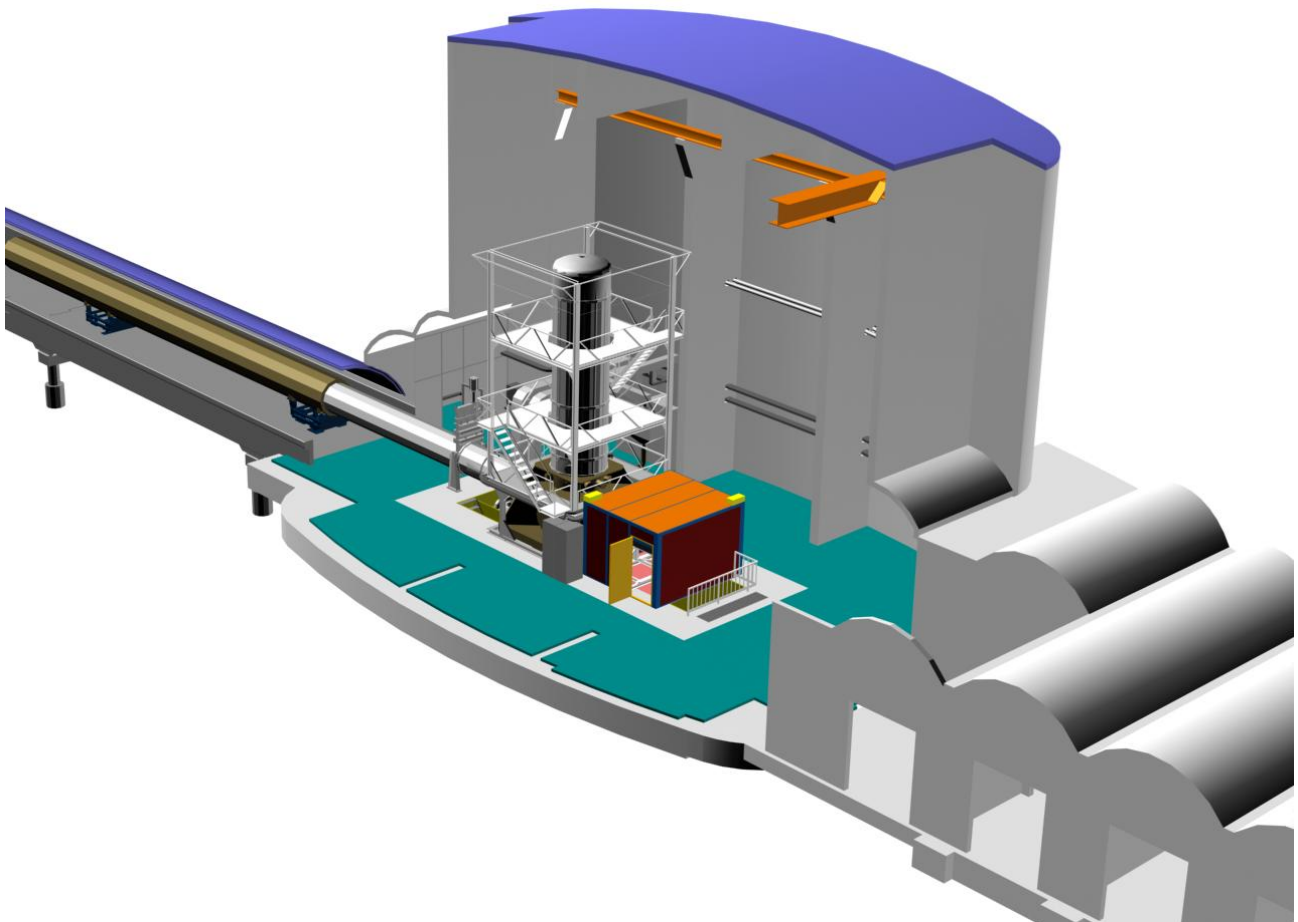
Figure 10. North Terminal Building; the North end tower is shown at the end of the North arm tube. The acoustically isolated cabin behind the tower hides the end optical bench.

All requirements and features are identical to those of Central and MC buildings: long term stability, mechanical resonant frequencies above 7.5 Hz, overpressure for cleanliness, bridge crane, clean room basement for payload installation.

The requirements have been met with a different design, with respect to the Central Building.

Walls and roof constitute a single concrete shell, with strong vertical stiffening ribs on the inside, resting on 30 m deep piles. The covered area is 17 m wide and 25 m long, in the arm direction; the height is 17 m.

The central part of the floor, 6 m wide and 15 m long, supporting the tower and the large valve, is separated by a 5 cm gap from the rest of the floor; this improves the isolation with respect to the building vibrations. In order to improve also the stability, this central part of the floor, together with the underlying clean basement, constitute a very stiff concrete box, founded on a longer set of piles, reaching a more stable gravel layer, 48 m deep at the North arm and 52 m deep at the West arm.

At the back of each building there is a one floor appendix hosting the 15 kV power connection, transformers, uninterrupted power supplies, Diesel generator and chilled/hot water generators for climatization.

3.5 The Tunnels

3.5.1 Arm tunnels

The function of the tunnels is to protect the arm vacuum tubes from external events of natural and human origin. The most relevant prescription is the stability with respect to subsidence, as described at the beginning of the Infrastructure Section. The inner cross-section (height 3.1 m, width 5.0 m) has been designed in order to allow an easy welding of the tube and the passage of a tube module at the side of the already installed tube (Figure 11).
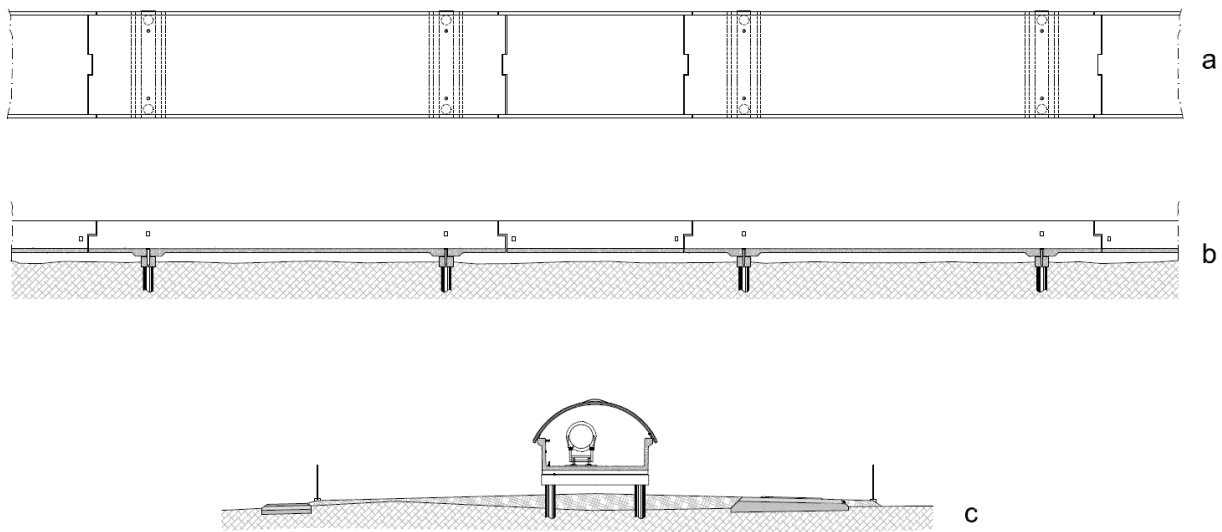
Figure 11. The tunnel; a- concrete beam structure plan, b- concrete beam structure longitudinal cross-section, c- transverse cross-section.

The floor and the walls of the tunnel belong to concrete beam elements, having a cross-section with the shape of a wide "U". The tunnel is covered by a light roof, made of curved sandwich plates (metal/insulation/metal), similar to those used for the central building walls. On the roof there are apertures with filters, to evacuate heat, during tube bake-out.

For a maximum of stability, every 15 m there is a pair of piles, 0.8 m in diameter, inserted 20 m deep, in the ground. On the capitals joining every pile pair, rests the tunnel, having the classical "Gerber Beam" isostatic structure (Figure 11). The concrete beam elements have been poured on site, in a casting factory set up on purpose at mid length of the West arm. There are 20 m long beams resting on two adjacent pile pairs and 10 m long beams joining the longer beams. All the elements touch each other through stiff rubber pads; this helps to avoid mechanical friction among rigid bodies and to damp any possible resonance. Beam resonance effect is, anyway, cancelled by the fact that tube supports are positioned exactly above the piles, that is the place less affected by oscillations of the structure.

The tunnel floor has been aligned to better than 1 cm, correcting for the earth curvature, which gives, on 3 km, a sag of about 20 cm. The corresponding angle between the vertical directions at the arm ends is about 0.5 mrad.

Main doors to enter the tunnel are located every 300 m, in correspondence of the foreseen position for the vacuum pumping stations. Further doors, located every 100 m, are present for safety reasons. Between the door wall and the tube there is a 2.5 m wide passage, for equipment and tube modules. On the other side of the tube there is a narrower passage, for cable trays and inspection.

3.5.2 Assembly Buildings

At mid length of each tunnel, there is a large hall about 40 m long and 24 m wide; the whole floor surface, including a 40 m long portion of tunnel, is served by a 5.5 tons bridge crane. The halls have been used for reception, preparation and buffer storage of tube modules, to be directed to the tunnel for installation. Since the end of the tube assembly, the North Assembly building has been converted to vacuum technology laboratory, mechanical workshop and storage. The West Assembly Building became cryogenic technology laboratory, silica fiber production laboratory and monolithic payload assembly laboratory.

3.6 The Clean Rooms

3.6.1 Central Building Clean Rooms

At the Central Building ground floor, a surface of about 300 m^2 is occupied by clean rooms, with different purposes (Figure 6).

The main clean block is subdivided in four rooms:
- o the entrance/dressing interface, class 10,000
- o the central room (class 10,000) giving access to the other rooms and to the lower clean gallery, under the towers, through a trap door for equipment and a personnel staircase;
- o the assembly laboratory (class 1,000), where payload assemblies can be performed inside an inner volume (class 100), confined by curtains
- o the mirror preparation laboratory, where mirrors are equipped with magnets and markers, inside a class 10 cabin.

On one side wall of the class 1000 payload assembly room, there is the exit door of a large washing/drying machine, with a 1 m^3 capacity. Components to be cleaned enter the washing machine through the entrance door, accessible from the washing room, containing also other ultrasonic cleaning facilities and a dedicated ultrapure water production plant.

The clean laser laboratory (class 100,000) has a separate entrance/dressing interface; it contains two optical tables for the laser source and the beam shaping optics. Part of the laboratory walls coincide with the

external wall of the Input tower; through the various optical windows, the main beam is injected into the interferometer and control beams reach sensors and cameras.

All the described rooms are supplied by the same air treatment unit, running at full power when there is activity in the clean rooms; during data taking, in absence of activity, the clean rooms are set in stand by, at low power, in order to reduce acoustic noise.

A dedicated air treatment unit supplies a separate clean room system, constituted by the clean basement and by the towers standing on its roof. The clean basement is the path to install payloads into the towers. When this operation has to be performed, the bottom lid is removed from the relevant tower, which is supplied at a higher level with filtered air. In this way the coming payload is subjected to a clean air shower, preventing the entrance of dust into the tower. The air fed to the tower is filtered at a class 100 level, but there is no real laminar flow, due to the uneven air distribution and to the large obstacles on the air path. The air return flow is taken at the basement floor level.

3.6.2 Terminal Buildings Clean Rooms

In the Terminal Buildings and in the MC Building there is only the clean basement, under the tower, for payload installation. It is a small, 20 m^2 clean basement, coupled to the tower, functioning exactly as the one in the Central Building.

3.7 Alignment and Survey

Alignment and survey have been based on a combination of optical instruments and satellite Global Positioning System (GPS). This method allows the optimization of measurement time and precision. The used optical instruments are last generation levels and theodolites fully automated and computer linked, able to measure up to distances of the order of several tens of meters. When used alone, such instruments would have allowed rms errors of about 15 mm on 3 km, due to the large number of measurement steps necessary to cover the full distance. The introduction, every 300 m, of a GPS measured point allowed to reduce the errors at the level of 5 mm. In this way, successive control surveys in limited regions, do not require to measure a full arm, from end to end, but only to measure the interval between two adjacent GPS points.

The points to be measured have been materialized on building and tunnel floor by precision brass bushes designed on purpose. The bushes have a cylindrical/conical standard hole, where any kind of target or instrument can be plugged in a reproducible way. About 450 such bushes have been cemented in precision holes, drilled on tunnels and buildings floors; every bush is closed with a dust tight protection cover. The tunnel bushes are considered also as tube reference points, since the tube is rigidly tied to the tunnel structure, through the supports. Reference points for the towers are materialized by four precision holes, drilled at the corners of the "square plate" of each tower basement.

Precision stands for GPS antennas have been developed in order to transfer the position of floor bushes outside the tunnel, through suitable holes in the tunnel roof.

3.7.1 Initial and Successive Surveys

A first survey of the site has been performed with the help of experts from the Engineering faculties of Roma-1 and Pisa universities, referring to IGM (Istituto Geografico Militare) points in a 50 km wide region. Several secondary reference monuments have been built on the site, to be used during tunnels and buildings construction.

The main surveys of the tunnels have been performed on the still open concrete structure, before to cover it with the roof panels. All the reference bushes, put every 15 m, in correspondence of the tube supports, have been carefully surveyed (±2 mm, rms). Successively tube supports and tube modules have been positioned with respect to the bushes (±1 mm, rms).

After the tube installation, all the bushes are surveyed at least once per year, to monitor tunnel/tube (ground) movements. When the displacements are larger than given limits (see Vacuum System Section) opposite correction displacements are performed, using the adjustment capabilities of the tube supports.

3.7.2 Ground Stability

Ground lowering rate at the Virgo site turned out to be of the expected order of magnitude: between 0 and a maximum of 30 mm per year (Figure 12).

North Tunnel subsidence
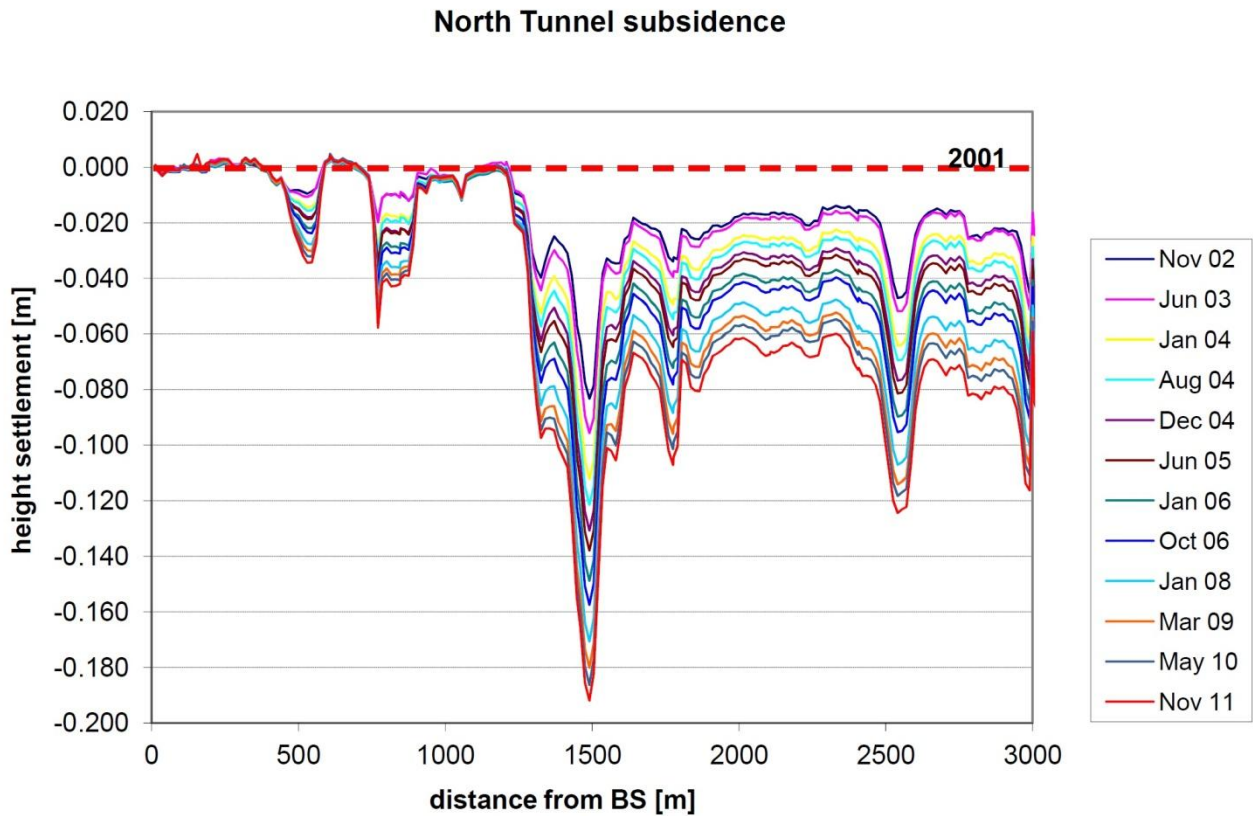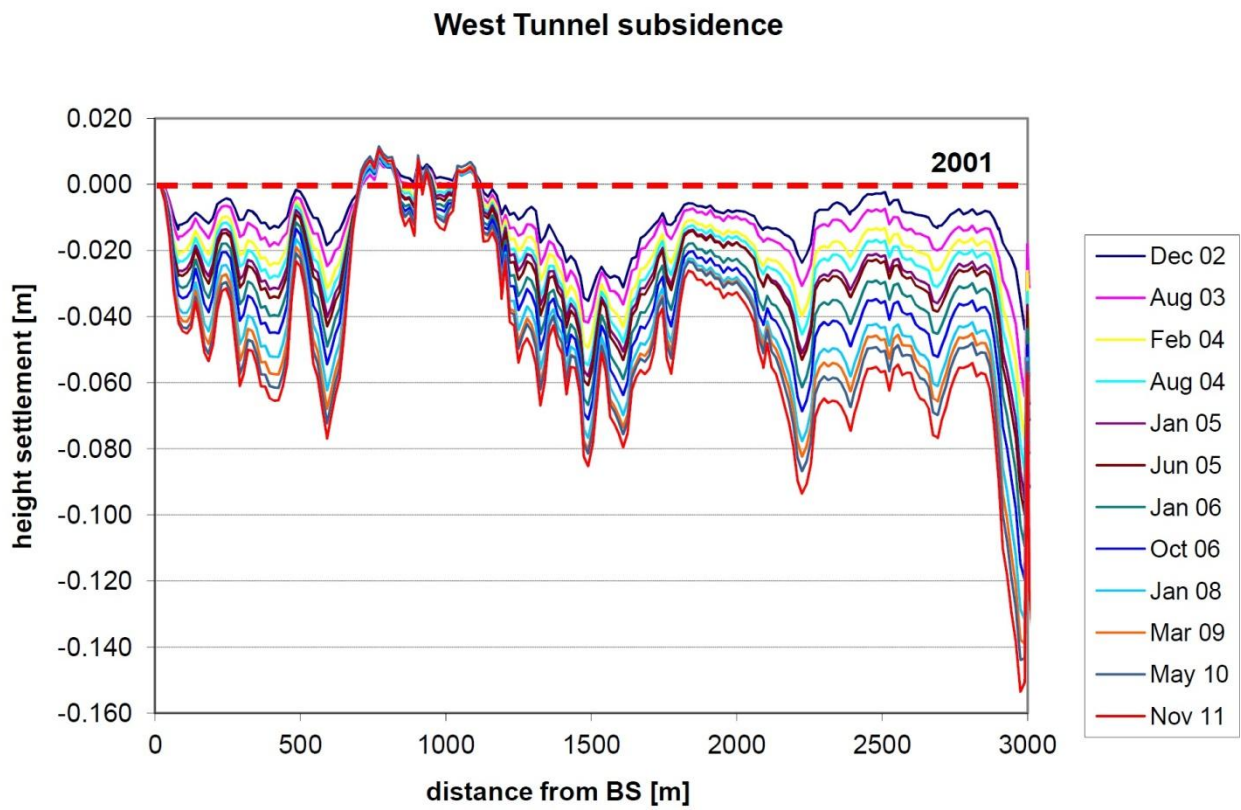
Figure 12. Subsidence profiles of North and West arms.

On the contrary only a limited saturation effect can be seen, even about seven years after the construction (Figure 13).

Largest settlement points of each tunnel
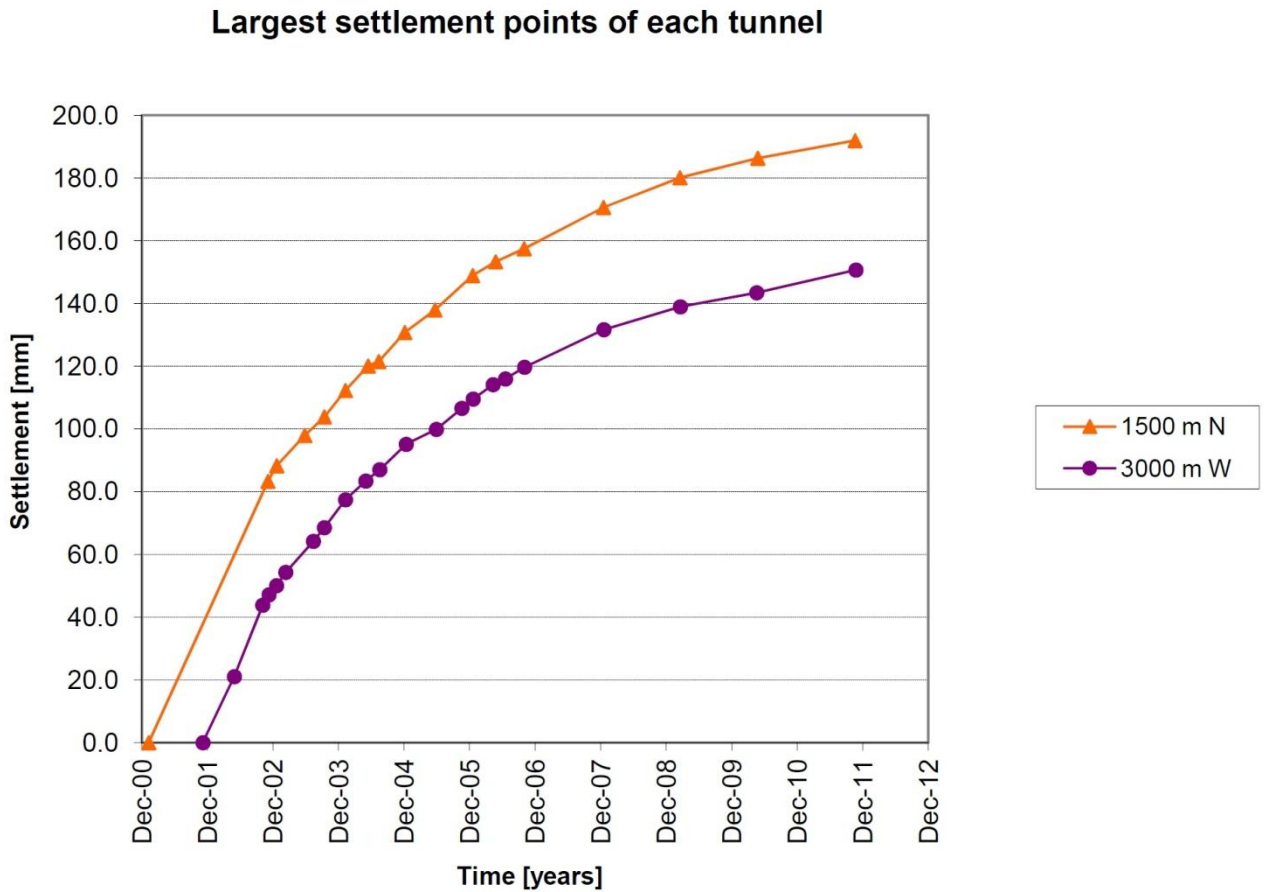
Figure 13. Subsidence time evolution.

In general the largest subsidence effects are located where the load added on ground is large, i.e. in correspondence of terminal buildings, of mid arm assembly buildings, of bridges and earth fills.

The Central Building, probably thanks to its deep foundations reaching a consistent gravel layer, remained stable, together with a large fraction of the first half of the North tunnel.

The Terminal Buildings, in spite of similar foundations on deep gravel, sink at a relatively fast rate: 8 mm per year at North and 12 mm per year at West. The end slabs of the tunnels, having less performing foundations, sink twice more quickly than the respective Terminal Buildings (Figure 14).

Differential settlement

Tunnels - Terminal Buildings
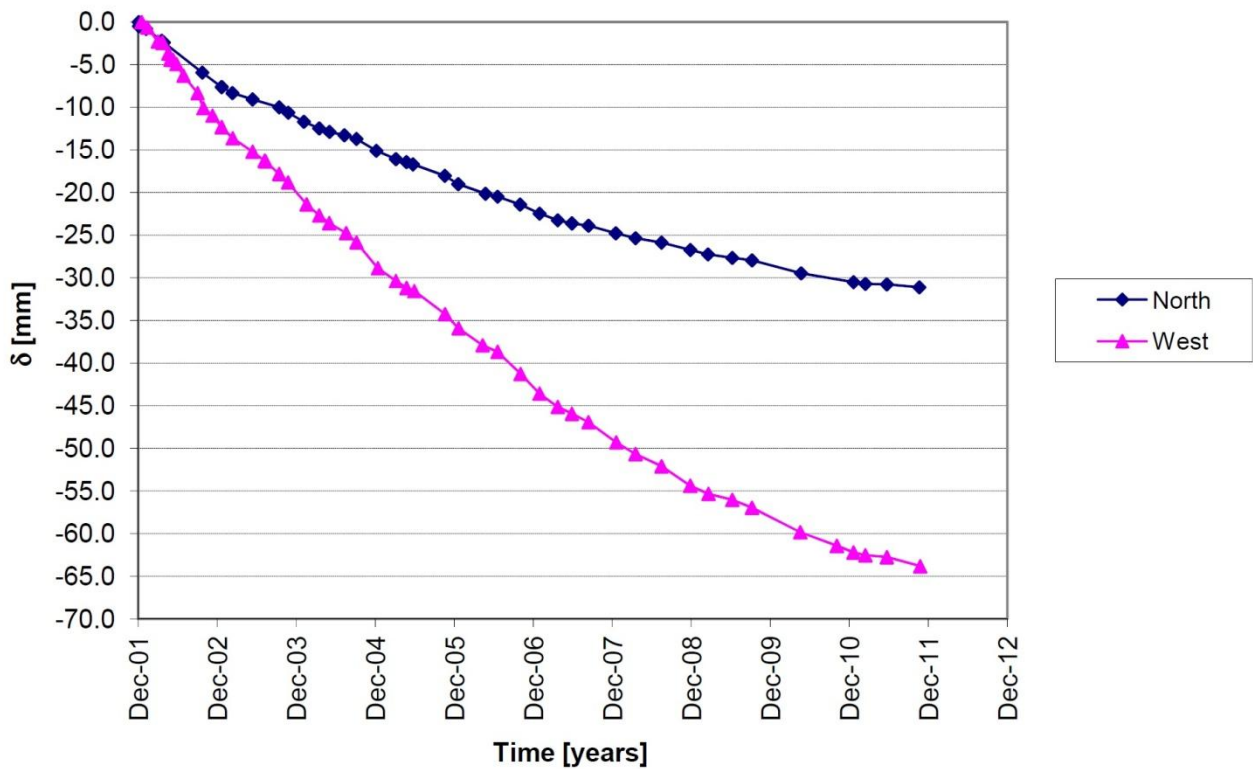
Figure 14. Tunnels sinking relative to Terminal Buildings.

This behaviour produces a vertical share strain on the last tube module, rigidly connected to the large valve. In order to keep this strain within acceptable limits, the last tube modules of each arm have to be realigned every few months, that is every 2 mm of displacement of the tunnel-end with respect to the Terminal Building. At the tunnel/Terminal Building interface, a multipoint hydraulic level system has been installed, to monitor continuously the relative displacements at 0.1 mm level.

Horizontal transversal ground displacements are, as expected, more than 10 times smaller than the vertical ones. Nevertheless in a few points it has been necessary to perform also horizontal tube adjustments.

Horizontal longitudinal displacements are expected to be also small and neutralized by the interaction among tunnel beam elements.

Even if the lowering rate will not decrease, adjustment capabilities of tube supports will allow Virgo operation for more than 20 years.

4. The Vacuum System

4.1 Vacuum System Function and Requirements

4.1.1 General requirements

The entire interferometer is put inside a large vacuum enclosure, in order to suppress several sources of noise, each one of them being strong enough, at atmospheric pressure, to prevent the observation of gravitational waves.

The vacuum vessel consists of several parts:
- two 3 km long straight tubes, 1.2 m in diameter, laying on ground perpendicular to each other; the laser beams propagate along the interferometer arms inside these tubes
- several vertical cylinders, called "towers", 2 m in diameter, up to 11 m high, containing the optical elements suspended to suitable antiseismic attenuators
- one 142 m long tube, 30 cm in diameter, containing the Mode Cleaner optical cavity
- several valves, with up to 1 m aperture
- several pumping groups, including many types of pumps and vacuum gauges.

The diameter of the 3 km long arm tubes has been chosen to be 1.2 m, to be able to contain two or even three independent interferometer beams. In this way the implementation of an additional interferometer would require major changes to the towers only.

The 1 m aperture gate valves at both ends of each 3 km tube, called "Large Valves", have been developed on a custom design. Their fundamental role consists in separating the towers from the tubes, allowing to keep the tubes in vacuum, while venting the towers; in this way it is possible to save a large amount of work and money, allowing frequent maintenance operations in the towers.

The noise sources suppressed by vacuum are:
- transmission of acoustical noise to the mirrors
- thermal noise due to damping of mirror suspensions by air friction
- excitation of mirror motion by gas molecules
- scattering of light by residual gas molecules
- refractive index changes due to statistical fluctuations of gas molecule density.

It can be seen that the last phenomenon is dominant. It is therefore sufficient to reach a pressure low enough to suppress this noise and all the other ones will be eliminated as well.

The noise level superimposed to the gravitational wave signal by residual gas pressure fluctuations has been carefully evaluated. The maximum residual pressure acceptable value has been chosen in order to keep this noise lower by one order of magnitude with respect to the shot noise. This condition must hold also for a future upgraded interferometer, having a sensitivity improved by a factor of 10, with respect to the Virgo design sensitivity.

Quantitatively, assuming a design sensitivity of 10^{-23} Hz$^{-1/2}$ above 300 Hz, and 10^{-24} Hz$^{-1/2}$ for an improved detector, the noise signal due to pressure fluctuations must be below 10^{-25} Hz$^{-1/2}$. This corresponds to a residual gas pressure of about 10^{-7} Pa (10^{-9} mbar). This value has been calculated for a residual gas constituted essentially by Hydrogen, which is the case for baked stainless steel vacuum enclosures. In the case of residual gas dominated by higher polarizability gases, the limit pressure should be lowered by one order of magnitude.

Baked vacuum systems have been considered, since, in order to reach the requested end pressure, it is mandatory to foresee a bake-out process for the whole tank, when it is already evacuated. Experimenting with prototypes allowed us to choose the most appropriate bake-out parameters to eliminate the H_2O molecular layers present on the inside surface of tubes and towers. The best choice turned out to be heating the tanks, once under vacuum, at 150°C for about 100 hours.

Furthermore the residual gas must be free of condensable organic molecules (hydrocarbons), in order to keep the optical surfaces clean. A hydrocarbon partial pressure of 10^{-11} Pa (10^{-13} mbar) is required if one wants to avoid the cumulative deposition of one monolayer of molecules on the optical elements in 4 years. This value has been chosen theoretically, because of the lack of experimental data. A reasonable sticking

probability of 0.1 for hydrocarbon molecules has been used, together with other more conservative hypotheses:

- o that one monolayer of molecules deteriorates mirror surfaces
- o that hydrocarbon molecules polymerize under the intense Fabry-Perot beams (10 kW), while it is more likely that they are photo-desorbed.

The retained target values for the average partial pressures on the optical path of the interferometer beams are:

gas species	partial pressure
H_2	10^{-7} Pa (10^{-9} mbar)
all other gases	10^{-8} Pa (10^{-10} mbar)
hydrocarbons	10^{-11} Pa (10^{-13} mbar)

These very stringent conditions (Ultra-High-Vacuum) are necessary on the 3 km optical paths and in the lower part of the towers containing the main optical components. A 10^3 times higher pressure (High-Vacuum) can be accepted in the towers containing the Input and Detection optical benches, the Mode Cleaner cavity and in the upper part of all the towers, where most of the electromechanical parts of the antiseismic suspensions are contained. In order to cope with a HV regime (10^{-4} Pa), a careful material selection has been performed for all SA components, and suitable vacuum/thermal treatments have been developed. UHV volumes and HV volumes are separated by vacuum tight optical windows or by low conductance apertures, allowing to preserve the pressure difference operating in a differential vacuum regime.

Pressure fluctuations in the vacuum enclosure can be produced also by bursts of molecules released by the vessel walls or by internal components. The origin of bursts can be mechanical (deformation or friction) or thermo-electrical (discharges in ion pumps). Molecule bursts release will be reduced to very minimum by the absence of moving parts in the UHV volumes, pumped only by Titanium evaporation pumps and Ion pumps, and by the extreme cleanliness of components, allowing a very low load on the pumps themselves.

Residual gas bursts effect, still present in the gravitational wave signal, will be vetoed by their peculiar time structure. Their shape should be characterized by a rise time well below 1 s [12], due to the fast emission process, and by a decay time larger than 100 s, due to the ratio V/S of the volume V over the pumping speed S of the corresponding pumping group.

Figure 15 shows a schematic lay-out of the vacuum system.
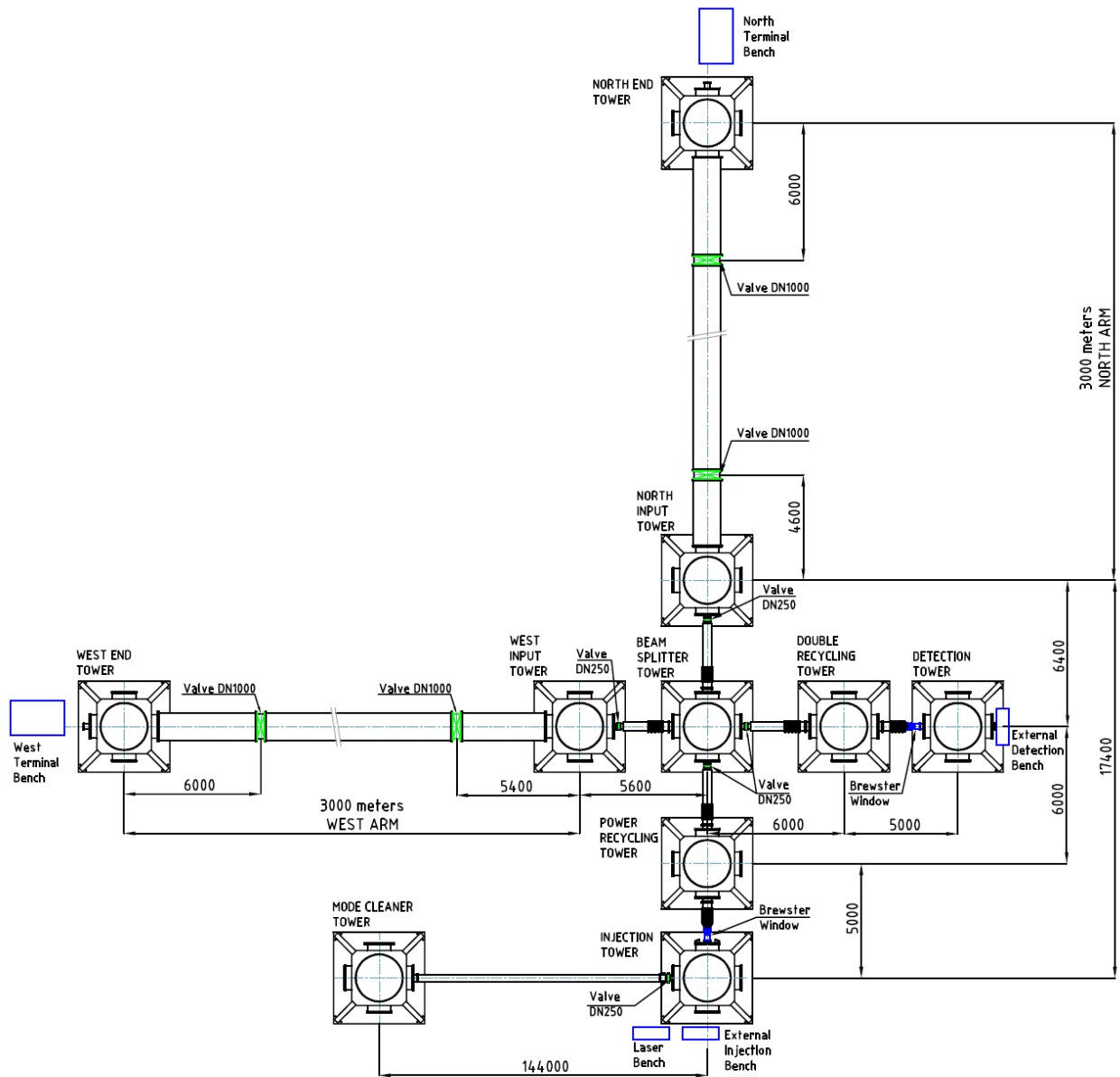
Figure 15. Schematic lay-out of the vacuum system.

Finally the evacuated volume has to be kept free of dust, in order to avoid optics contamination. This request holds, in particular, for the tower lower part, where optical components are located. Quantitatively, the fraction of mirror surface covered by dust grains should be kept at the ppm level, that is the same level prescribed for scattered light losses.

In order to cope with all the requirements, the material for towers and tubes construction has been selected to be stainless steel 304L. Possible alternatives could have been: higher quality stainless steels or aluminum alloys. 304L stainless steel has been preferred, after preliminary dimensioning of the various alternatives, as being the less expensive and most reliable solution. The following main points have been considered:

- o mechanical characteristics
- o cost and availability of the raw material
- o welding reliability and crack-less deformability
- o raw material outgassing rate and possible reduction processes

o   construction experience inside CNRS and INFN
o   experience inside companies candidate for construction
o   compatibility with existing vacuum instrumentation.

Among the different stainless steel grades, 304L has been retained, as the best compromise between cost, procurement easiness, absence of ferromagnetic behaviour.

Diffused light influence on the interferometer depends strongly on vacuum enclosure properties. In fact stray light can be diffused back into interferometer beams after bouncing on vacuum enclosure walls; in this way seismic modulation can spill in the gravitational wave signal. To avoid these problems a thorough investigation of diffused light propagation has been performed, as described in the relevant section. As a result, a large set of baffles and absorbers has been installed inside the vacuum volume, with the mission to cut the path of diffused light from mirrors to vacuum walls, back to the mirrors. Inside the 3 km arm tubes there are stainless steel baffles. Inside the tower volume, up to the large valves, there are baffles made of special infrared absorbing glass.

4.1.2 Ultimate vacuum

As explained in the introductory section, an end pressure below 10^{-7} Pa has to be reached on the light beam path.

This pressure value becomes a real challenge if it has to be reached in a large volume, with kilometric dimensions and a huge wall surface. In a vacuum enclosure without inner gas sources, with negligible permeation effects and without leaks, the end pressure close to the pumping ports is determined by the ratio:

$$end\_pressure = \frac{wall\_surface \times outgassing\_rate}{total\_pumping\_speed}$$

In the case of Virgo, the vacuum enclosure has a wall surface above 25000 m^2. The only way to keep the pumping system at an economically affordable level is to reduce the wall outgassing rate. While designing Virgo, available experience on very large systems was that the best outgassing rate reachable, after bake-out, was of the order of 10^{-10} Pa $\cdot$ l / cm^2 $\cdot$ s. Before Virgo and LIGO construction, the largest existing UHV systems were at least one order of magnitude smaller. The outgassed gas species are largely dominated by hydrogen, trapped inside the whole sheet thickness in the stainless steel production process, at a concentration of a few ppm in weight. With the given values the total pumping speed should be 10^6 l/s, with a moderate safety factor of 4. The cost of a similar pumping system, distributed along a 6 km length would have doubled the Virgo construction budget.

The problem has been solved experimenting and developing the air firing treatment on material samples and on several tube and tower prototypes. Firing consists in heating the raw material or the already built tank elements at several hundreds of degrees Celsius, in order to increase hydrogen atoms mobility and rapidly reach the equilibrium with the much lower H_2 concentration in the atmosphere. After cooling down, hydrogen concentration in the metal sheets and outgassing rate are reduced by more than two orders of magnitude. Air firing is a cheaper alternative to traditional vacuum-oven firing, which is not applicable to very large systems.

For Virgo, a very large oven has been built by the CNIM company (La Seyne sur Mer, Toulon), capable to reach 450 ^{o}C, meeting the requirement of a H_2 outgassing rate well below $5x10^{-12}$ Pa $\cdot$ l / cm^2 $\cdot$ s. Similar results have been obtained for the large valves components and for the tower lower vacuum tank, fired in the same oven for a longer time, given the larger thickness of the metal sheets to be hydrogen depleted. The firing temperature has been chosen to be well below the brittle temperature for 304L stainless steel.

The systematic study on stainless steel hydrogen outgassing, besides developing the air firing technology, allowed us to obtain relevant results in vacuum technology [13,14,15]. In particular we have demonstrated that, for our commercial cold-rolled austenitic stainless steel sheets (Avesta, Sweden), diluted

hydrogen is really desorbed by air firing while surface oxide layers don't play a significant role in reducing outgassing [16].

Air firing and 150 ^{o}C bake-out, together with a strict application of standard washing procedures allowed to meet also the hydrocarbon maximum pressure requirement.

4.2 The Towers

4.2.1 Function and specifications

The vacuum towers have been conceived to host in vacuum the interferometer optical elements and their antiseismic suspensions, called Superattenuators (SA). The various optical elements require seismic isolation at different levels, hence SA's and the respective towers have different height. The main mirrors (Beam Splitter, Power Recycling, North Input, North End, West Input and West End), acting as gravitational test masses, have long suspensions inside 11 m high towers (Figure 16).
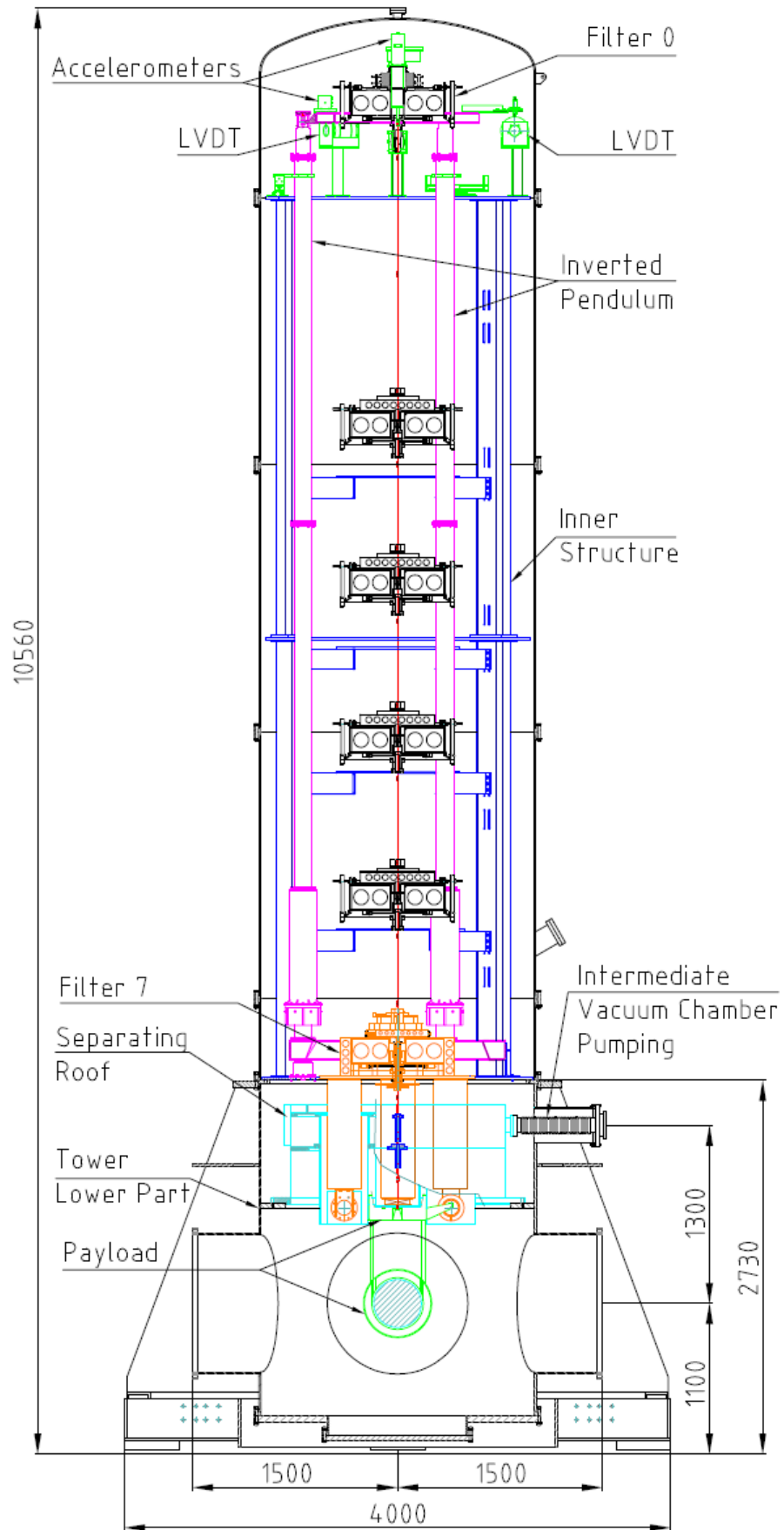
Figure 16. Vertical cross-section of a high tower, showing inner details and the SA.

The Mode Cleaner mirror, the Input Bench and the Detection Bench have short suspensions and 6 m tall towers (Figure 17).
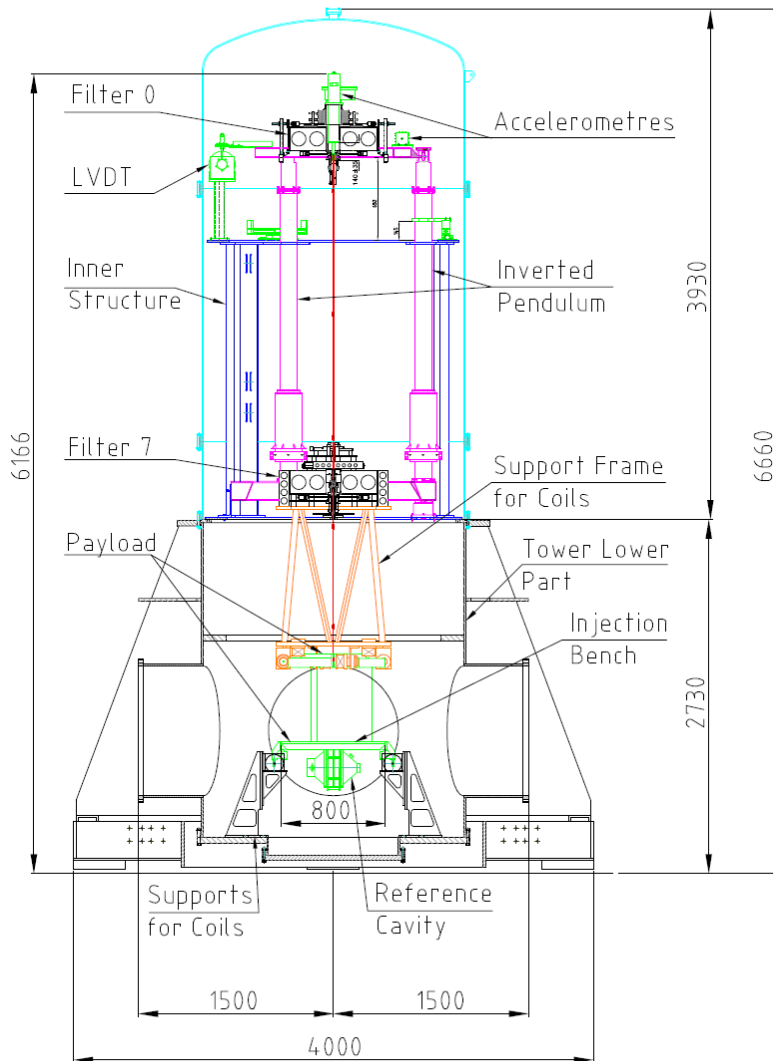
Figure 17. Vertical cross-section of a small tower, showing inner details.

The mirrors contained in the high towers require an Ultra High Vacuum level (10^{-7} Pa), not compatible with the electromechanical elements of the suspensions, by which they are supported by means of metallic wires. Hence the long towers are vertically split in three compartments: the lowest one (10^{-7} Pa) containing the mirror "payload" and the propagating light beams, the upper one (10^{-4} Pa) containing the antiseismic suspension, the intermediate needed to obtain by differential pumping the appropriate pressure difference between upper and lower compartments. The three volumes are pumped independently and are connected just by a 16 mm hole for passage of the payload suspension wire. In order to keep the conductance between the three compartments as low as possible, the holes are equipped with 200 mm long "conductance tubes".

UHV conditions in the tower lower part can be reached by respecting strict cleaning conditions followed by a 150°C bake-out process. To this aim the long tower bases have been enclosed inside appropriate ovens.

The MC mirror and the optical benches require only a High Vacuum level (10^{-4} Pa), hence the short towers have one single compartment and no ovens.

Only the base of a tenth tower has been installed between Beam Splitter and Detection Bench. This is provisional for the installation of a Signal Recycling mirror and its corresponding suspension.

The tower bases are linked by vacuum tubes for the interferometer beams propagation; the link tubes among the central towers have 300 to 400 mm diameter; the arm tubes, containing the 3 km long Fabry-Perot cavities have a 1.2 m diameter (Figure 15). The link tubes are equipped with suitable aperture gate valves, to allow independent evacuation of the towers. Link tubes connecting towers with different working pressure are closed by vacuum tight optical windows, set at the Brewster angle with respect to the light beam, in order to reduce unwanted reflections.

Tower bases are equipped with several optical window ports, for the passage of auxiliary laser beams, used for mirror position feedback control and for monitoring purposes.

4.2.2 Mechanical design

A unique feature of Virgo is its sensitivity, starting at a frequency as low as 10 Hz. This is achieved with the SA, able to reduce the seismic motion of the test masses (the mirrors) already at that frequency. As a consequence all the resonant frequencies of the mechanical structure supporting the SA have been pushed above 10 Hz, i.e. well above the SA cut-off frequency (a few Hz). A tower design in agreement with these conditions has been achieved by detailed modeling via a simulation code. Also the SA structure, described in a following dedicated section, has been taken into account. The mechanical simulation has been performed in all possible conditions, including bake-out under vacuum. The lowest collapse factor turned out to be 12.8.

The mechanical structure of the tower consists of a stiff base, allowing an accurate positioning and a strong clamping to the building floor, and of an upper part, made of modular cylindrical pieces. All pumping ports, feed-through and windows are located on the base; so no equipment has to be disconnected when opening the tower.

4.2.3 The tower base

The tower base hosts the optical payload and serves as a high stability support for the SA. The base (Figure 18)

Figure 18. A tower base.

consists of a cylindrical tank (2000 mm diameter, 2740 mm height, 15 mm wall thickness), welded to an upper square flange (2400 mm x 2400 mm x 60 mm), which is tak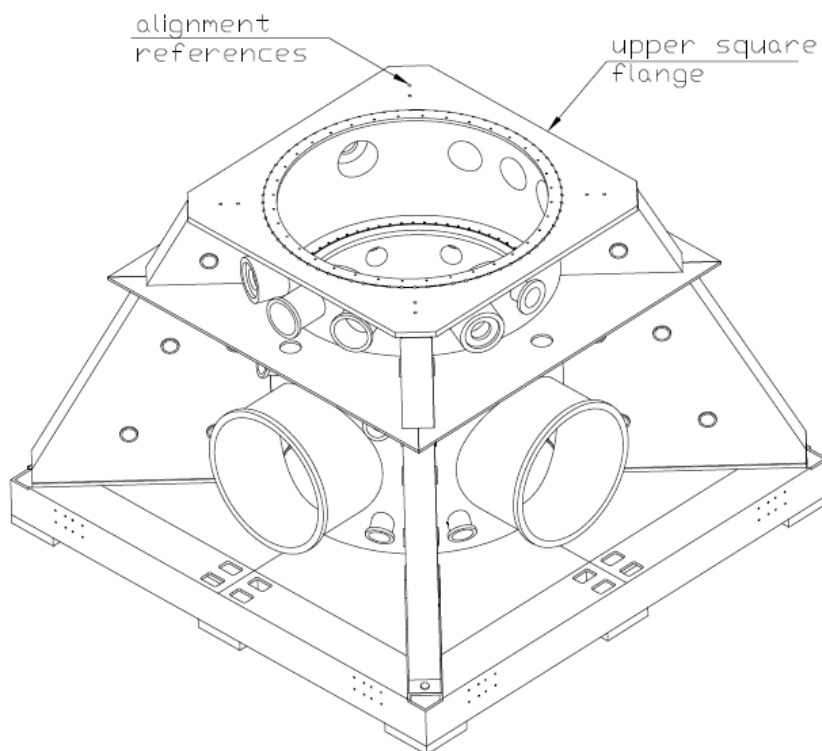en as a reference for the tank geometry and for the tower positioning. To this aim four precision holes have been drilled at the flange corners. The tank is welded to a very massive (4000 mm x 4000 mm x 300 mm) square pedestal clamped to ground. Pedestal, tank and upper square flange are bound with four vertical triangular stiffening wings.

Each tank has four large perpendicular ports, in the horizontal plane, at the interferometer beam level, i.e. 1100 mm above the building floor. All the ports have a 1000 mm diameter, except the ports connected to the arm tubes, having a 1200 mm diameter. The 1000 mm ports are closed by flanges equipped with 400 mm ports for the passage of the main interferometer beams, through the link tubes. The pumping ports for the three tower compartments are all located on the upper part of the tower bases, just below the square flange. Several smaller ports and optical windows are present for the main laser beam and monitoring and control beams.

The bottom wall of the towers consists of a circular 2 m diameter lid, bolted under the tower to an appropriate flange. In the center of the lid there is a 1 m diameter aperture, closed, in turn, by a secondary lid. The 1 m aperture allows the installation of the payload from below, through the clean gallery existing under the floor of the buildings. Exceptionally the 2 m lid could also be opened.

The bases of all the towers are structurally identical, differences concern only positions of optical windows and access ports. All the large ports (1 m, 1.2 m, 2 m) are closed by bolted flanges and metal gaskets (Helicoflex Delta, by Cefilac, France); this is particularly important for bakeable towers. Only the lower 1 m lid has a temporary Viton gasket, being opened relatively often to work on the payloads. The 400 mm ports connecting the tower bases through the link tubes, have bolted flanges with Helicoflex gaskets. Ports with diameter of 250 mm or smaller have standard Conflat flanges and copper gaskets.

4.2.4 The separating roof

The two horizontal disks dividing vertically the high towers in three volumes with different vacuum levels constitute one single rigid block called "Separating Roof". This system is located inside the tower base, just below the upper square flange and rests on an appropriate inner flange. Besides the limited gas flow through the low conductance tubes (2 l/s each, combined in series), the vacuum tightness between upper and lower compartment is reached without gasket thanks to the very high quality machining of this flange and of the lower surface of the separating roof. The two surfaces can slide one over the other, without loosing tightness. This feature allows to adjust, within a 25 mm radius, the separating roof position on the horizontal plane, following the adjustment of the mirror suspension wire, operated at the inverted pendulum top stage. Minor adjustments, up to a few mm, can be accommodated inside the conductance pipes; larger adjustments require to move the separating roof. This operation is achieved from outside, by a vacuum tight system of micrometric screws and bellows. The wire position inside the conductance pipes may be visually inspected by a set of mirrors and a TV camera (periscope).

The separating roof structure is complicated by the following features. The last SA stage, suspended above the roof has four legs supporting the coils acting on the magnets of the "marionetta", the underlying SA stage (see chapter 6), located under the roof. To keep separated the upper and lower tower compartments, the separating roof is traversed by four cylindrical pots enveloping the coil legs. At the end of every pot there is a thin Kapton window allowing the steering coil/magnet interaction, without magnetization effects. Pumping and venting speeds have been dimensioned in order not to break the thin windows with too high pressure differences (below 600 Pa).

The marionetta supporting wire passing through the conductance tubes and coils and magnets located on opposite sides of the Kapton windows demand for an extremely difficult submillimetric positioning of all the parts. All this does not hold for the short tower, not equipped with separating roof.

4.2.5 The upper cylinder

Above the base there is a 2 m diameter, 40 cm high, cylinder, called "technical ring", with four 250 mm ports equipped with all the needed electrical feed-troughs for in- and out-going signals.

Above the technical ring, the tower tank is completed by three (one for the short towers) standard cylinders and a top cap. The 2 m flanges coupling the cap, the standard cylinders and the technical ring to the base, have Viton gaskets, not being part of the UHV compartment, hence not included inside the bake-out oven.

4.2.6 Construction

The towers have been built by the company SDMS (St. Romans, Grenoble). The fabrication took place in a clean environment, free of dust and of oil vapors, in order to meet outgassing and cleanliness requirements. To the same aim, the inner surface of the tanks has been electropolished (RA 1.6 μm, rugosity, following international mechanical standard). The different tower parts have been processed by thermal treatments in air, up to 450 ^{o}C and under vacuum up to 200 ^{o}C, for mechanical tension relieving, hydrogen outgassing and accurate degreasing.

At the end of the fabrication process, every tower base has been carefully surveyed, using, as reference, the four precision holes on the upper square flange. Once cleaned, the base tanks have been sealed and conditioned under vacuum until their installation on site.

4.2.7 Cleanliness

As explained in the requirements section, it is extremely important to protect the optical payloads against both hydrocarbons and dust. Having done this during tower fabrication, cleanliness may be endangered when the towers are opened for SA or payload installation.

To this building air conditioning and clean air circulation circuits are arranged in order to have slightly increasing pressure in the following series of volumes: the external atmosphere, inside the Central (Terminal) Building, the clean rooms and the gallery, inside the tower base. The environment becomes cleaner and cleaner moving in the same sequence, up to class 10 inside the towers, in absence of operators.

To prevent dirt entering the towers, bases are equipped with two 200 mm pipes blowing-in, just below the separating roof, 1200 m^3/h of filtered air, derived from the main clean room air system. In this way, when the tower base is opened from above, for SA installation, an overpressure is formed in the UHV payload compartment and clean air flows upwards, through the conductance pipe, preventing the entrance of dirt. The separating roof acts as a sort of umbrella against dust. Moreover the work volume above the tower is confined by a plastic tent, enveloping the whole service scaffolding.

When the tower is opened from below, for payload installation, the filtered air flow acts as a real air shower, keeping clean components and operators entering from the underneath clean gallery. In order to establish a regularized circulation of clean air, appropriate apertures, close to the gallery floor, suck-in air returning it to the filter units. The established regime is not at all a laminar flow, due to the insufficient inlet aperture and to the relatively large dimensions of payload and operators, with respect to the UHV chamber. As it is described in the payload section, dirt accumulation is monitored with silicon wafer located in the most exposed points of the chamber.

4.2.8 Link tubes

The link tubes are the 400 mm vacuum tubes connecting the towers in the Central Building to allow the passage of light beams. The link tubes have to account for:
- o their own dilatation and tower dilatation due to 150°C bake-out
- o misalignment between tower bases
- o mechanical tolerances on tower flanges and on link tubes construction

o installation of tower/tower sectioning gate valves
o installation of stray light absorbing glass baffles.

Hence a link tube, up to 3.0 m long, includes an elastic bellows and a 250 mm aperture gate valve. The bellows allows elastic longitudinal displacement of ±40 mm and transverse displacements of ±15 mm. The whole link tube, including valve and glass baffles, is bakeable. All the gaskets used for the link tubes are metallic, apart the valve gate sealings, which are Viton, bakeable up to 200°C. The link tubes serve also as connections to the permanent pumps for the tower UHV chamber. Such permanent pumps are constituted by two large tanks with Ti evaporators, coupled with an Ion pump; given their large dimensions, these groups cannot be installed directly on the towers.

4.2.9 Bake-out ovens

In order to bake-out the tower bases, they have been enclosed inside large hot air flow ovens, integrated with the lower part of the scaffolding surrounding the towers. The upper part of tower bases, where all the pumping ports are present, is outside the oven; it is thermally insulated with soft blankets, in order to reach a sufficient temperature on all the walls of the UHV chamber. The structure is permanent, while the insulating walls and the heating fans are movable. In each tower the available power is 20 kW, distributed by a circulating air flow of 2000 m^3/h. Under the tower there is a 3 kW heating disk for the tower bottom lid. The power supply and control unit installed in the central building is able to power two tower ovens at a time.

The ends of the link tubes, including the gate valves, are inside the oven volume; the tube external part is heated by tape resistors and covered by insulating blankets.

4.3 The Arm Tubes

4.3.1 Vacuum performances and related constraints

As stated in the requirements section, the maximum tolerable pressure in the arms is 10^{-7} Pa. This low pressure requires a very small outgassing rate of the tube material, which should be $< 5 \cdot 10^{-12}$ Pa·l/s·cm^2 for hydrogen, and $< 5 \cdot 10^{-16}$ Pa·l/s·cm^2 for hydrocarbons; this cleanliness, together with the absence of fluorine, being mandatory for avoiding pollution and chemical attack of the mirror coating.

The design final pressure (10^{-7} Pa) is reached by a bake-out of the whole evacuated arm tube at 160°C for removing water vapour.

Finally the gas flow due to leaks has to be well below the one due to the walls outgassing. Hence the maximum acceptable leak rate for an assembled arm tube has been established to be 10^{-5} Pa·l·s^{-1}, summing up the contribution due to the tube modules, as built in the factory, and the contribution due to the circular welds performed on site to assemble the modules. With 200 modules per arm, each module cannot leak more than $3 \cdot 10^{-8}$ Pa·l·s^{-1}.

4.3.2 Mechanical design of the arm tubes

The main mechanical constraints retained for the tube design are:
o resist to a 3 bar external pressure (operate in vacuum with a safety factor of 3)
o remain in the elastic domain for a temperature between 5 and 160°C (bake-out)
o axis of each module of the 3 km tube inside a 10 cm diameter cylinder
o accept a vertical shift up to 1 cm between adjacent supports
o have the possibility to remove and replace an already installed tube module
o presence of baffles inside the tube for stopping scattered light.

Two completely different concepts have been considered to cope with these prescriptions: plain tube pieces interleaved with bellows and a completely corrugated tube.

In addition to the choice of a mechanical principle for the tube, there were geometrical constraints, one of which related to the choice of having the possibility to host 3 interferometers, which implied a minimum diameter of 1.2 m, the other being a realistic length of tube prefabricated modules to minimize the work for welding the modules together, while being transportable by truck.

4.3.2.1 The basic Module

After the construction and test of several prototypes, either straight tube or corrugated modules, it was decided to build 15 m long stainless steel elementary modules, with diameter 1.2 m, with outer stiffening rings, and one bellows per module allowing for dilatation. Stainless steel "lips" at both ends will allow to weld the modules together and easily separate them cutting out the welded portion of the lips.

The different components, and then the complete tube, were modeled and optimized with SYSTUS, a finite elements program, [17] determining the following parameters for the basic components:

o   wall thickness for the tube: 4 mm
o   distance between 2 stiffeners: 1.2 m
o   bellows wall thickness: 2 mm, 10 waves with a shape as in figure 19 (Bezier shape)
o   lip thickness: 2 mm, with a shape as in figure 19
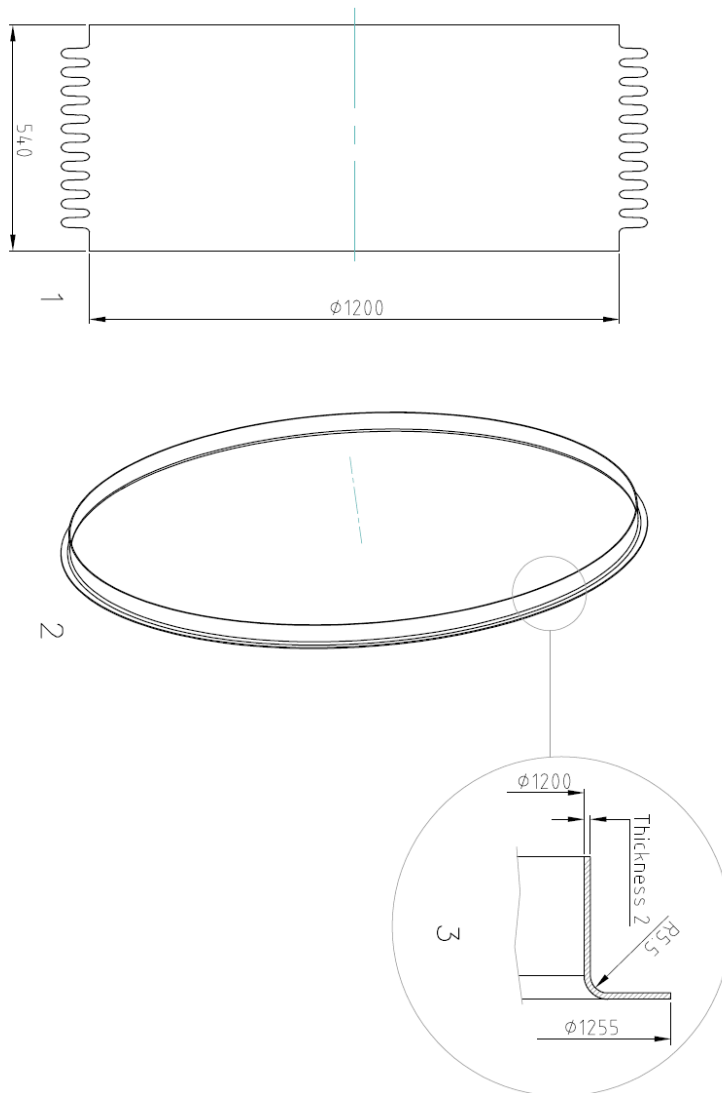
Figure 19. Bellows and lip shape.

    o   defect of circularity of the external edge less than 0.5 mm for assembling two modules with a welding robot.

Once welded together, it must be possible to disassemble the modules by nibbling the welded lips with a cutting robot. Since it has been decided that 3 nibblings should be possible, the height of the lips has been fixed to 22.5 mm.

4.3.2.2 Composition of one arm

A complete 3 km tube is composed of 300 m long basic sections, with 20 modules each, the first one and the last one being respectively a "reinforced module" and a "pumping module" connected to a pumping station. Each arm tube is composed by eight such sections and, at both ends, by two "end sections", also 300 m long, which include large valves and special short modules to link the valves with the towers (Figure 20).
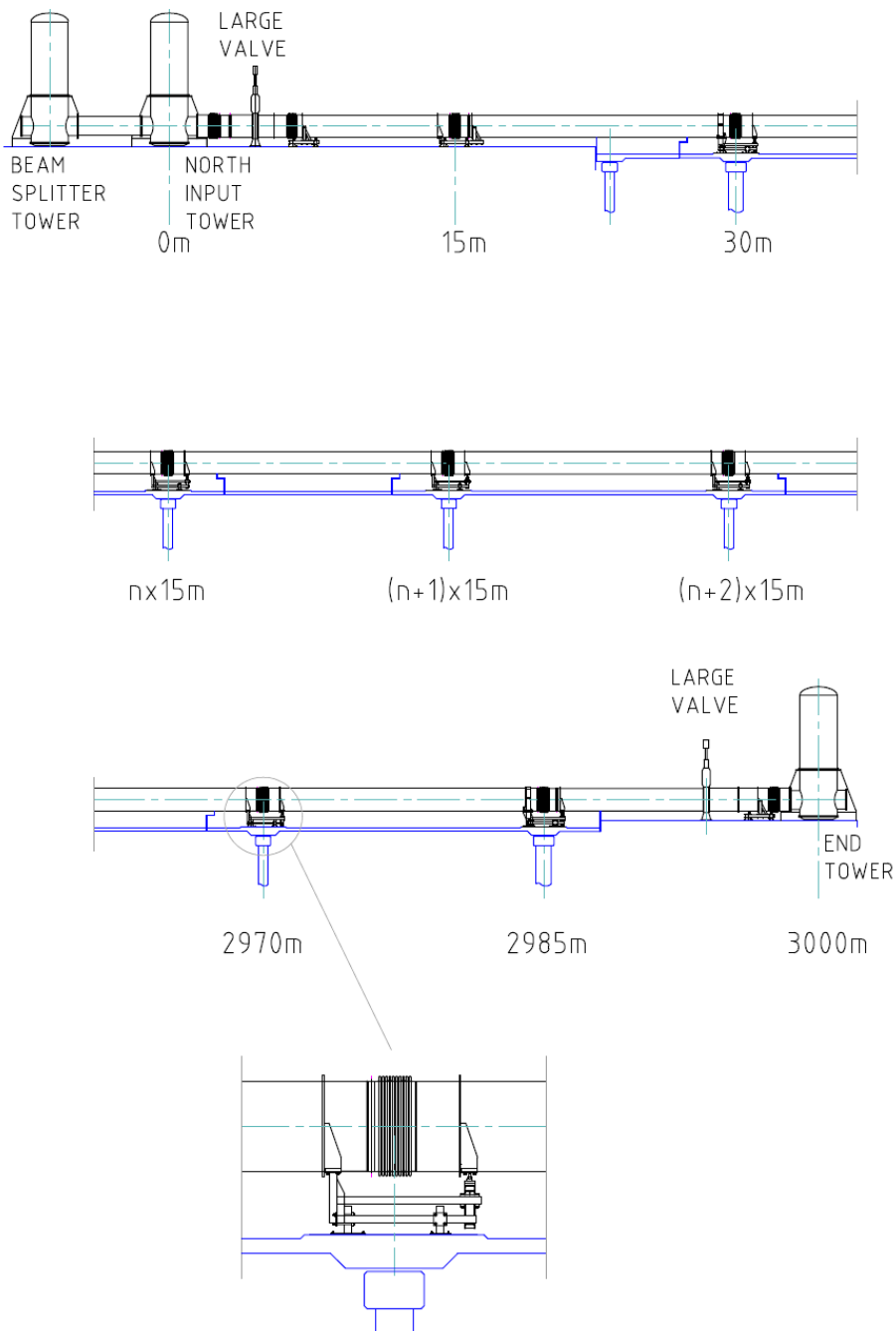
Figure 20. Composition of an arm tube, showing the first modules, some intermediate modules and the end modules.

Each section has been planned to be vacuum tested independently, closed provisionally by welded curved end caps, when being tested. So both end surfaces stand the atmospheric pressure (12 t force) and transmit it longitudinally via the module feet to the tube supports, rigidly fixed to the tunnel floor. This implies that the two end modules and their supports, of every section, are especially reinforced.

This leads to several types of modules:

o basic module: (Figure 21), 15 m long, made of 3 stainless-steel (4 mm thick) plain cylinders welded together, with stiffening rings 1.2 m apart. At one end of the module there is one bellows 54 cm long, with 10 waves 68 mm high, and a lip; on the other end the module is terminated by a simple lip.
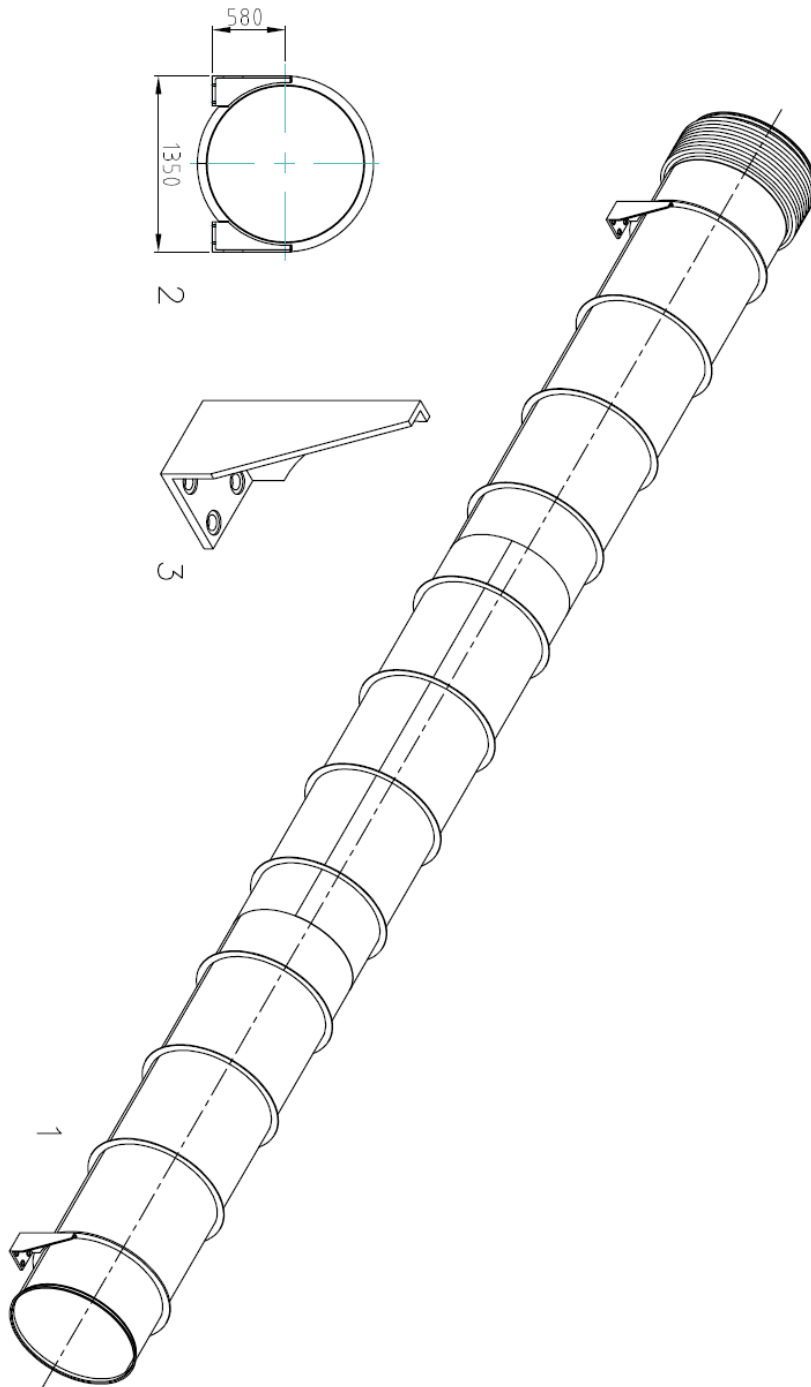
Figure 21. Basic module, its cross-section and one foot.

o   reinforced module: essentially the same as the basic module, but without bellows and with more
    stiffening rings (every meter).The absence of the bellows leaves a free space between two sections to
    install, then remove, the end caps for the vacuum test of the sections. The bellows have been
    installed later, to join the tested sections to compose a 3 km arm tube.
o   pumping module: the same as the basic module, but with 3 pumping ports: two DN200 for
    intermediate and permanent pumping, one DN63 for measurement instrumentation.
o   link modules: (ϕ 1200 mm) of different lengths to connect tube, valves and towers. When necessary
    the link modules contain a bellows.

From the previous description, it turns out that the large majority of the modules building a 3 km arm tube are connected by welds. This is, by far, the most reliable and economically convenient solution. Only the connections of tubes to towers and large valves are made by bolted flanges, coupled by metal gaskets. For a maximum of tightness and reliability, Helicoflex gaskets have been used. On the large valve side connected to the arm tube, the metal gasket has been doubled by an Viton gasket, to facilitate the leak search.

The modules rest on supports fixed on the ground of the tunnel, by mean of stainless steel feet (Figure 21) welded on the last stiffening rings on each side of the basic module, or to special double rings at one end of the pumping module and at one end of the special reinforced module. On these 2 last modules (reinforced and pumping), the feet transfer the 12 tons longitudinal force due to atmospheric pressure from the tube end cap to ground through the support, which has to be specially strong.

4.3.2.3 Module construction

For the construction of the 404 modules, a call for tender was launched in 1997, and the contract signed with Société CNIM from La Seyne-sur-mer (France); the raw stainless-steel (1.4307, equivalent to 304L) has been supplied by Avesta (Sweden). CNIM developed a specific industrial tool, with huge benches for: cutting the stainless steel plates, rolling them in cylinders, longitudinal welding, circular welding for assembling the different parts of a module (Figure 22),
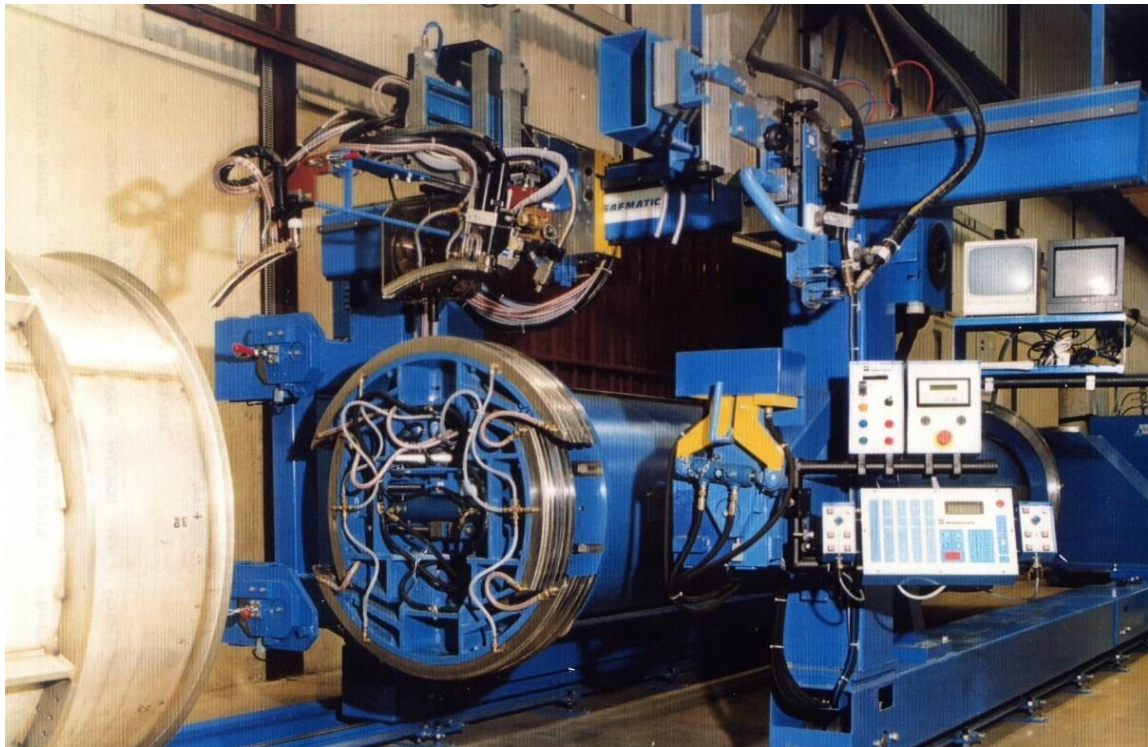
Figure 22. Picture of CNIM circular welding machine.

and a specific tool for precisely installing the stainless steel baffles (see the dedicated chapter). All this avoiding contacts of the module inner surface with materials other than clean stainless steel. Then in a 'white' hall (class 10000), the modules have been washed with alkaline soap in warm water, then rinsed with demineralized water, in a 17 m long washing machine. After drying they have been geometrically controlled on an on purpose built reference bench. A big oven ($17 \cdot 5 \cdot 5$ m^3) with electrical heaters and two permanent independent airflows (to remove the desorbed hydrogen inside and outside the modules), allowed to heat 4 modules together at 400°C for 96 hours for hydrogen desorption and residual hydrocarbon evaporation. Finally on a helium test bench the tightness of the module has been tested, together with its cleanliness, by Residual Gas Analysis (RGA).

The bellows, as stated above, have been optimized in the complete model [17], for a maximum compression of 37.8 mm between 5°C and 160°C while remaining in the elastic domain.

They were "hydroformed" at the SFZ (France) firm and tested, then heated at 400°C at CNIM before measuring the stiffness of all of them to insure it was in the expected range. After the 400°C heating, the length had increased by a small value (up to 3 mm) but a little different for every bellows. In order to keep the tolerance on the module length (15000 ± 1 mm), CNIM had to build the straight part of the tube adapted to the actual length of the associated bellows. After the final 400°C heating no change in length has been detected.

Lips also have been built at SFZ, with the right tolerances, which were not kept just after the TIG (Tungsten Inert Gas) welding on the modules; hence, in order to keep the required tolerance (0.5 mm on circularity), they had to be remachined once welded on the modules.

The whole industrial process has been validated with a first module ("module 0"), which has been fully tested, including bake-out at 160°C to eliminate water vapour. The results showed that the obtainable pressure limit was correct. The hydrocarbon rates being slightly too high required new efforts for improving the cleanliness throughout the whole process, then the production could begin.

Finally the mass production of the modules (404 modules or links) lasted from 1999 to 2002, with a maximum production rate of 20 per month. For each module the results of the tests are part of a report, summarizing all the geometrical measurements, tightness results, cleanliness (Figure 23) shows the result of a RGA analysis), and data on the stainless-steel quality
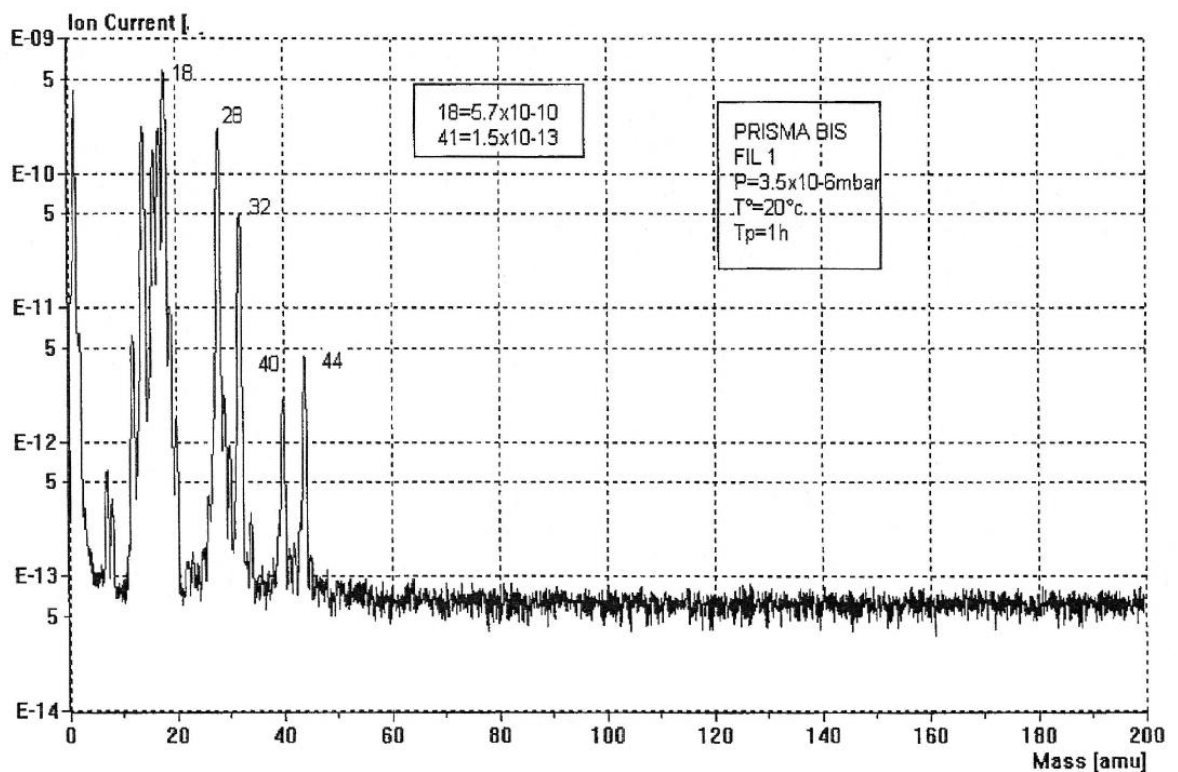
Figure 23. Typical residual gas spectrum for a finished tube module.

After the last tests the modules have been closed with tight stainless steel end disks; the inner volume remained connected to the external atmosphere by a small hose through a Teflon/active carbon filter, in order to keep the inside of the module in equipressure with the outside (breathing modules). Then the modules have been carefully packed to be transported by truck or train.

4.3.3 Thermal Insulation

Before going to Cascina the modules have been shipped to Mantova at the Belleli premises (the company in charge of the assembly on site) in order to be equipped with a thermal insulating cover. This insulation is necessary for minimizing the heat loss when heating the tube with electrical current for the bake-out process. The cover installed on the rigid part of the module is made of two overlapping rockwool layers (160 mm total thickness) covered with an aluminium sheet to provide a high uniformity temperature distribution. After assembly on site, also the bellows have been covered with insulating mattresses to complete the insulation. With this equipment the average power for getting a 150ºC temperature is about 200 W per meter of tube.

At the same time thermocouples have been installed on the module body in order to control the temperature during bake-out.

After this installation, the modules have been shipped to Cascina, by truck, where they have been assembled to compose the arm tubes.

4.3.4 Bake-out system

The tubes are heated by Joule effect, sending a DC current through the electrical resistor constituted by the tube wall itself; this is possible since every arm tube is completely welded over 3 km and the tube feet are electrically insulated from supports and ground by fibreglass washers. The DC current choice has been necessary for safety reasons and to avoid unwanted electromagnetic inductance effects (high impedance, uneven current density distribution). Current is supplied to the tube at five points (300 m, 900 m, 1500 m, 2100 m, 2700 m) by AC/DC converters. Intermediate points (0 m, 600 m, 1200 m, 1800 m, 2400 m, 3000 m) are grounded. In this way the maximum voltage is safely limited at 55 V and the current (about 1700 A) flows from each supply point, in opposite directions, to the two next ground points. Power is supplied by diesel generators, to save the high cost of two permanent supply lines, 3 km long, each with a total power above 0.6 MW. The diesel generators are rented since the bake-out operation lasts only a few weeks per arm and has to be performed very seldom (only once, up to now). The AC/DC converters have been purchased, being custom designed and built; since one arm tube is baked at a time, six converters have been bought (five plus a spare one). Every 300 m a suitable copper current connection is bolted to a tube stiffening ring; they are alternatively connected to ground and to 55 V. The return current conductor is constituted by a 10x200 mm^2 pure Al bar, attached to the tunnel wall, having a resistance five time smaller than the tube one.

4.3.5 Tube Supports

The functions of each support [18] are:
o   Bear the ends of two adjacent modules allowing only longitudinal relative displacements (Z direction) due to thermal expansion, exploiting the elasticity of the intermediate bellows; relative transversal displacements (X, Y) of the module ends have to be strictly prevented to preserve the lip weld integrity.
o   Hold the forces coming from temperature variations of modules and from vacuum.
o   Allow for the alignment of the modules in X-Y plane (perpendicular to the tube axis) referred to the given reference line.
o   Allow for the fine adjustment of the module position in Z direction referred to the reference mark on the ground of the tunnel.
o   During assembly, allow the fine adjustment of the modules to fit two adjacent lips in the same circumference; to allow correct lip welding.
o   Allow the re-alignment of the modules after installation if it is necessary to compensate for ground subsidence.

The carrying capacity is determined by the fact that a standard module has a maximum weight of about 3400 kg including thermal insulation and a pumping module has a maximum weight of about 3800 kg, including thermal insulation and vacuum equipment.

One further requirement for the supports, is that they should not induce any vibrations on the tube when accommodating movements due to temperature changes, pumping etc. So rolling or sliding systems were rejected, and the chosen solution was leaf springs, which allow displacement by bending "elastic" steel plates.

4.3.5.1 Basic support

A view of one basic support is shown in figure 24.
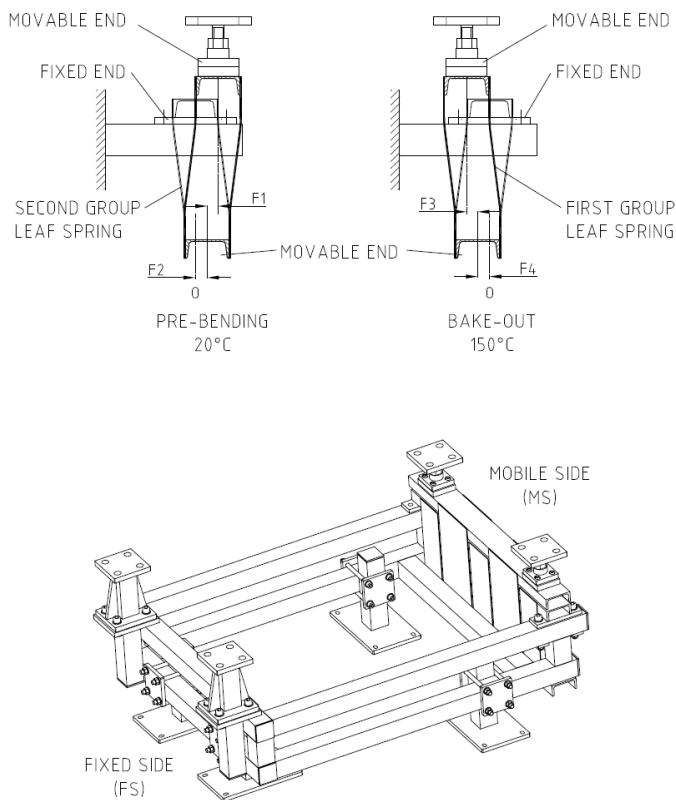
Figure 24. A basic support and the principle of its mobile side.

It consists of a strong steel frame resting on four adjustable legs bolted to the tunnel floor. On top of the frame there are four plates supporting the two feet at the end of one module and the two feet at the end of the adjacent module; in the region between the two feet pairs there are the expansion bellows and the lip weld joining the two modules.

Each support has a fixed side (FS, connecting rigidly the module feet to ground) and a mobile side (MS, connecting the module feet to ground, but allowing longitudinal displacements only). The fixed parts are blocked to ground and the 2 feet of each module on the side without bellows are bolted to this fixed part. The other part, which receives the feet on the bellows side of the adjacent module, is mobile in order to allow for the 37 mm dilatation of the module (from 5 to 160°C). At module installation, the position of FS is fixed at first, while the position of MS has the possibility to match the module feet with their fabrication tolerances.

Before performing the lip welding, a fine adjustment to fit the two lips is performed.

45

Figure 24 shows also the cross-section of the mobile side of a support, based on steel leaf springs. In order to allow only parallel (horizontal) displacements of the plates supporting the module feet, leaf springs have always been used in pairs, welded to an upper and a lower U-beam. The use of two sets of leaf springs in series, one set going down and one set coming up, reduces virtually to zero vertical displacements of the upper mobile U-beam; only the lower U-beam can have unimportant vertical displacements. At module installation, at about 20°C, the leaf springs have been pre-bent in order to have the two extreme temperatures, 5°C and 160°C, corresponding to leaf springs bent by the same amount, but in opposite directions. The use of tools and clamps with precision screws allowed to adjust module ends with submillimetric accuracy, before lip weld execution.

The adjustment ranges allowed by the supports in X, Y and Z directions are shown in figure 25.
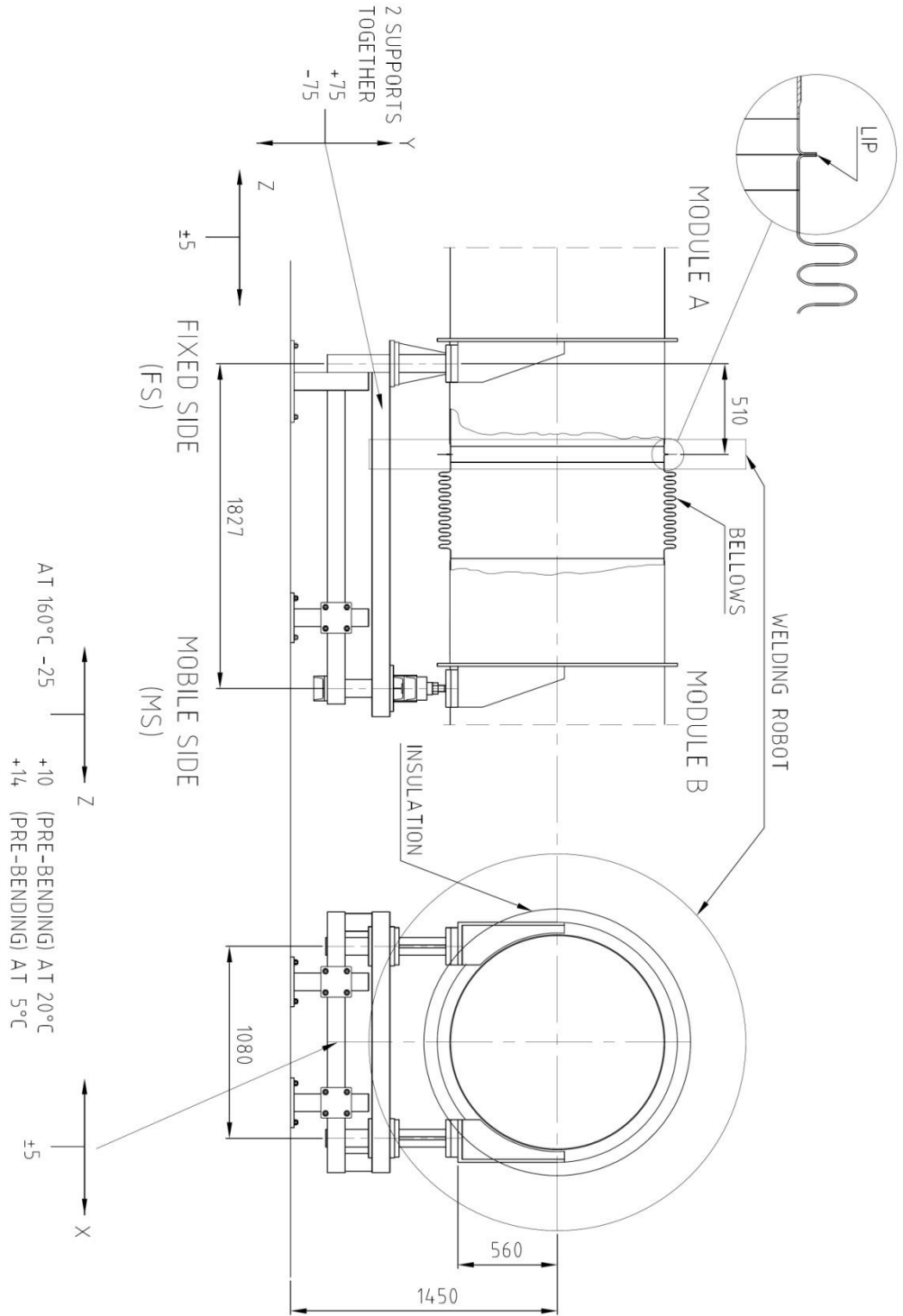
Figure 25. Support adjustment ranges in x, y, z, expressed in mm.

4.3.5.2 Special supports

Every second basic support, has been slightly modified in order to obtain some mobility (a few mm) also on the "fixed side" (FS), introducing short leaf springs. This has been necessary in order to compensate for the thermal dilatation of the tunnel concrete beams. These supports are called "balance supports".

There are also "Superfixed" supports for the ends of the 300 m sections, which have to stand an axial force of ~ 12 tons, because of the atmospheric pressure, during the preliminary vacuum test. These supports are reinforced with strong inclined beams.

Other special supports [18] had to be built for link sections near towers and valves.

4.3.5.3 Electrical insulation

Since the bake out of the tube is done by D.C. current flowing through the tube (U_{max} = 60 V), the tube must be electrically insulated from the ground. Insulation fibreglass blocks have been inserted between support upper plates (made of carbon steel) and module feet.

4.3.5.4 Construction

The supports have been built at the firm Belleli, who insured also their positioning and mounting in the tunnel.

4.4 Mode Cleaner Tube

The Mode Cleaner tube links the injection tower with the mode cleaner tower. These three items constitute a vacuum chamber separated by a window from the rest of Virgo, the required pressure (10^{-4} Pa) being not as low as in Virgo tubes and central towers. The Mode Cleaner is a resonating optical cavity conceived to reduce sources of laser noise, such as acoustic waves, thermal gradients on the optical path, motion of dust, etc.

The tube is 142 m long, 300 mm in diameter, with a stainless-steel (1.4307) wall thickness of 3 mm. It is composed of 25 modules, 5.5 m long. Four bellows are spread out over the whole length, for a working temperature between -10° C and + 40° C. Except for 2 modules on each end of the tube, modules and bellows are TIG welded together. Close to the Injection Tower a DN 250 valve allows to isolate the Mode Cleaner; it is followed by 2 modules mounted with bolts and Viton gaskets, having two ports, one CF63 for measurements and one CF100 for an eventual additional pumping group, the tube being normally pumped via the Mode Cleaner Tower. The two modules close to this tower are also mounted with bolts and viton gaskets; one of them allows the adjustment of the tube length.

The tube rests on 25 adjustable supports (3 fixed and 22 sliding supports). The three fixed supports, together with the two towers, define four independent sections with one bellows each. The tube has been aligned in such a way that its axis remains in a 10 mm diameter cylinder.

The leak rate has been measured as $Q < 3 \cdot 10^{-7}$ Pa·l·s^{-1}. A residual pressure of $< 10^{-4}$ Pa has been obtained. It must be remarked that there is no need of performing a bake out of this tube.

4.5 The Large Valves

It is mandatory to have the possibility to close the whole volume of each tube (3.400 m^3) while venting the towers, so large valves are necessary at both tube ends. Such valves, with ~ 1 m aperture, are not available off the shelf for ultra-high vacuum. The study and design have been made by Virgo, and the main requirements [19] are:
- o It has to be a gate valve with horizontal axis, made of stainless-steel with a 1 m aperture diameter
- o The gate gasket has to be in elastomer (Viton), 15 mm diameter cord.

- The leak rate must be $< 2 \cdot 10^{-7}$ Pa·l·s^{-1} for Helium, for the gate and $< 5 \cdot 10^{-5}$ Pa·l·s^{-1} for the gate body
- The outgassing rates are $<5 \cdot 10^{-6}$ Pa·l·s^{-1} for H$_2$, for all stainless steel parts, and $< 4 \cdot 10^{-5}$ Pa·l·s^{-1} for the Viton gasket
- The working differential pressure at the gate is 100,000 Pa in both directions, and 1000 Pa max. at opening or closing
- The valve can be baked out, when closed, at 150° for 100 hours, with its own heating device
- The valve is fixed to the ground by means of 2 feet supports. The tightness must be kept when a 12 tons stress due to atmospheric pressure is applied along the horizontal axis on either of its sides
- The gaskets for the junctions of the valve to the tube links are made of stainless-steel
- The opening and closing times must be less than 60 seconds

After a call for tender the VAT-SARL firm (Verrières-le-Buisson, France) has been retained, the valves being built at the VAT factory (Haag, Switzerland). A complete valve, 4200 mm high, 1610 mm wide and 600 mm thick, is shown in figure 26.

Figure 26. A large valve.

The gate is moved by a pneumatic actuator, separated from vacuum by a bellows, and controlled by a double effect electrovalve receiving air from a pressurized air bottle. The times for opening and closing the valve have been measured respectively as 53 s and 30 s.

The stainless steel pieces (except the piston bellows) have been air-fired at 400°C for 100 hours in the Virgo oven at SDMS. The Viton cord received a special thermal treatment in three steps (made by Virgo), in order to eliminate fluorine which could corrode the mirrors.

The heating device is made of two mobile insulated boxes on each side of the valve, which can roll and form a big closed box around the valve, with resistors and a fan to sweep the warm air, so heating the valve at 150° C by convection. This action has to be done at the same time as the arm tube bake out or during the bake out of the adjacent tower.

The four valves were all tested at VAT, then at Cascina after their installation in the halls. All the requirements have been met.

The complete control of the four valves will be detailed below, with all the vacuum controls.

4.6 Towers and Tubes Assembly

4.6.1 Survey

The knowledge of the position of the vacuum system components is fundamental, since they support all the interferometer optical elements. Tubes and towers have been positioned with respect to the precision reference bushes installed in tunnels and buildings, as described in the Infrastructure section. Taking into account that fabrication tolerances are ±5 mm for tower bases and ±2 mm for tube modules, main installation precision requirements are:

- o misalignment among towers in the Central Building: ±5 mm
- o misalignment between input and end towers of each 3 km arm: ±5 mm (in addition to ±5 mm measurement errors, due mainly to GPS)
- o misalignment between adjacent tube supports: ±2 mm
- o the center of every arm tube cross-section must be inside a 100 mm diameter cylinder.

It has been also necessary to take into account the earth curvature in order to have really straight arm tubes. Earth curvature produces also a 48 mrad angle between vertical directions at 3 km distance; the same angle exists between the horizontal floors of Central and Terminal buildings. Moreover the West arm has an average inclination of about 1.5 m, over 3 km, since the West Terminal Building floor has an elevation lower by 1.5 m, with respect to the elevation of the ground level of the Central Building. All these features have been accounted for to position correctly tubes and towers.

4.6.2 Tower positions

The interferometer optical elements must be centered on the axes of the light beams, which are not straight lines, since they cross the beam splitter at a 45° angle. Moreover a few optical elements have a wedge angle between the two faces; this makes the outgoing beam not parallel to the entering one. On the other hand, each optical element and its support wire are nominally aligned on the mechanical axis of the respective tower; the adjustment features of the inverted pendulum top stage and of the separating roof have been exploited to correct tower mechanical imperfections and positioning errors. As a consequence the towers are located, in the Central Building, according to the beam propagation path. In the Virgo reference system, where the horizontal orthogonal axes coincide with the interferometer arms, pointing approximately towards North and West:

- o Injection and Power Recycling towers are translated by 20 mm westward
- o Beam splitter and Signal Recycling towers are translated by 20 mm northward

the link tubes, where necessary, are connected off center to the towers, according to the given translations.

The towers are placed on the buildings floor, in correspondence with the holes giving access to the underlying payload installation gallery. The holes have been shaped in order to allow some adjustment and some asymmetry in the tower positions along the arm directions, as required by the interferometer locking scheme. The horizontal coordinates of tower centers in the Virgo reference system are listed below, together with adjustment ranges.

Tower	West coordinate (mm)		North coordinate (mm)	
Input Bench	+20		-11000	
Power Recycling	+20		-6000	-600/+1000
Beam Splitter	0		+20	
North Input	0		+6400	±400
North End	0		+3006400	±1500
Detection Bench	-11000		0	
Signal Recycling	-6000		+20	
West Input	+5600	±400	0	
West End	+3005600	±1500	0	
Mode Cleaner	+144000		-11000	±2000

It must be clear that tower position adjustments are major changes, since they involve cutting link tubes and/or arm tubes and displacing very large objects of the order of 20 tons each. The MC tower (the easiest one) has been displaced in 2003 by 800 mm, requiring about two months of work. Very small displacements, of the order of millimeters, can be "easily" performed, if they can be accommodated in the elasticity range of link tube bellows.

Tower positions in the Central Building have been measured at the very beginning, when only tower bases were there and all lines of sight were free of obstacles. Later, after oven and scaffolding installation, only very limited checks have been possible. There is evidence, anyway, that the building behaves like a rigid box. Moreover the Central Building seems to be very stable with respect to the site external topographic references. The position of the only tower contained in each Terminal Building is, by definition, stable with respect to the stable floor plate, where it is clamped. The plate, in spite of its strong foundations, is steadily sinking at a relatively fast pace: about 20 mm/year at West terminal and 10 mm/year at North terminal. It is not a problem, for the interferometer control system, to follow such displacements angularly steering the central mirrors by several µradians.

4.6.3 Tower installation

In the tower installation process, the most challenging operation was the introduction of the seven tower bases in the Central Building through the ad hoc foreseen trap doors. It has to be considered that each base is a pyramidal object with a 4 m x 4 m square base and a weight of 17 tons. The tower bases, arriving from France on a special transportation chariot, have been lifted by a giant mobile crane, then lowered in the building through the trap doors. Once on the floor, the bases, sliding on strong rollers, have been pulled in position by capstans. The correct positioning, within a few mm, has been achieved in few iterations, for the two horizontal coordinates. The vertical positioning has been obtained with suitable shimming, necessary also as thermal insulation, during bake-out. A similar procedure has been followed to install tower bases in the Terminal Buildings and in the Mode Cleaner Building, facilitated by having the external road at the same level of the inner floor.

The system to clamp towers to ground must be strong enough to stand unbalanced forces due to atmospheric pressure. The worse case is during standard operation, when the end towers and the arm tubes are in vacuum: in this situation the end tower base is subject to a 11 ton force toward the BS. On the other hand, during bake-out, the tower base must be free to thermally expand (about 8 mm). The solution consisted in clamping very strongly to ground the oven/scaffolding structure containing the tower and leaving the

tower square base plate free to expand on three sides, against suitable springs. The springs push the plate against the fourth side, serving as fixed reference. The fixed side has been chosen for the different towers according to the particular situation of atmospheric pressure unbalance.

With the tower bases in position, the oven/scaffolding structure has been assembled and strongly clamped to ground. Then the systems of shims and springs mechanically connecting towers and ovens have been installed.

Main successive operations have been: external cleaning, pumping system installation and vacuum testing, bake-out oven testing, intermediate vacuum chamber installation and positioning, link tubes installation, SA installation, payload installation, final vacuum testing. All these operations are described in the relevant sections of this paper.

4.6.4 Tube module preparation

Tube modules arrived by truck from Belleli premises in Mantova fully equipped with thermo-couples and thermal insulation, still sealed with tight end disks and breathing filters. They were first carefully vacuum cleaned from dust on outer surface passing through a transit tent, then they entered in the assembly hall, at mid length of each arm tunnel. It has been considered as very important to preserve the cleanliness of the assembly hall and of the adjacent tunnel, since in this environment the modules had to be opened to be welded one to the other. In the hall, serving also as buffer storage for up to 10 modules, the plastic envelops protecting the lips and the end discs were dismounted. Then, with the help of a bridge crane, each module was loaded on an electric train and sent in the appropriate half tunnel.

4.6.5 Tube support installation

Tube supports have been installed in the tunnel well before the module delivery, as soon as the tunnel sections were available and equipped with surveyed reference bushes. The supports have been bolted to the tunnel floor and the four upper plates of every support were individually positioned to ±2 mm with respect to the local reference bush, ready to accept the feet of the modules.

4.6.6 Tube module positioning and welding

At installation, the two front feet of the new module were posed on the tube support already holding the two rear feet of the previously installed module. The bellows at the interface between the two modules was kept compressed with an appropriate tool, to leave room for the still present end disks, protecting the lips to be welded. The following operations were performed in sequence:
   o   fine adjust the new module position with respect to the tunnel reference bush, using the precision markers drawn on the modules, at the factory
   o   slide on the welding zone a movable clean tent, equipped with filtered air supply, enclosing about 6 m of tube, including the support, and wait for the establishment of a clean environment
   o   clean with solvents all the surfaces inside the tent
   o   start blowing filtered air into the already installed tube and into the new module
   o   as soon as the overpressure is sufficient, slide off the two adjacent end disks
   o   clean the lips
   o   release the compressed bellows, bringing to contact the pair of lips to be welded
   o   fine adjust the position of the new module feet, to have a perfect lip correspondence, to better than 0.5 mm
   o   install around the tube the welding robot and bring into the tent the PC controller
   o   let the robot chariot perform a test full turn around the lips
   o   start the welding turn and check continuously the electric parameters and the melted metal shape on the screen
   o   inspect carefully the whole weld
   o   dismount the robot and slide away the tent.

It happened only a few times to have a visually not satisfactory weld, in general due to inaccuracy of the position of the torch with respect to the lip edges. The defecting weld portions have been corrected by a second torch passage.

The initial program foresaw to assemble tube sections 300 m long (20 modules, 19 welds), with welded endcaps, to be He leak tested separately. After the absence of leaks in the first two sections, we decided to build longer sections, to speed up the assembly. The last assembled section was as long as 1.5 km, i.e. the whole last half of the West arm.

Out of more than 400 circular welds, only two were leaking and required to be cut by the nibbling robot and rewelded on the fresh lip edges.

The cutting head of the robot has been used also to cut out the welded endcaps of the tested sections, before joining them together with appropriate 1 m long bellows sections.

4.6.7 Tube leak detection

The tube leak detection has been performed with a classical procedure, made exceptional by the enormous volume of the system, in particular when a whole 3 km tube was tested for the section joining welds. Waiting times larger than 1 hour have been necessary.

Every circular weld to be tested has been enclosed by a band of silicon rubber (standing bake-out temperature) glued to the tube wall, on the two sides of the welded lips. Having connected a He leak detector to the pumping port, gaseous He was fed in the volume under the rubber band surrounding the lip weld. According to the design specification a maximum acceptable leak rate of $3 \ 10^{-11}$ Pa m^3 / s ($3 \ 10^{-10}$ mbar l / s) has been used.

A test bake-out has been performed on all the tube sections, but the leak test has not been repeated after bake-out, since the reached ultimate pressure and the residual gas composition witnessed the absence of harmful leaks.

4.6.8 Arm tubes geometrical stability

The ground subsidence has to be continuously corrected for two main reasons.

First because a support sinking much more than the support at the other end of the same module may produce an angle between two modules, hence stress in the lip welds. The maximum acceptable angle has been evaluated to be about 0.7 mrad, corresponding to one support sinking by 10 mm, between two completely stable supports. Before to reach this limit, the relative displacements of the modules can be safely accommodated in the elasticity of bellows and lips and in the tolerances of bolted connections.

Second because the tube axis must be straight within ±50 mm. Beyond this limit tube walls and baffles start entering the beam gaussian tails. This limit has been retained, even if it has been evaluated for the case of three interferometer beams in the tube.

Tube supports have been conceived in order to allow vertical tube realignment to recover tunnel subsidence. This is easily and safely achieved, using hydraulic jacks and safety adjustable shims, keeping the tube under vacuum. It turned out that there are zones, involving up to 20 supports, with a maximum sinking of 20 mm/year. In this case two realignment operations per year are necessary.

Particular care has to be paid at the far arm ends, since the last tunnel slabs sink more rapidly than the terminal buildings, producing a share stress on the tube. Since in these points the tube is not equipped with bellows, the maximum acceptable relative sinking is only 2 mm, requiring more frequent adjustments. These actions have been made very easy and quick, replacing the standard legs with mechanical jacks, on the two last tube supports. Very high precision hydraulic levels are being tested to monitor subsidence in these zones.

4.7 The Pumping System

4.7.1 Pumping system function and concept

The pumping system includes all the devices necessary to produce and monitor the vacuum environment for the proper functioning of the Virgo interferometer. The vacuum enclosure is composed by several volumes separable by gate valves, in order to make their vacuum status independent from each other; for the same reason, each separable volume has its own pumping and control system. There are 12 separable volumes, but the two 3 km arm tubes have 6 pumping stations each, to make their pressure profile sufficiently uniform, over the huge length. Moreover the six long towers have two main compartments each, with different vacuum regime. This gives a total of 22 pumping stations, distributed along 6 kilometers; to make control and maintenance easier, standardization of components has been enhanced as much as possible.

All pumps and gauges are connected to the vacuum tank through valves. In this way, in case of failure, the defecting equipment is separated (automatically, by the remote control system) from the vacuum tank without interrupting interferometer operation. Given the very high conductance existing among all parts of the vacuum tank, shutting down for limited time one pumping group does not change qualitatively the vacuum level.

The valves separating the arm tubes from the rest of the vacuum system have a 1 m diameter aperture and have been custom designed and built. The "Large Valves" have been described in a dedicated section (4.5).

All the other valves are standard, with aperture diameters up to 250 mm; shutter gaskets are in Viton, except valves normally closed against atmosphere, where metal gaskets are used.

The whole pumping system, valves included, is remotely controlled through one control/command crate per pumping station, linked to the Slow Monitoring network of Virgo. The control can be operated from the main workstations in the control room, from a portable PC connected locally to the network or, exceptionally, in local manual mode, in case of network failure. Any action on pumps, valves and gauges is subject to hard-wired and software safety conditions, in order to make impossible wrong or dangerous operations.

The main vacuum requirements, described in more detail at the beginning of the chapter on vacuum, are 10^{-7} Pa (10^{-9} mbar), in the UHV volumes, and 10^{-4} Pa (10^{-6} mbar), in the HV volumes.

Since UHV regime is reached through 150 °C bake-out, all the connected valves, pumps and gauges have to be able to stand the same treatment and have been equipped with appropriate heaters.

4.7.2 Cleanliness

In addition to maximum pressure requirements, there is the cleanliness issue: hydrocarbon vapors below 10^{-11} Pa (10^{-13} mbar) and absence of dust. All lubricants are forbidden and great care is put in avoiding dust pollution. For this reason, most of the primary pumps are of the dry type ("scroll") and all the large turbomolecular pumps have magnetic not lubricated bearings. This solution is fundamental also to reduce vibrations, very dangerous for an apparatus to detect gravitational waves.

For sake of hydrocarbon and dust cleanliness, all electromechanical components to be installed in vacuum have been carefully selected and tested; appropriate solvents have been used and heat treatments under vacuum have been developed.

4.7.3 Tower pumping

As previously explained, in the high towers there is a bottom UHV compartment, where the suspended optical element is located, and a top HV compartment, where there is the antiseismic suspension. This device contains several electromechanical components, magnets, motors and hundreds of meters of cables, summing up to a surface of plastic material of about 100 m². Between the two compartments there is the Separating Roof, described in a previous section (4.2.4), confining an intermediate volume to be pumped independently, to limit the gas flow from the HV compartment to the UHV one.

The top and the bottom compartments are pumped by two similar groups, each one made of a 1600 l/s magnetic bearing hybrid turbomolecular pump and of a 25 m³/h scroll pump, serving both as roughing pump and backing pump. It has been calculated and experimentally verified that during rough pumping the

pressure difference across the Kapton windows of the Separating Roof is correctly limited and that the air flow is not strong enough to move accumulated dust particles.

HV regime is reached in two steps: "rough pumping", from atmosphere to 10 Pa with the scroll pumps, and "intermediate pumping", down to 10^{-4} Pa, with the turbomolecular pumps. To reach UHV in the bottom compartment a third step is necessary, continuing the turbomolecular pumping action, with the addition of bake-out. After cooling down, when the pressure is below 10^{-6} Pa, the "permanent pumping" is started to reach 10^{-7} Pa or less. This last step is performed opening the valves in front of the Ti evaporation pumps, each consisting of two 250 l tanks equipped with Ti evaporators. The effective pumping speed, about 3000 l/s, is determined by the conductance of the connection pipes; the saturation of a fresh Ti layer is reached after about one year of operation. One of the tanks gives access to a 200 l/s Ion pump, necessary to pump noble gases, not captured by titanium. The Ti evaporation pump is connected to the tower lower compartment through one of the link tubes.

During evacuation, the intermediate vacuum chamber is pumped by the upper and lower pumping groups, through the conductance pipes. When the bake-out is nearly finished, in order to allow reaching 10^{-7} Pa in the lower compartment, an Ion pump, connected to the intermediate chamber by a bellows, is put in operation, to achieve the wanted gas flow reduction between top and bottom compartments.

In standard operation conditions, the permanent pumping is constituted by the turbo/scroll group operating on the top compartment, the ion pump operating on the intermediate chamber, and the Ti evaporator/ion pump operating on the mirror compartment.

Thanks to the very low outgassing of the tower walls and of the SA, it has been demonstrated that the scroll pump backing the turbo can be operated only five minutes per week. This is very important, since it allows to eliminate a possible source of mechanical noise.

In a system where such huge volumes have to be evacuated, the duration of all these operations has to be carefully considered. The sizes of the pumps chosen to meet the pressure requirements give relatively convenient evacuation times.

For towers, high or small:
- o rough pumping: about 16 hours
- o intermediate pumping: a few hours to reach 10^{-3} Pa.

This means that a tower can be evacuated overnight.

The bake-out time, at the chosen temperature, is much larger: about one week, including cooling down. Due to this fact, Virgo is presently operating in pre-bake-out HV regime. This is necessary because, during commissioning, the towers have to be opened rather frequently and would require a bake-out after any evacuation, to reach UHV regime. This is not a problem, since the intermediate pumping system already allows reaching a pressure close to 10^{-5} Pa, in the mirror compartments. This pressure value is absolutely acceptable from the point of view of noise induced by vacuum fluctuation; a lower value would be required if all other noises could be pushed well below the present design sensitivity. A few bake-out runs have been performed for test purposes.

Tower venting time has been set at about 14 hours (one night). This is due to the need to avoid moving dust particles and to limit to a few hundred Pa the maximum pressure difference across the Kapton windows of the Separating Roof. The impedance created by dust filters and air dryer on the inlet line helps to this aim. Given the large volume, venting air comes from atmosphere; hence it has to be dried to avoid potentially dangerous water condensation.

All what has been said for the high towers holds also for the small ones, limited to the HV regime; since small towers have one single compartment, no bake-out is performed and there are no Ti evaporation pumps.

The Mode Cleaner tube, 142 m long, is cut by a gate valve close to the IB tower. Hence the MC tube is evacuated together with the MC tower.

Also the Signal Recycling tower has one single compartment, but being part of the UHV volume, it is equipped with a Ti pump.

4.7.4 Tube pumping

Each 3 km arm tube is equipped with six pumping stations, at 600 m distance, very similar to the tower lower compartment pumping stations, including a 1600 l/s magnetic bearing hybrid turbomolecular pump backed by a 25 m^3/h scroll pump. There is also a single volume Ti evaporator with a 200 l/s ion pump. The turbo/scroll group is used as intermediate pumping and during bake-out, the Ti/ion group is used as totally vibration free permanent pumping, in the regime 10^{-6} Pa to 10^{-8} Pa.

Due to the huge volume, the tubes cannot be rough pumped by the scroll pumps, in fact it is necessary to employ a group able to pump against atmospheric pressure for more than one day. This heavy duty is performed, on one tube at a time, by a large group made of a 1000 m^3/h Roots pump, backed by a 250 m^3/h oil free pump. The roughing group ultimate pressure is 10^{-1} Pa, but intermediate pumping is started at 10 Pa, in order to avoid any backstreaming.

Tube pumping times are much longer than the tower ones:
- rough pumping: about four days
- intermediate pumping   about one day.

The chosen bake-out time is two weeks, to compensate for possible temperature disuniformities in such a long system.

Such long times have no drawback, since the large valves allow to maintain the tubes in vacuum, when opening the towers. On the other hand, since the tubes do not contain any equipment, there is no need to vent them. In fact the arm tubes have been evacuated only once, in 2003, and they have never been vented, since then.

Tube venting time is of the order of a few days; venting will be performed, when needed, using filtered atmospheric air.

As for the towers, also the tubes will be definitively baked-out only at the end of the commissioning phase, when venting a tower will happen very seldom.

4.7.5 Control instruments

Most control instruments and vacuum gauges are installed on dedicated ports ("Instrumentation Bottles"), connected through valves to the vacuum system. In this way, in case of failure or maintenance, they can be accessed without venting the large volumes. In general there is one instrumentation bottle per pumping group.

Different type of pressure gauges have been chosen, according to the required performances and to the pressure range: Pirani, Capacitance, Inverse Magnetron, Bayard-Alpert. On almost any instrumentation bottle there is also a RGA. This instrument proved to be very useful to monitor the vacuum quality, to monitor hydrocarbon contamination and to detect leaks.

High sensitivity differential gauges have been installed across the Large Valves, to prevent operations with pressure differences higher than 2000 Pa.

All the instruments are read and controlled remotely, as described in detail in the following sections.

4.8 Vacuum Control System

The vacuum control system [20] has been designed in such a way that the main vacuum elements of the Tubes (Tu), Towers (To), Link Valves (LV) and Large Gate Valves (LGV) stations can be controlled and monitored remotely. That includes all basic actions needed to reach the vacuum level required in the different parts of the vacuum chamber and the continuous acquisition of all slow control channels giving information about the state of the vacuum itself (pressure values, pumps activity, valves status) as well as the vacuum control elements.

Moreover, the vacuum control system includes safety protections for all actions considered hazardous for the personnel or dangerous for the equipments. The philosophy of the safety protection architecture is to introduce redundancy for all protections against hazardous commands: at least two completely independent safety conditions are required, one of them being hardwired. The hardware safeties are implemented in every bench (Tu, To and Valves), and the software safeties are implemented in a local

server for Tu and To, and in the top Supervisor (VTTVSU) for the valves. The software safeties allow combining information of the different parts of the vacuum chamber. For instance the large valves cannot be opened if the two capacitance gauges installed on each side of them read a pressure difference greater than 500 Pa (5 mbar). The safety protection can be conditional or active: a conditional safety forbids for instance to act on a pump if a condition is not fulfilled. An active safety monitors permanently the activity of a pump and executes a specified action when a given condition is detected [21].

4.8.1 Vacuum Control Hardware

There are 6 pumping benches for each tube and 10 pumping benches for the towers, among them are 7 benches for UHV (high) towers and 3 for HV (small) towers as shown in figure 27.
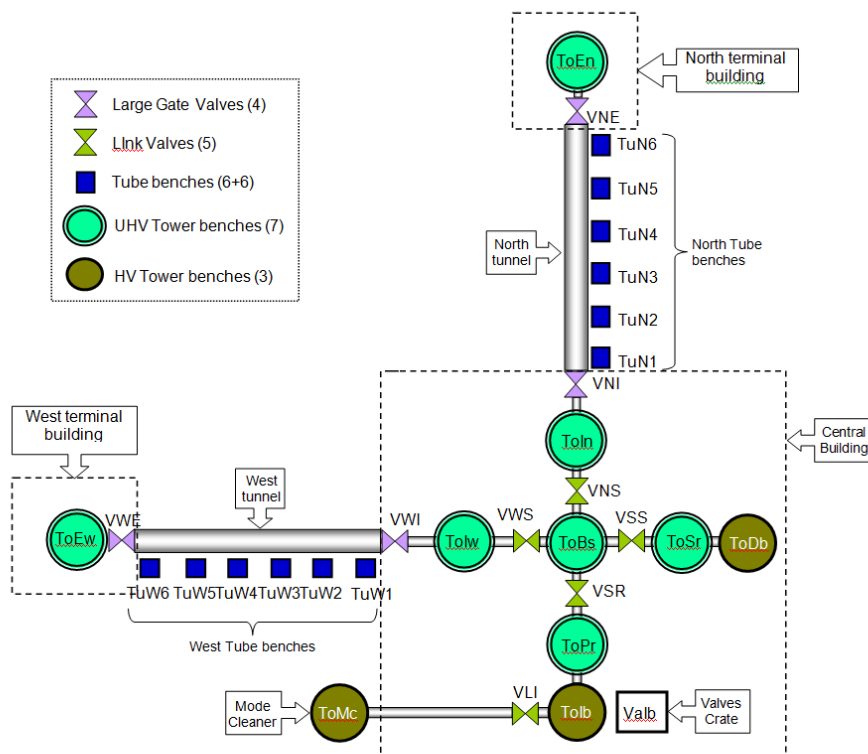
Figure 27. Schematics of the vacuum control system.

A pumping bench is typically in charge of controlling the pumps, the valves and reading gauge pressures. The power to the benches is delivered by dedicated UPS lines. Each bench is composed of an electrical part (power breakers, relays, power supplies, …) and an electronic crate managed by a CPU board (Motorola 68040 processor) on which runs the OS9 Operating System. The tube and tower pumping benches are based on the same electronic architecture, while the electrical part is very specific as a tower vacuum bench is much more complex. In addition to this, the racks contain specific controller boards associated to the pumps, valves and gauges. At the startup of the electronic crate, as a first step, a boot program is uploaded from a dedicated server (*os9boot*) located in the Data Acquisition (DAQ) room (Central Building) which in a second step loads in the CPU memory the specific server program associated with Tube or Tower functionalities, then running permanently.

58

The valves are of two kinds: there are 5 link valves (LV) located between the towers and 4 large gate valves (LGV) to isolate the tubes from the rest of the vacuum chamber. These 9 valves are controlled only by one crate, hosted in the Injection Bench tower pumping rack, linked through a local network FIP to seven control boxes (one for each valve except for the 2 large gate valves located in the central building which share a control box with a link valve). The valve crate implements the same CPU as tower and tube crates.

4.8.2 Vacuum Control Software

The vacuum control software is based on a client-server architecture. The servers running on OS9 CPU are unique: there are 12 tube servers, 10 tower servers and 1 server for all the valves. The vacuum control software has been developed in the framework of the Supervisor (see the section on Interferometer Control). It hence benefits from this architecture. For instance, it makes use of the mastership communication protocol implemented in the Supervisor in order to arbitrate which software element is allowed to take the mastership on the control of a pumping bench at a given moment: only one client (a graphical user interface) can send orders to a server to perform a specified action, such as opening a valve or turn off a pump. Until the mastership has not been released, no other client can obtain it.

The architecture of the vacuum supervisor is hierarchical as shown in figure 28: the tube servers are controlled by two instances of a supervisor (TuVSU) controlling the 6 tube servers of each arm.
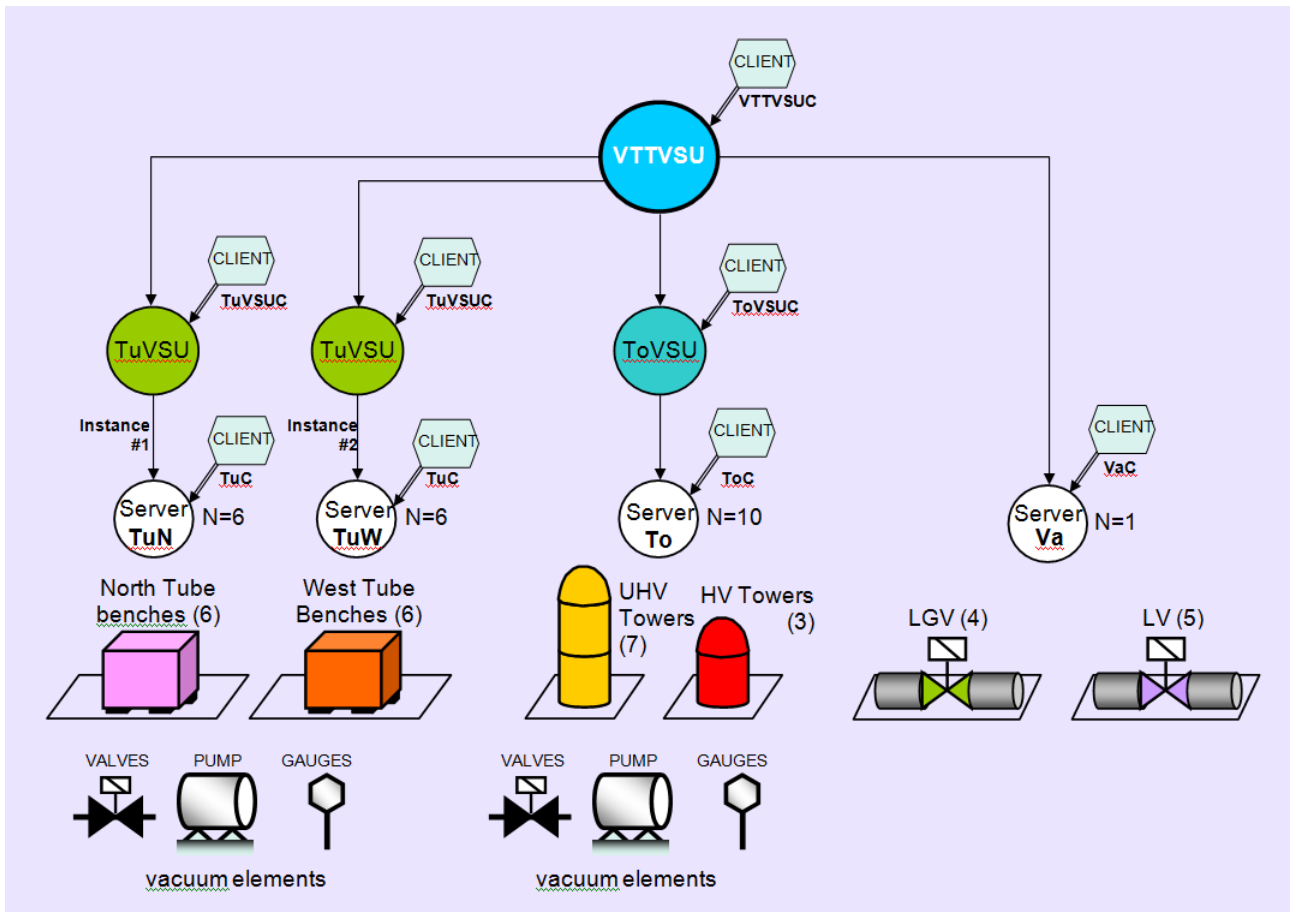
Figure 28. Schematics of the vacuum control software.

The choice has been driven for being able to operate each arm independently from the other. The 10 towers are controlled by another supervisor (ToVSU). These 3 supervisor servers are then run through a top supervisor VTTVSU (VTT for Valve Tube Tower) which controls directly the valves' server. The different VSU (ToVSU, TuVSU and VTTVSU) have specific user interface clients displaying some information about the status of the different vacuum control elements (pressure, gauge status, valves status, server status, …)

which are refreshed typically each second. Alarms are also gathered and displayed in real time on the user interface. The vacuum VSU are also in charge of forwarding the alarms sent by the servers to the ErrorLogger daemon which collects error messages coming from all servers running in Virgo.

The software safety protections for the towers and tubes actions have been implemented in each tube and tower server while they have been implemented in the VTT server itself for the valves because it requires the knowledge of some information (mainly pressure) provided by the tower servers.

Finally, the OS9 servers send slow monitoring information to the DAQ system (slow frame builders Fbs) every 10 seconds in order to acquire vacuum data which could be important to understand the apparatus at a given time.

4.9 Vacuum System performances

As explained, at present, in the commissioning phase, the vacuum system is kept in pre-bake-out HV regime.

Most towers have been evacuated and vented several times. Each high or small tower is pumped by one scroll-turbo group and the backing scroll pump is put in operation only 5 minutes per week, when a consistent quantity of gas (up to a pressure of 500 Pa) has been accumulated by the turbo. A typical residual gas spectrum for the upper compartment of a long tower is shown in figure 29. Short towers behave as the upper compartments of long towers.
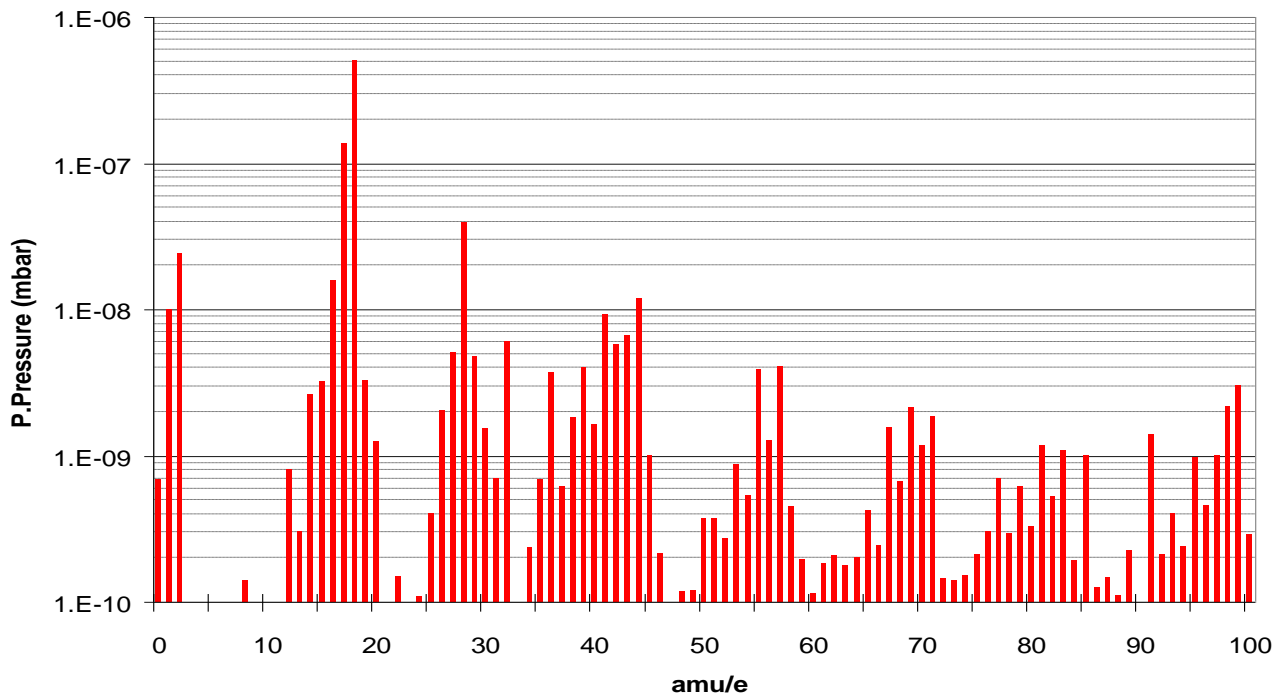
Figure 29. Residual gas spectrum for the upper part of a long tower.

Bake-out of a tower lower compartment has been performed only for test purposes, so far, on towers fully equipped with SA. The residual gas spectra of a lower tower compartment, before and after bake-out are shown in figure 30.
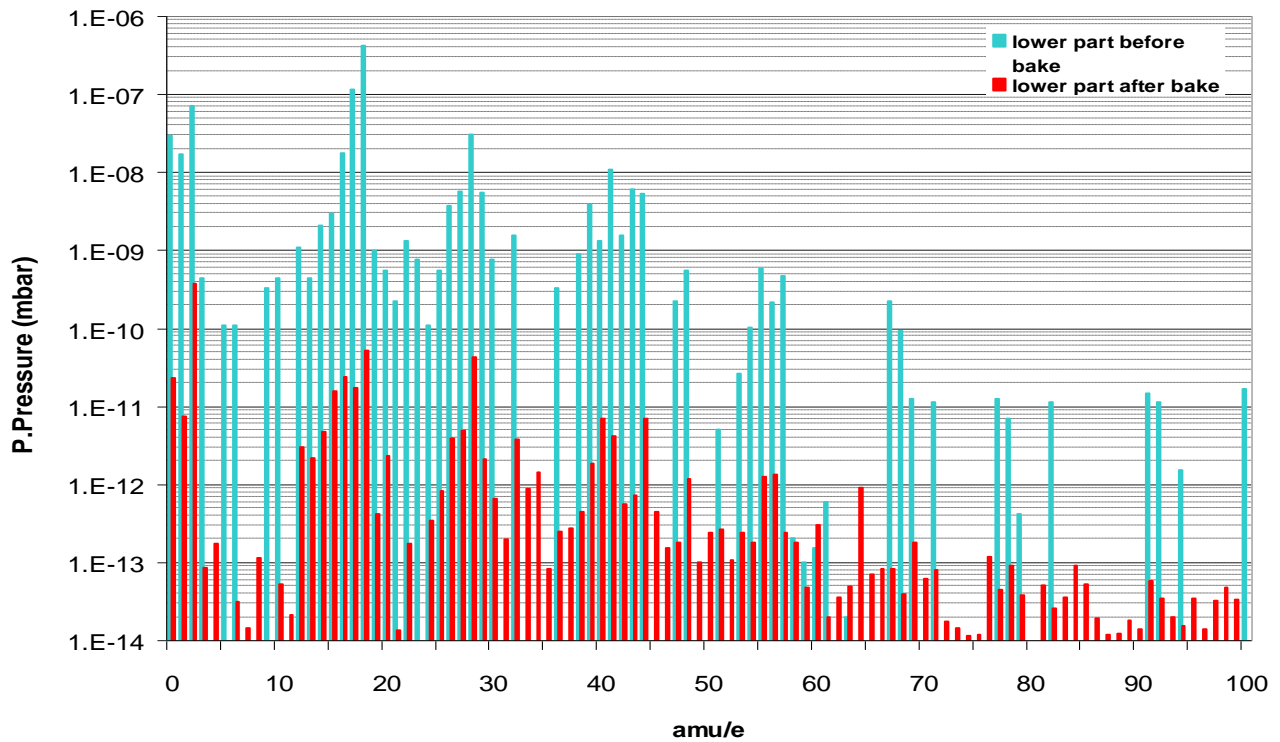
Figure 30. Residual gas spectrum for the lower compartment of a long tower, before and after bake-out.

The 3 km arm tubes have been evacuated only once, in 2003, and never vented any more. As for the towers, the final bake-out has not yet been performed. At present they can be kept well below 10^{-4} Pa, pumping with only one scroll-turbo group per tube, thanks to the excellent outgassing and cleaning procedures, adopted during fabrication and installation. In these conditions, the pressure profile along a tube varies between 0.4×10^{-4} Pa and 0.8×10^{-4} Pa.

One full tube has been baked-out for test purposes, achieving an average end pressure of 0.5×10^{-7} Pa. The residual gas spectra of a tube before and after bake-out are shown in figure 31.
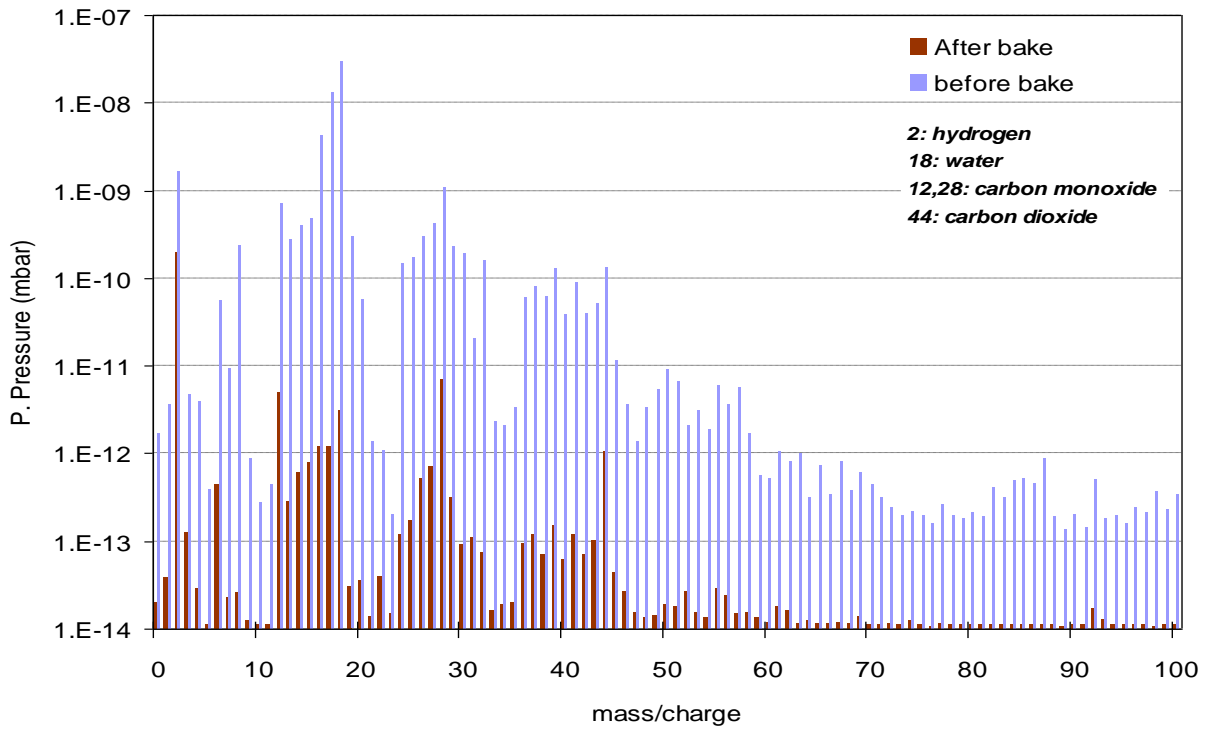
Figure 31. Residual gas spectrum for a 3 km arm tube, before and after bake-out.

5. Scattered light noise

5.1 Introduction

The sensitivity of the interferometer can be limited by the noise due to scattered light propagation and recombination in the interferometer beams.

The total light scattered by the mirrors is of the order of 100 ppm, mainly due to mirror "flatness" (i.e. large scale polishing defects), resulting in diffraction at low angles (or in low order modes), so in a loss of power and contrast. Mirror roughness (small scale defects) results in light scattered at "large" angles ($> 10^{-4}$ rad) at the level of some ppm, responsible of the "scattered light" noise considered here.

This scattered light propagates in the vacuum chamber, and after reflections and diffusion from the walls, may recombine with the main beam, with a different phase due to the different optical path. The vibrations of the chamber make the phase shift time dependent, resulting in noise in the phase of the interference signal.

5.2 Noise evaluation

A careful noise evaluation of possible ``killing'' baffle systems was performed. The initial ideas of this evaluation have been formulated by K.Thorne [22].

We have developed a statistical approach of the scattered light propagation [23].

The information on trajectories obtained from a particle analysis is supplemented by additional information regarding phase modulation coming from the wave picture. Scattered light was represented by optical rays, extracting information on the noise from the statistics of photons received by the mirrors. Then the options for a baffle system have been evaluated by a Monte Carlo simulation. Coherent effects, such as diffraction or back reflection by the baffle edges, were computed analytically [24].

As a first result, the noise in a plain tube has been evaluated to be $h(f) \sim 10^{-23}/\sqrt{Hz}$ at 10 Hz. Being of the same order as the foreseen sensitivity, it is obvious that a system of baffles had to be designed and implemented in the arm tubes. The simulation has been confirmed by analytical calculations

5.3 Baffles in the arm tubes

It was decided to allow the possibility of having three interferometers side by side inside the vacuum tank. For this a free aperture of 1 m is necessary, which leaves a space in the tube cylinder between ϕ 1000 mm and ϕ 1200 mm available for baffles.

The best performing material was absorbing black glass for welding protection with an anti-reflective coating (Schott-Desag Athermal 11, thickness 3.2 mm, transmission $\sim 10^{-7}$, reflection between 3.10^{-3} and 10^{-2} depending on incidence angle, negligible diffusion, at $\lambda = 1064$ nm). A satisfactory glass prototype was realized, with the shape of a quasi perfect light trap, but finally these baffles were found too fragile for installing in the 3 km tubes. The black glass was used only in the central area and in the links between valves and towers. The baffles in the 3 km arm tubes have been built in stainless steel.

5.3.1 Steel baffles

Stainless steel baffles with a conic shape are more efficient than simple rings normal to the tube axis. Stainless steel has a small reflection coefficient, but there is a large reflectance distribution function (BRDF), and the absorption is close to 50%. The BRDF has been measured for the sandblasted stainless steel used for the baffles, and was introduced in the Monte Carlo computation.

Finally, steel baffles have the shape of a truncated cone with an external diameter of 1184 mm, internal diameter of 990 mm and an angle of 55° with respect to the cone axis. The steel thickness is 1.5 mm. The internal edge is serrated in order to suppress diffraction (Figure 32).
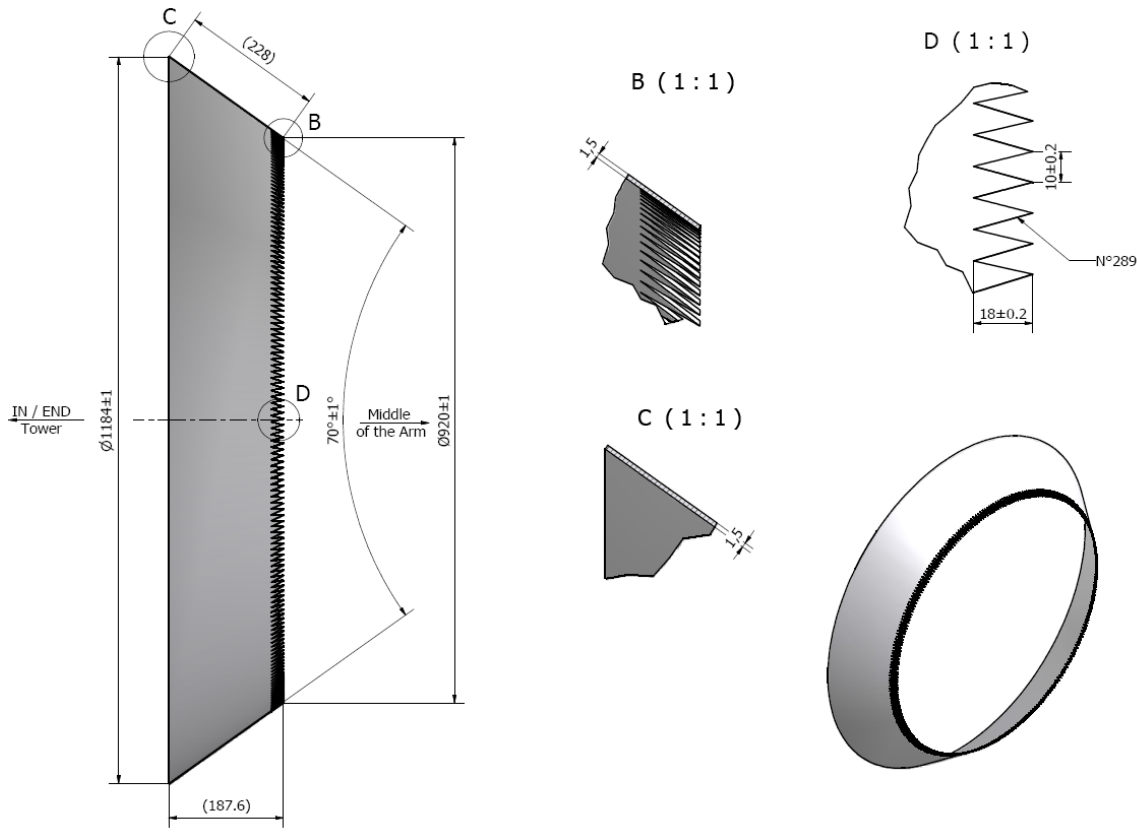
Figure 32. Shape of a conic metal baffle with serrations at the inner edge.

The conceptual requirement was to cover completely the solid angle as seen by the beam spot at each Fabry-Perot mirror. A simple calculation gives the distance Zn of the nth baffle to the mirror through the law:

$$Zn = Z1 \left(\alpha \, \frac{r}{r-h} \right)^{n-1}$$

where r is the tube radius, h is the baffle height, and α is a coefficient for getting some coverage between the shadows of each baffle. The total number of steel baffles is 160 per arm. They have been realized by several firms near Paris and soldered inside the modules at CNIM before the washing, by mean of 4 small lugs on their external part. They have been installed only in the tube part in between the two large valves, which is supposed to remain untouched hopefully for the Virgo lifetime.

5.3.2 Glass baffles

In the links joining the large valves and the towers, large glass baffles have been installed for covering all discontinuities like valve or tower flanges, bellows etc... In this area glass baffles are allowed, since they can be relatively easily replaced, in case of breaking. All these link baffles are 1160 mm diameter disks made out of black glass, with a large central hole. Inside each link, there are 4 rings, one in front of each flange (tower and valve), and one on each side of the bellows. The inner hole diameter ranges from 600 mm to 850 mm according to the baffle location and the laser beam size. Their sizes and positions are displayed in figure 33.
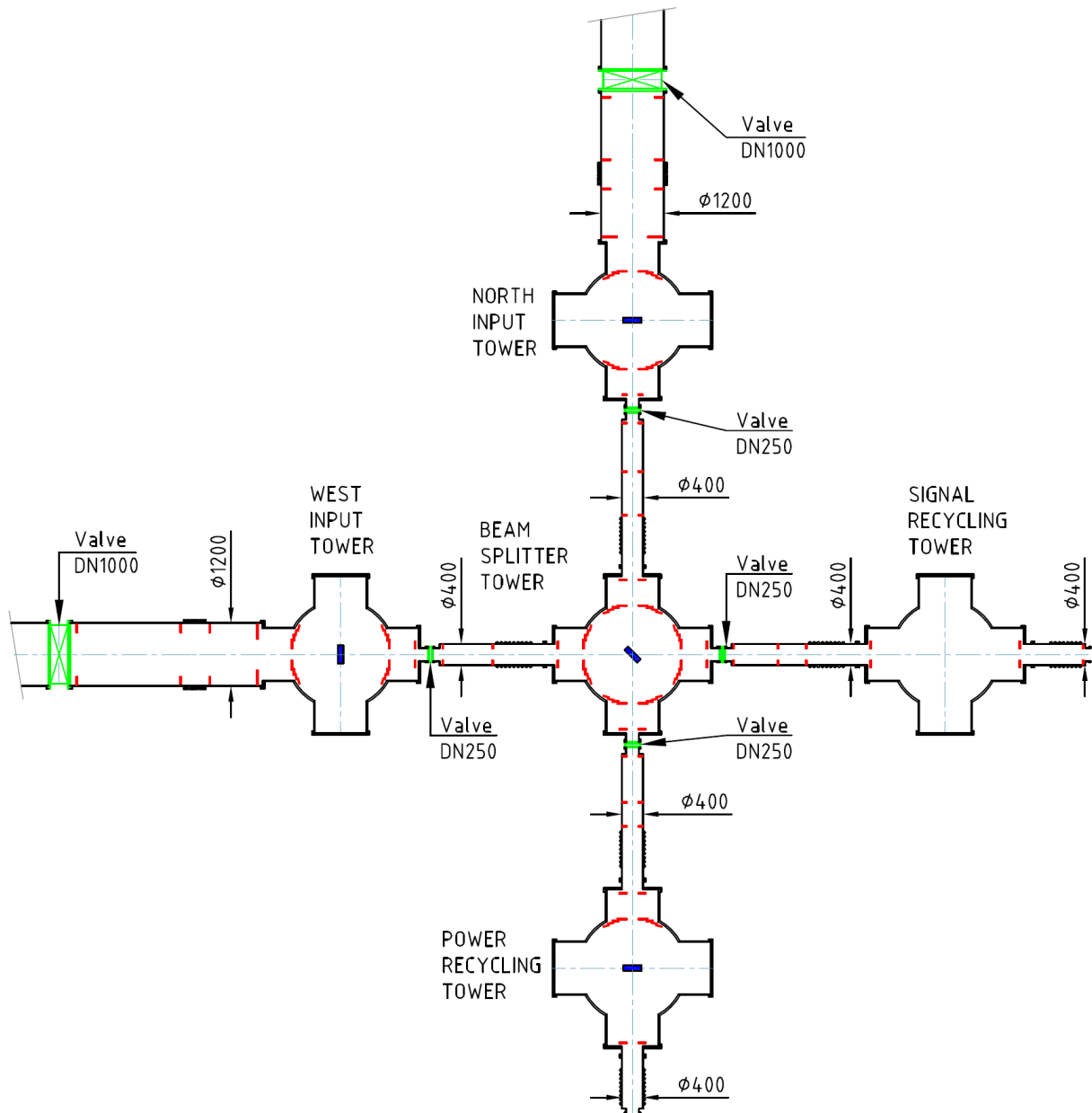
Figure 33. Scheme of the central area and location of glass baffles, represented in red.

With these stainless steel and glass baffles, the evaluated noise in the arm tubes is $h = 6.5 \times 10^{-25}/\sqrt{\text{Hz}}$ at 10 Hz.

5.4 Baffles in the Central Area

The central area is constituted by 5 towers, their mirrors (Figure 34) and the 4 junction links (small links). To evaluate the noise with a Monte Carlo simulation, all possible processes for re-scattering of photons off all elements have been listed. The geometry of the tanks, links and mirrors, and the optical properties of all surfaces, have been taken into account [25]. Photons coming from the main beam have been generated and their scattering off each element has been followed in all their possible paths until a possible recombination. The total noise is the incoherent sum of the contributions of all scattered light generation processes through all recombination processes.
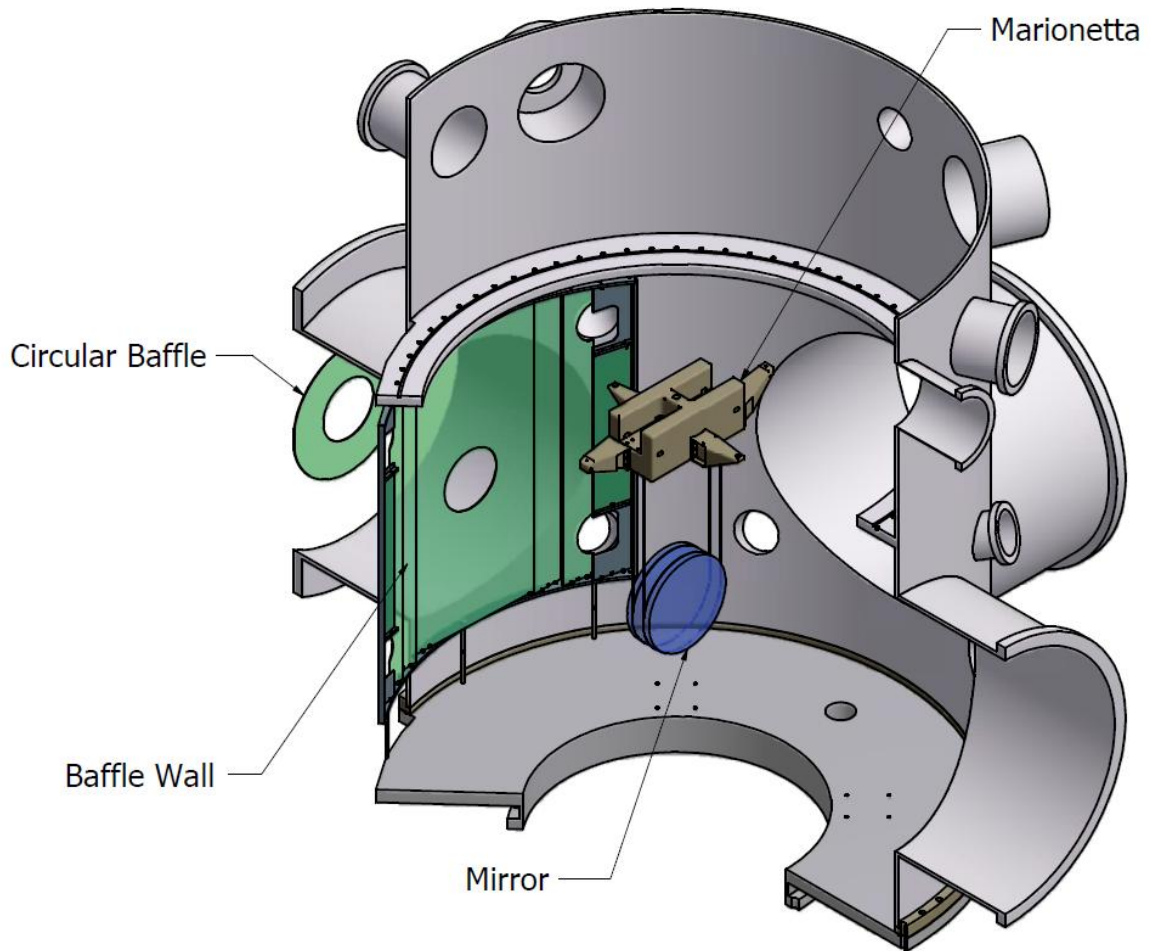
Figure 34. Glass baffles covering the tower inner wall around the laser beam path.

The resulting actions for reducing the noise are given below together with the final result.

For the small links, the steel tube diameter must not be less than 400 mm, to avoid the effects of grazing diffusion on its walls. Black glass disks with external diameter 380 mm, and a central hole of diameter 230 mm, corresponding to ± 5 beam waists, have been inserted inside the links. Their position was chosen for hiding the 250 mm diameter valves and the bellows waves (Figure 33). With these baffles (14 altogether) the noise coming from the small links is negligible.

Among the towers the most delicate situations can be found around the two input mirrors and the beam splitter, due to the complex geometry and the high light intensity. In fact all possible diffusion or reflection areas in the tanks have to be covered with black glass, with ± 5 waist holes for beam passage. In order to be as close as possible to the tower cylinder, the baffles inside the towers at the junction of

the big links have the shape shown in green figure 34: in the centre a big plate 1150×600 mm^2 with a hole having a radius equal to 5 times the beam waist, and on each side three 1150×120 mm^2 plates installed as shown in the side view in figure 34. The beam splitter tower has 4 such devices, covering most of the cylinder (Figures 33 and 35), the input towers have 2, the end towers have one and the recycling tower has one also.
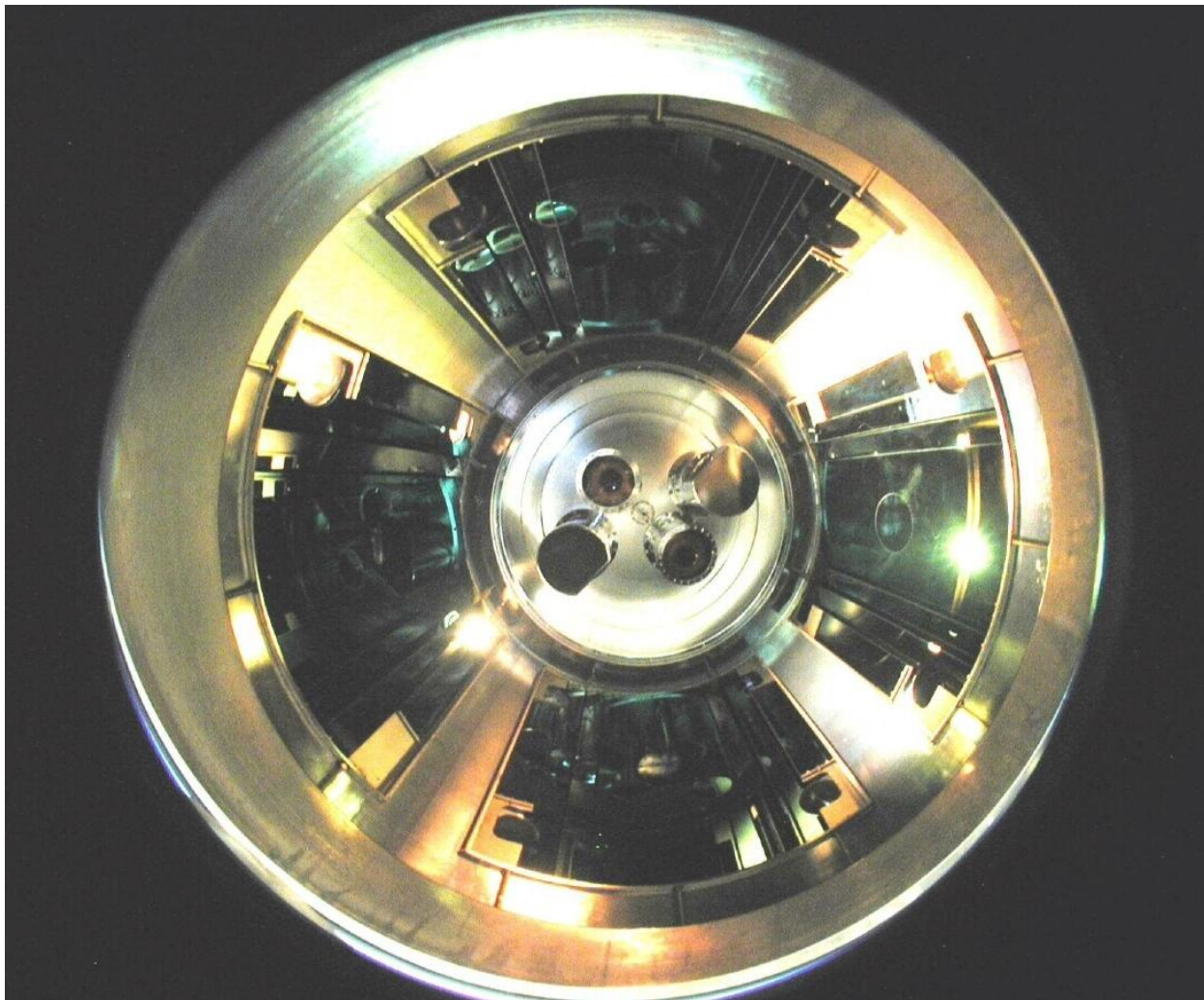
Figure 35. Picture of the 4 glass baffle sets inside the beam splitter tower, taken from below with a fish-eye lens before mirror installation.

The resulting noise from the central area is reduced to ~ some $10^{-25}/\sqrt{Hz}$.

6. Mirror suspension

6.1 Seismic isolation

Seismic motion, always present on ground, even in absence of earthquakes, is a very powerful noise source for gravitational wave detectors. The typical linear spectral density of seismic displacement in all three space coordinates can be approximated, in the frequency range of Virgo, by:

$$\tilde{x} \cong \frac{\alpha}{f^2}$$

measured in m $Hz^{-1/2}$, as a function of the frequency f and of the parameter α, which ranges typically between 10^{-6} and 10^{-9} m $Hz^{3/2}$, depending on the geographical location.

From the previous equation, it turns out that the seismic motion reaching the test masses (the mirrors) has to be reduced by at least a factor 10^{12}, in order to have an acceptable sensitivity in the 10 Hz region.

Very performing devices have been developed in order to suspend the Virgo mirrors, strongly reducing the seism induced motion; those devices have been called: "Superattenuators".

6.2 Superattenuator working principle

The SA design is based on a simple idea. If the suspension point of a simple pendulum moves in the horizontal plane at a frequency f higher than the pendulum normal mode (f_0), the oscillation is transmitted to the suspended mass with attenuation proportional to $(f_0/f)^2$. The wire length l connecting the suspension point to the mass sets the pendulum normal mode frequency according to the equation:

$$f_0 = \frac{1}{2\pi}\sqrt{\frac{g}{l}} \; .$$

Therefore a device suspending a mirror based on the working principle of a simple pendulum, represents a good isolation system against horizontal seismic noise at frequency $f \gg f_0$.

A better attenuation performance is obtainable by a pendulum chain where each pendulum is attached to the mass of the upper one forming an n-stage pendulum (Figure 36).

Ø2000

Inverted Pendulum

Pendulum Wire

Inner Structure

Pendulum Chain

10560

Separating Roof

Mirror
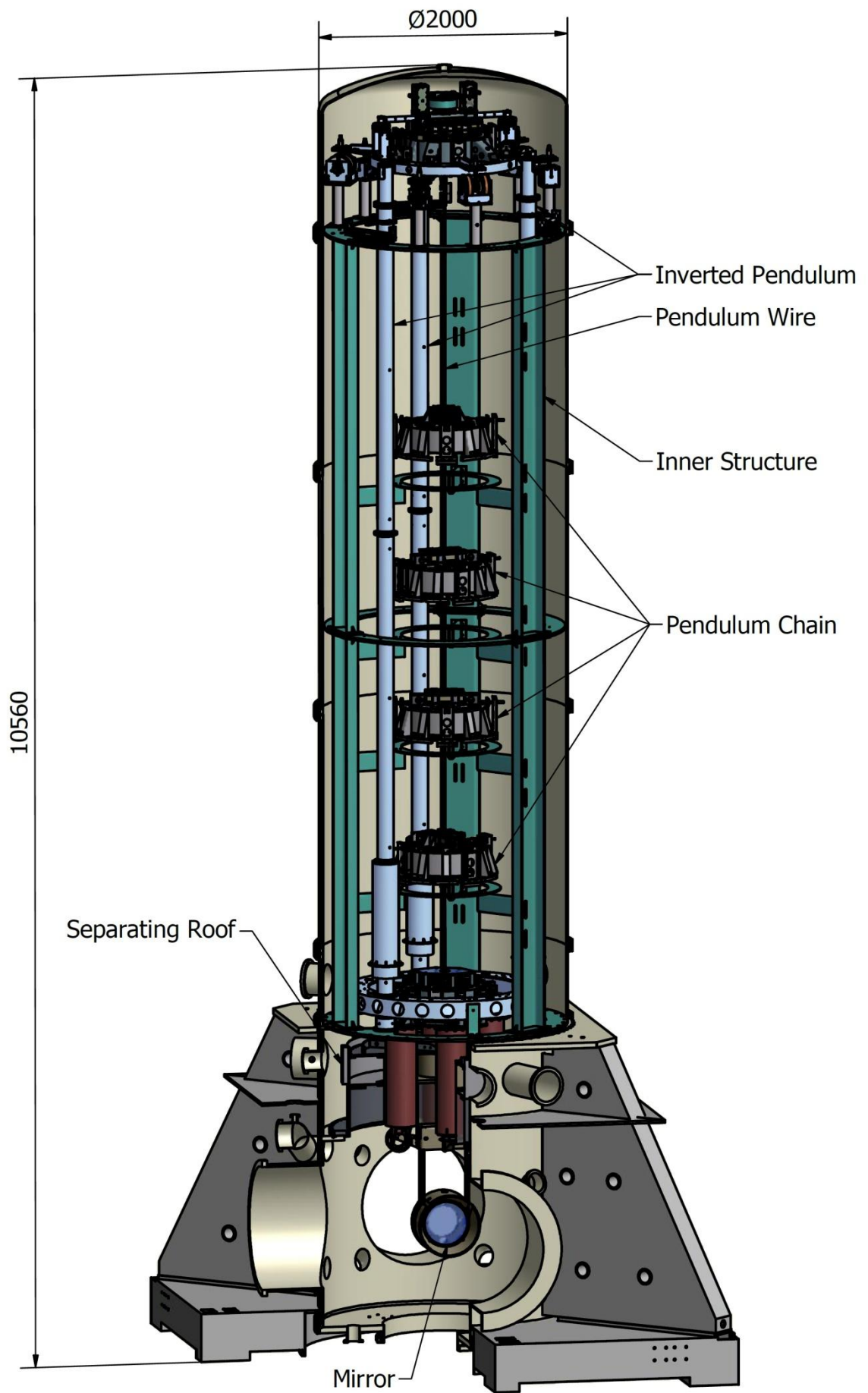
Figure 36. The VIRGO Superattenuator. The three legs metallic structure of the Inverted Pendulum, the six seismic filters and the payload of a long suspension chain are shown inside their long tower.

With this system an oscillation at a frequency f higher than the frequencies of the chain normal modes ($f > f_n > ... > f_1$), is transmitted to the suspended mass with attenuation proportional to f^{2n}. In particular, the ratio between the linear spectral density of the last mass displacement (the optical component) and the linear spectral density of the suspension point displacement (where the excitation is applied), decreases as A/f^{2n} where $A = f_1^2 \cdot f_2^2 \cdot ... f_n^2$ and n is the number of stages. In this way a very large attenuation of seismic noise horizontal component can be obtained in the frequency region above the highest pendulum resonance frequency simply increasing the number of stages.

Unfortunately the pendulum wires supporting the end mirrors, 3 km away in the arms of Virgo, are misaligned with respect to one another by about $3*10^{-4}$ rad because of the different directions of the plumb line on the curved Earth surface. This means that they are not perfectly perpendicular to the laser beam, hence vertical seismic motion introduces significant changes in the distance between the mirrors. In addition any vertical vibration will be partially transmitted to the interferometer horizontal axis (laser beam direction) because of unavoidable mechanical couplings among different degrees of freedom. Thus vertical ground motion will cause a change of the laser beam optical path.

Following all these considerations it is clear that a vertical attenuation of seismic noise comparable with the horizontal one is fundamental.

With a multistage pendulum this goal can be achieved by replacing each suspension wire with a spring to form a cascade of vertical oscillators. The spring should support a heavy load and, at the same time, it should be soft enough to exhibit a low resonant frequency. In this way it is possible to confine the vertical resonances of the chain in a low-frequency region obtaining a strong attenuation, starting from a few Hz, as it happens for the horizontal pendulum resonances. Helicoidally shaped springs may have internal low frequency resonances that would spoil the SA isolation performance. This problem has been overcome by using normal metallic suspension wires, attached to triangular cantilever springs clamped below each pendulum mass (Figure 37).
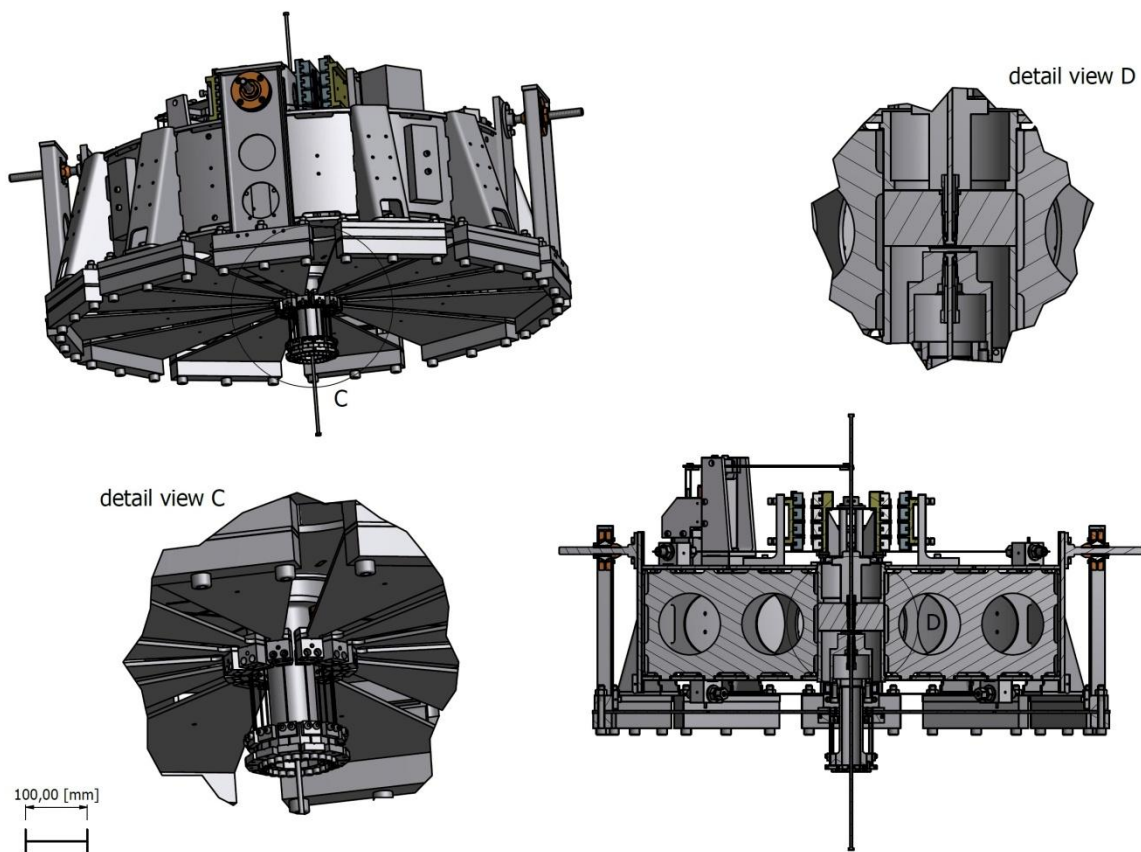
Figure 37. Technical drawing of a mechanical seismic filter.

With this technical solution the masses of the SA act as "mechanical filters" in the vertical direction.

Also the unavoidable mechanical couplings between rotation of the pendulum masses and horizontal mirror displacements can cause optical path changes. To confine these rotational mode frequencies below the detection band, each pendulum mass has been designed to have high momentum of inertia. In addition, the diameter of the suspension wire, connecting two consecutive stages, has to be small enough to reduce its restoring torque, determining the rotational frequencies. Furthermore upper and lower wires have to be attached as close as possible to the center of mass of the filters, assuring low frequency rotational modes and negligible coupling effects on horizontal displacements of the test mass.

A drawback of such a complex system is that seismic motion is amplified in correspondence of its resonance modes. This is cured by active damping, as described in the section on SA control.

6.3 The Superattenuator design

The Virgo SA, which represents one of the peculiarities of the apparatus, has been designed taking advantage of the working principle of a multistage pendulum [26]. In addition to the pendulum chain, each SA includes a "top stage" and a "payload". The top stage consists of a three leg inverted pendulum with a top platform. The payload consists of an upper mass, called "marionette", supporting an optical component. The optical component may be either a mirror (a test mass) or an optical bench with several optical and electronic elements. In the mirror case the marionette supports also a so called "reference mass", suspended behind the mirror and acting as reaction mass for the actuators controlling the mirror position.

71

Two different size SA's have been designed to fulfil the different needs in isolating mirrors and optical benches. Each mirror, indeed, is suspended to a long SA chain with 6 filters (Figure 36), while a bench is suspended to a short chain with two filters only (Figure 38.).

Figure 38. One short Superattenuator. This figure is relative to the Injection Suspension where a marionette with the shape of a disk is shown as well as the optical bench under which the reference cavity for the laser beam is attached.

Long and short SA's are accommodated inside towers 11 m and 7 m high, respectively.
Here below we describe a long SA while additional information on each single chain element can be found in reference [27].

6.3.1 The Inverted Pendulum top stage

The top stage of the SA is designed to fulfil three main functions:
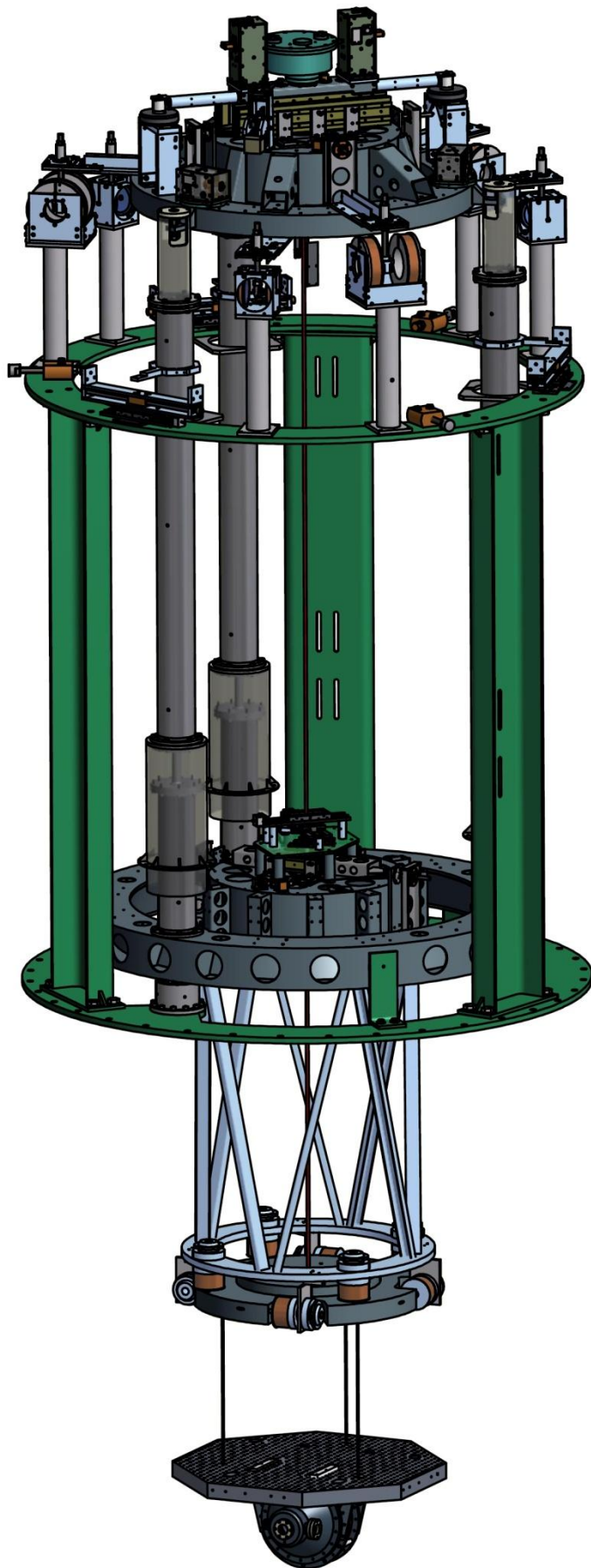- to introduce an additional very low frequency (~30 mHz) horizontal filtering stage;
- to provide the SA with a suspension point positioning system: the tidal strain over 3 km, of the order of one hundred microns over a period of 6 hour, is far beyond the dynamic range of the actuators exerting the steering forces upon the mirror. Therefore tidal drifts are compensated by moving softly the SA suspension point, upstream the seismic attenuation chain.
- to provide a soft suspension stage on the top of the chain allowing active mode damping and seismic noise reduction by means of inertial sensors, position sensors and electromagnetic actuators. In addition, any noise introduced by acting on the top stage is filtered out by the SA chain.

To fulfil all the above requirements in the horizontal plane a device based on the principle of the inverted pendulum (IP) has been realized. An IP is a suitable device for several reasons:
- an ideal inverted pendulum can be conceived as a mass-less vertical bar of length l connected to ground by means of an elastic joint with stiffness k and supporting a mass M on its top. In such a pendulum the gravity acts as an anti-spring and the resonant frequency, given by

$$f_{IP} = \frac{1}{2\pi} \sqrt{\left(\frac{k}{M} - \frac{g}{l} \right)}$$

can be tuned to be very low (about 30 mHz in Virgo);
- the force required to displace the chain suspended from an IP resonating at 30 mHz is very low: the force required to move the 1 ton SA chain by 1 cm is less than 1 N. Therefore soft electromagnetic actuators can be used to control the mirror position. For this reason the IP is a good platform to act upon for the active damping of the SA normal modes.

The Virgo IP (Figure 36) consists of three metallic legs clamped through flexible joints to a bottom ring resting inside the base of its vacuum tower. A steel ring is suspended to the top ends of the three legs, by three thin wires (31 mm long). This ring surrounds the first filter of the chain (hereafter called Filter Zero) to which it is rigidly connected. The Filter Zero together with the top ring form a platform to which the whole pendulum chain is suspended. The bottom ring is not bolted to the tower but it rests on three hollow steel feet to be used for the installation of piezoelectric actuators under it, in order to correct for seismic ground tilts.
Each leg is a 26 kg aluminium pipe with an inner diameter of 125 mm and a 2.5 mm thickness. The total length of the leg, from the bottom of the flexible joint to the suspension point of the SA is about 6.2 m. The leg is composed by three sections flanged together and reinforced with titanium inserts.
Due to the non zero mass of the leg, an extension below the flex joint is necessary to tune the percussion point [28], to preserve the isolation performance. A proper counterweight is attached to a bell-shaped 0.9 m long skirt bolted to the bottom of the leg. The flex joint is therefore mounted on top of a 0.8 m high rigid support.

The IP structure is surrounded by a rigid metallic structure (called inner structure in figure 36), holding the parts of sensors and actuators that need to stay "on ground". It is equipped with [28, 29]:

- 3 motorized sleds on the external structure in front of the leg tops. Each sled is connected to the corresponding leg top through a soft spring tangent to the top ring. The motors are used to set the IP roughly in its working point;
- 3 horizontal LVDT (Linear Variable Differential Transformer) position sensors set in pin wheel configuration. The secondary windings stay on the inner structure, while the primary ones are rigidly connected to the top stage;
- 3 horizontal coil-magnet actuators, set in pin wheel configuration. The coils, arranged as Maxwell pairs, stay on the inner structure, while the magnets are rigidly connected to the top stage.

6.3.2 The seismic Filters

As mentioned above, in the SA each pendulum mass is a vertical mechanical filter. A sequence of six filters is able to isolate the optical components from the vertical seismic noise with a working principle similar to that of a multistage pendulum. A detailed description of the design and performance of a single filter can be found in reference [30].

A seismic filter is a rigid stainless steel cylinder (70 cm diameter, 18.5 cm high for a total weight of about 100 kg) suspended as close as possible to its centre of mass (Figure 37). On the outer circumference of its bottom part, a set of triangular cantilever spring blades is clamped. Each blade (3.5 mm thick and 385.5 mm long) is bent at a constant curvature radius and with different base width according to the load to be supported. The different curved blades become flat and horizontal under loads ranging between 48 and 96 kg. Each blade tip is connected by a 1 mm diameter steel piano wire to a mobile central column, coaxial to the filter body. Any movement of the central column, apart from the vertical direction, is prevented by two sets of four centering wires stretched on the top and on the bottom of the filter body.

A crossbar, bolted on the upper part of the central column, is used as a mechanical support for the magnetic anti-spring system described in the next section. The central column and the crossbar represent the moving part of the mechanical filter from which the load of the lower stages is suspended by a steel suspension wire. By connecting each filter to the next one, a chain of mechanical oscillators in vertical direction is obtained.

The set of triangular steel blades mounted under each filter, sustains the weight of the lower part of the chain (Figure 37). The support capability of each spring set is tuned varying the number of blades from 12 to 4, the base width of each blade between 180 mm and 110 mm and the curvature radius without load.

Once properly loaded the main vertical resonance frequency of each filter is about 1.5 Hz. In order to reduce the peak amplitude of the blade first flexural mode (about 100 Hz), a rubber/metal damper is mounted in the middle of each blade. Another special damper, mounted on the crossbar, suppresses a mode at about 50 Hz, due to the suspension wire connecting the crossbar to the next filter and acting as a stiff spring [30].

"Maraging©" steel has been used in place of standard steel for blade construction minimizing micro-creep effects [31, 32] due to the high load applied. The same material has been used to machine the suspension wires with nail-heads at both ends [33]. Since the suspended load decreases going from the top to the bottom of the chain, the wire diameter changes along the chain in the range 4-1.85 mm. In this way it has been possible to confine the wire violin modes within the high frequency band and to reduce their angular stiffness, which determines the rotational frequencies around the vertical axis.

The two nail-heads of the wires connecting a filter to the upper and to the lower one are screwed in the central part of its body at a relative distance of 5 mm, very close to the filter center of mass. As mentioned above, this guarantees a small return torque to rotations of the filter around a horizontal axis and thus a low tilt frequency.

6.3.3 The magnetic anti-spring

The chosen suspension wire length of 1.15 m sets the pendulum resonant frequency of each stage at about 0.5 Hz. In the vertical direction the stiffness of the triangular blade springs fixes the natural resonant frequency at about 1.5 Hz.

In order to reduce the vertical stiffness of the blades, and then to confine the main vertical resonant frequency of each filter below the pendulum one, a system of "magnetic anti-springs" [30, 34] has been conceived. It consists of four sets of permanent magnets (two assembled on the crossbar and two on the filter body) facing each other with opposite horizontal magnetic moment (namely in a repulsive configuration). The two matrices screwed on the crossbar move in vertical direction only.

The working principle of this system is sketched in figure 39.
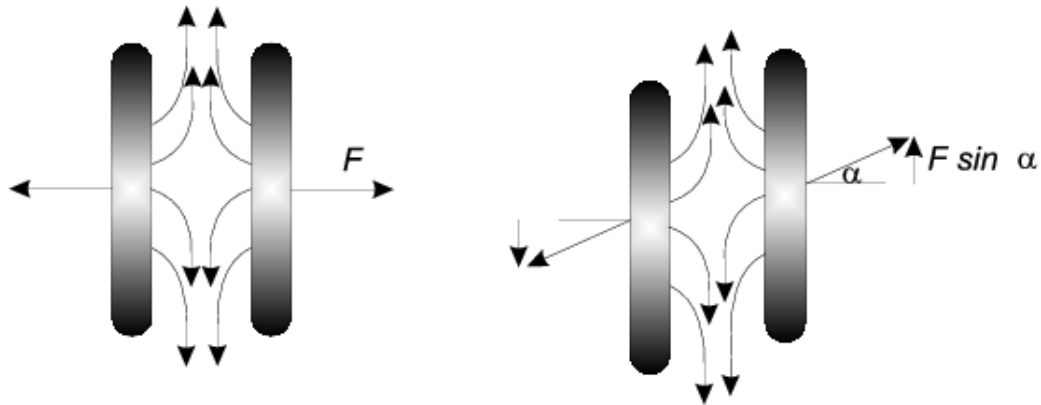
Figure 39. The working principle of the magnetic anti-spring system. When the magnets are displaced in the vertical direction (right side) a vertical component of the repulsive force appears.

When the magnets are perfectly faced, the repulsive force has a null vertical component, but as soon as the crossbar (and its magnets) moves in the vertical direction, a vertical component of the magnetic force appears. Considering a small relative displacement (Δy), the vertical component of the repulsive force (F_y) is proportional to Δy:

$$F_y \approx F_0 * (\Delta y / d)$$

where F_0 is the module of the repulsive force and d is the magnet separation (Figure 39). Such device is equivalent to a vertical spring with a negative elastic constant (anti-spring) whose module is F_0/d. Its rest position is thus the position for which the two couple of matrices are perfectly faced.

On a seismic filter the magnetic anti-springs act on the crossbar in parallel with the blade mechanical springs, so that the overall elastic constant is reduced and the vertical mode frequencies of the chain are confined below the highest frequency of the horizontal ones.

The device working principle requires that in the rest position all the magnetic anti-springs are perfectly aligned, in order to null the vertical component of the magnetic force. To this aim a small remotely adjustable cantilever blade (the so called "fishing rod") has been added on top of each filter, to bring the anti-springs to the correct working point.

6.3.4 The Filter 7

The last mechanical filter of the chain is the so called Filter 7 [35]. Since it has been designed to steer the payload, it has been equipped with four aluminum legs (about 900 mm long and 250 mm in diameter) bolted under the filter body bottom part. These legs are used as a mechanical support of the coils

mounted in front of the permanent magnets screwed on the marionette wings. The coil-magnet pairs are used to apply forces and torques to the marionette, controlling its position in three degrees of freedom: translation along the beam direction (z), rotation around the vertical (y) and transverse axes (x).

In addition the Filter 7 is equipped with different vacuum compatible stepping motors. Two of them are dedicated to the filter alignment around its vertical axis. The first one is accommodated on top of the filter body and it is used to rotate the filter with respect to the upper part of the SA moving also the whole payload. The second one is mounted under the filter and it rotates the marionette and the rest of the payload with respect to Filter 7 adjusting the relative positions of coils and magnets.

A second pair of vacuum compatible stepping motors moves two small masses attached to mechanical trolleys on top of the filter body, performing a fine adjustment of the tilts (rotations around the two horizontal axes).

The set of sensors and actuators is completed with three positioning sensors with permanent magnets screwed on the cylindrical filter body mantle. They are installed reproducing the geometry of the IP top stage (pin-wheel configuration at 120° each other) and, together with a set of three 110 mm diameter Maxwell pair coils mounted on the ground connected bottom ring, represent the system to feedback control the Filter 7 position during the interferometer alignment. The large size of the coils, ensuring a field gradient uniformity of better than 2% over a 30 mm distance makes sure that the noise reintroduced at this stage is negligible.

6.4 The mirror payload

The mirror payload, composed by the marionette, the mirror and its reference mass, is suspended under Filter 7. The mirror and its reference mass are independently suspended to the marionette. The payload was designed to provide two separate levels of action to control the final mirror position: Filter 7 on marionette and reference mass on mirror. The actuators consist of coil-magnet pairs. The mechanical resonance frequencies of the payload have to be as high as possible to limit thermal noise and to reduce cross talk between the various degrees of freedom to be controlled.

The marionette is composed of a body and four arms carrying the small permanent magnets of the electromagnetic actuators. The marionette body is made out of stainless steel AISI 304L and its mass is 108 kg. The four arms, are made out of amagnetic steel AISI 316 L, to avoid spurious magnetization effects.

The marionette is suspended to the SA by means of a 1 m long Maraging® steel wire with 1.8 mm diameter. This wire is clamped to the marionette center of mass in order to minimize the torques needed to control the angular position. The vertical position of the attachment point can be adjusted with an accuracy of the order of 0.1 mm. A motorized mass of about 240 g housed in the lower part of the marionette allows to adjust the inclination around the *x*-axis within ±7 mrad . In this way the marionette can compensate the mirror θ_x offset.

The mirror rests on a pair of thin steel wire loops, descending from the marionette and transferring directly to the mirror the steering action made by Filter 7 coils. The reference mass is supported in an identical way and has two notches to allow the passage for the mirror support wires, without any contact.

The reference mass has the shape of a hollow cylinder, coaxial with the mirror and containing it. In this way, the two centers of mass are coincident. This allows to reduce the coupling between the various degrees of freedom when a force is applied on the mirror by the reference mass actuators. Moreover, the reference mass has the function of protecting the mirror and its delicate coatings from contamination, mainly during assembly, and to avoid any mirror damage by supporting it in case of wire breaking; The present reference mass is made out of Al alloy 5056, for an easier machining. It is planned to replace it with a dielectric reference mass to avoid eddy currents.

All the payload components are ultra high vacuum compatible and the reference mass shape limits the dust contamination of the mirror during the assembly phase and in operation.

The marionette is steered by means of the coil-magnet actuators along four degrees of freedom: translation along the vertical (*y*) and optical (*z*) axes, rotation (θ_x) around the transverse horizontal axis and (θ_y) around the vertical axis (Figures 40, 41, 42). Another set of coil-magnet actuators permits to apply forces directly between the reference mass and the mirror, along *z*, *x*, θ_x and θ_y for automatic alignment and locking

purposes. To this aim, the reference mass is equipped with four coils facing four small magnets glued to the rear face of the mirror and two coils facing the magnets on the mirror sides.
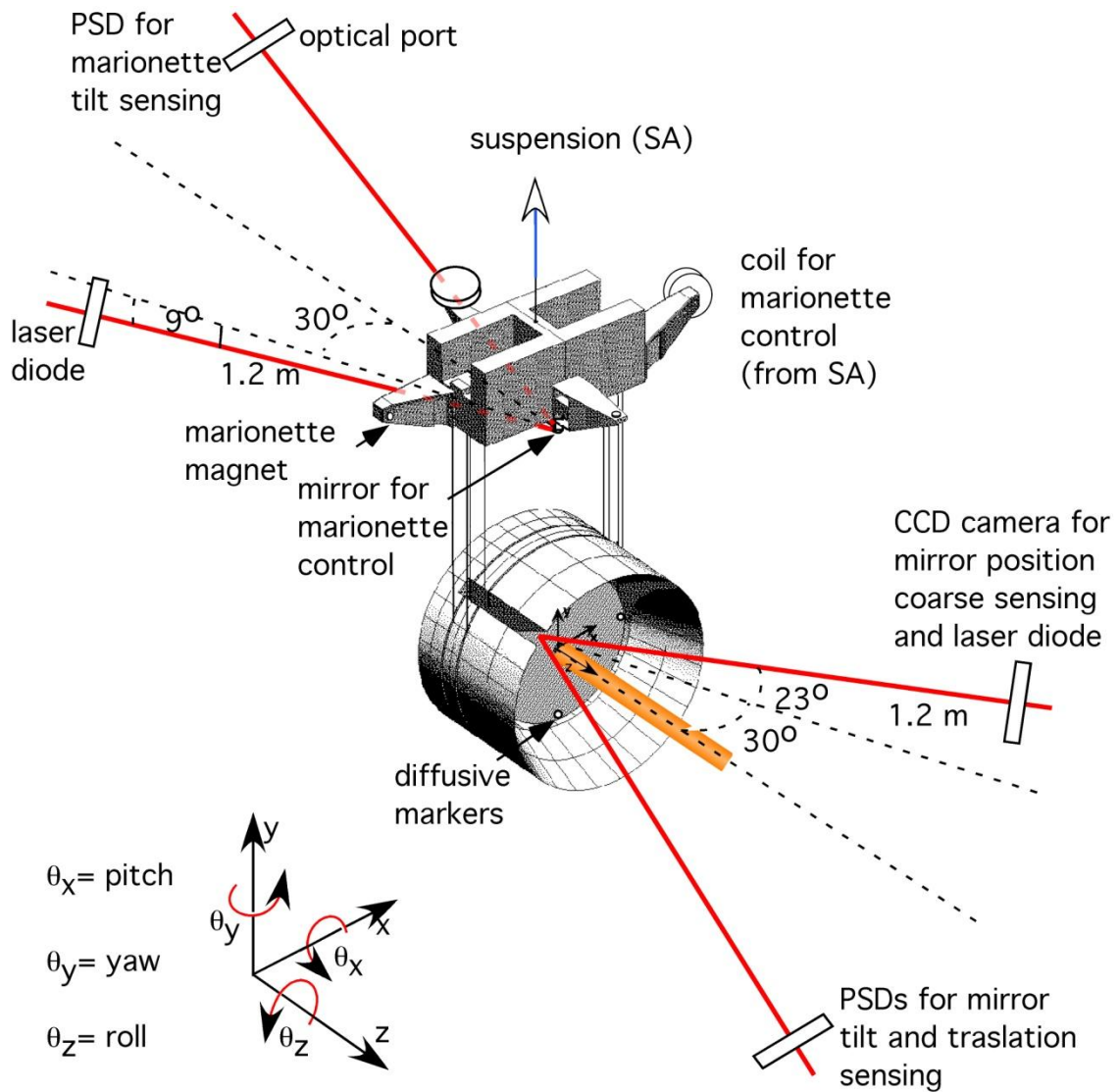
Figure 40. The mirror payload and the standard reference frame used to describe the motion of the optical elements of the Virgo interferometer.
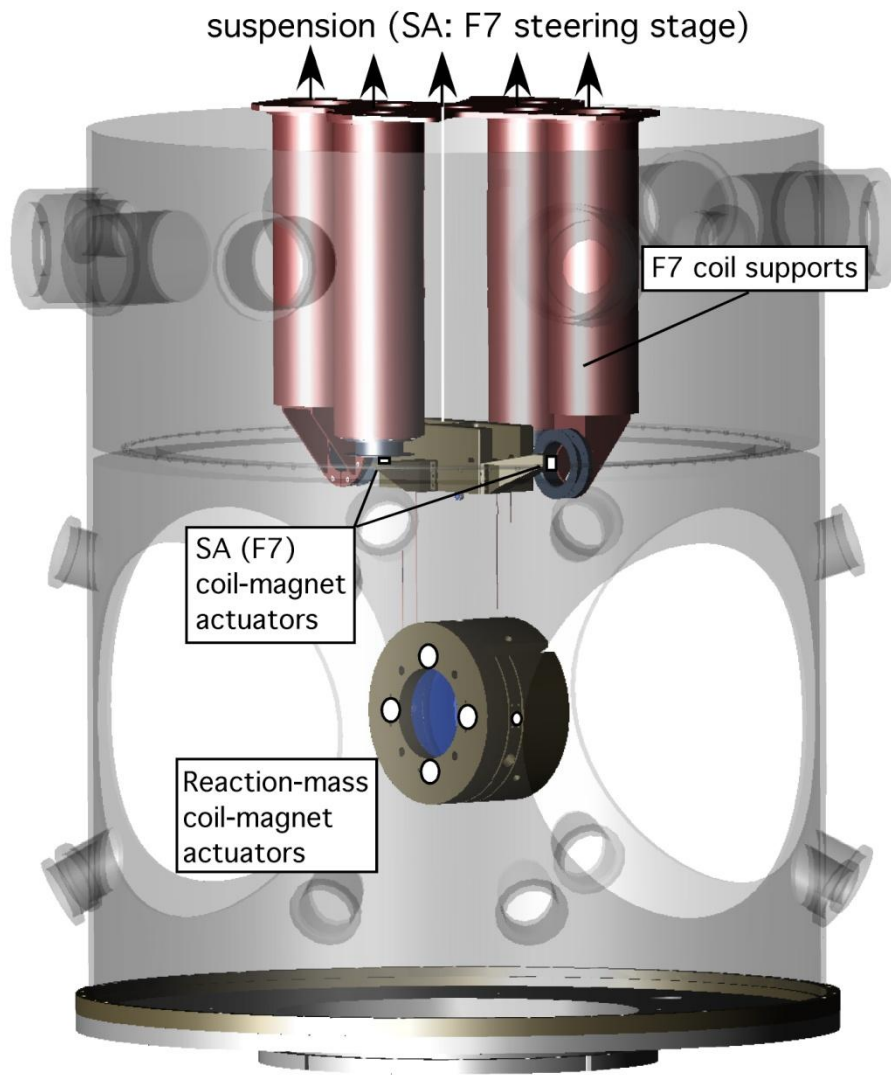
Figure 41. 3-D representation of positions of coils and magnets for the local controls.
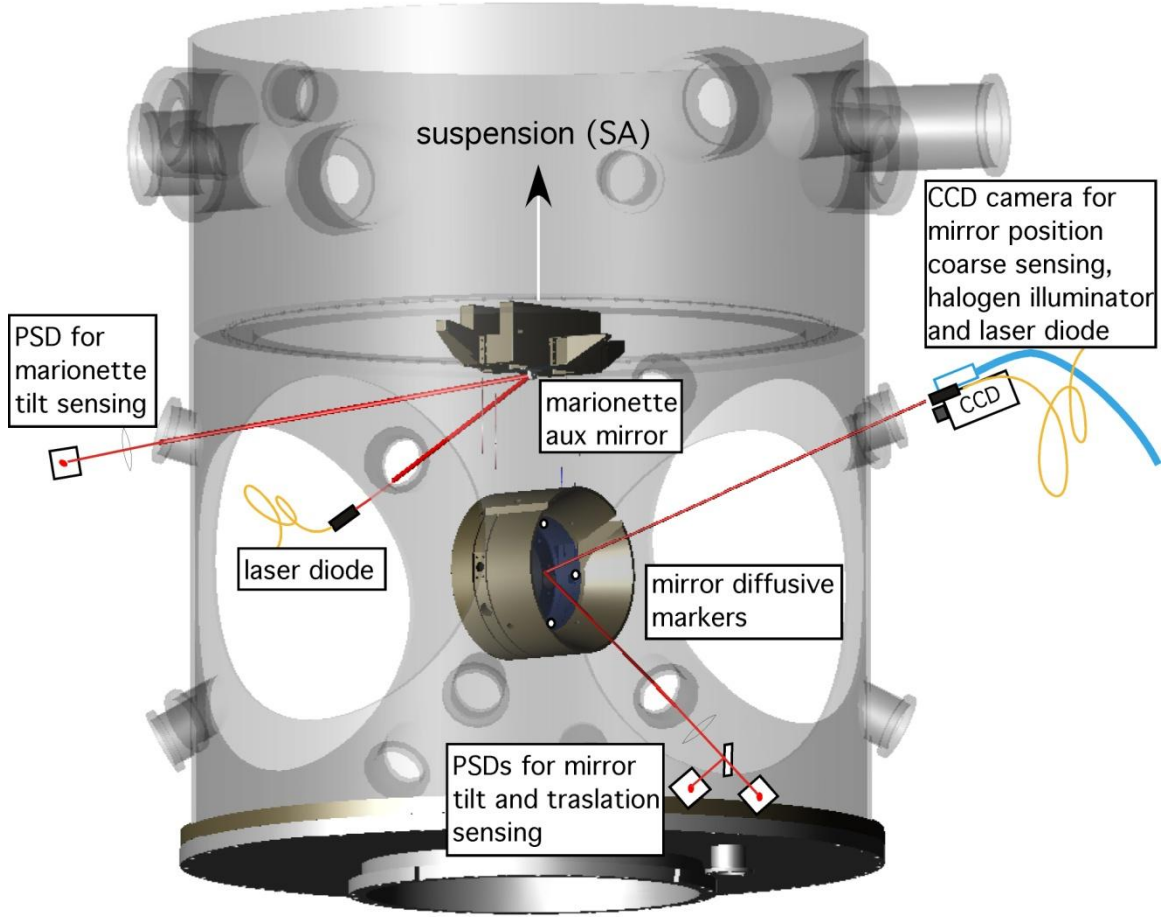
Figure 42. 3D representation of sensors for the local controls.

6.4.1 Mirror suspension wires

Present limitations in interferometer sensitivity below 100 Hz are mostly due to thermal noise from the mirror supporting wires [36,37,38]. The noise spectrum is given by the Fluctuation-Dissipation theorem [39] that relates the position fluctuation spectrum $x^2(f)$ to the system dissipation or, in the following expression, to the pendulum transfer function $H_{pend}(f)$:

$$\left(x^2\left(f\right)\right) = \frac{4k_B T}{2\pi f} \Im\left\{H_{pend}\left(f\right)\right\}$$

where k_B is the Boltzmann constant and T the system temperature. The imaginary part of the pendulum transfer function contains the dissipation terms that determine the quality factor Q. A full treatment of the thermal noise behaviour of the Virgo suspension can be found in [40].

For the mirror wires C85 steel has been selected as the best compromise [41] between internal dissipation and breaking strength requirements.

Relaxation of wires under tension ("creep") could be a source of mechanical shot noise. This has been investigated in [42] and a thermal treatment has been developed to reduce the noise contribution: the

suspension wire is left under tension at 150 °C for one week in a Nitrogen atmosphere with a U shape to facilitate further mirror assembly.

Also the dissipation occurring in the wire clamping system of the marionette and at the contact point on the side of the mirror must be taken into account. For this reason the clamps in the marionette have been designed [43] in ~~such~~ a way to minimize stick-and-slip processes that could increase the mechanical energy dissipation: the wire is clamped in a stainless steel clamp through two hardened steel inserts, where a groove has been realized through an electro-erosion process. The clamping pressure is then controlled, in the assembling phase, through a dynamometric wrench. To reduce the friction between the suspension wires and the lateral surface of the mirror a fused silica prism (so-called "spacer") is bonded to the lateral surface of the mirror. Silicate bonding [44, 40] is used to preserve the mirror mechanical quality factor. The performance of this suspension has been evaluated in [36] and a quality factor of about 10^6 is expected.

6.4.2 Payload assembly

The payload assembly is a complex procedure performed in a class 100 clean room respecting the strict requirements on accuracy for the mirror and reference mass positioning with respect to the marionette, and on mirror handling and cleanliness.

To this aim a stainless steel assembly structure was built. This structure was equipped with 4 micrometric sleds, to adjust the position of the reference mass and of the mirror with a mechanical accuracy of 0.1 mm along the translation degrees of freedom x, y, and z. Similar adjusting gears are used to control tilt of marionette, reference mass and mirror.

Before the assembly of the whole system both the reference mass and the marionette were equipped with coils and motors, and electrically cabled.

The fused silica supports for magnets were attached on the mirror rear face by silicate bonding. The magnets were then fixed with a UHV compatible ceramic glue. On the front face of the mirror near its edge, where the reflective coating is absent, four markers for mirror position measurement were bonded.

Then the real assembly work started, requiring about one day per mirror. The most delicate phase was when the mirror was taken out of its class 1 box and placed on a cradle below the marionette. Then a sucking disk flange was positioned in front of its coated side using the positioning gear. Contact on the uncoated external area was achieved through a circular gasket. After evacuation the mirror supports were released. In this way the lateral surface of the mirror was made available to position the suspension wires.

The reference mass was then put on a cradle and positioned around the mirror. Its suspension wires were then clamped to the marionette.

At this point all the elements of the payload were secured to the assembly structure and protected from dust with a multi layer hermetic plastic cover.

The payload was then lowered through a trap door from the clean room floor into the gallery which leads under the suspension towers. An air cushion trolley was then used to take the payload to the proper tower. The tower trap door was then opened and clean air flushing started. The trolley arrives under the tower and the payload was lifted. Then two operators entered the tower to suspend the payload and make the electric connections. The end mirrors were taken to the end buildings through the 3km tunnel using a low pressure tire electric trolley.

The suspension procedure lasted about 4 hours for two operators in the tower. The most delicate part was when the payload was balanced and rotated in order to be aligned with the coils attached to Filter 7 and the upper suspension was tuned.

6.5 The bench payload

The payload of the short suspension was equipped with a marionette having a different geometry. In this case, indeed, the Filter 7 legs were replaced by an aluminium structure (see figure 38) supporting eight coils

(four vertical and four horizontal). The coils are faced to eight permanent magnets screwed into a disk shaped marionette (800 mm in diameter and 105 mm thick). With this setting-up the coil-magnet system is used to control the payload on four degrees of freedom: the displacement along the beam axis (z), the rotation around this horizontal axis (θ_z), the rotation around the second horizontal axis (θ_x) and the rotation around the vertical axis (θ_y).

These short suspensions have been conceived with an Inverted Pendulum supporting a filter chain with two mechanical passive filters only to be used for the Injection, Detection and Mode Cleaner payloads. In the first two SA, the payloads consist of a marionette with the geometry mentioned above and an octagonal optical bench, while in the Mode Cleaner SA a small reference mass surrounding a curved mirror (80 mm in diameter) is hung to the marionette.

The different marionette geometry mounted on the bench payload has been chosen because the short towers are not equipped with a separating roof dividing the vacuum volume in two sections: the upper part with a low vacuum level and a lower part with high vacuum environment dedicated to the high optical quality mirrors. This marionette, indeed, has also a protection purpose of optical elements and electronic devices mounted on the benches.

6.6 Mirror control

The overall task of this system is to drive the interferometer mirrors from a incoherent to a coherent state where the mirrors are in a fixed relative position at the level of picometers and nanoradians according to the Global Control correction signals. Due to the large position range of the Virgo suspensions a hierarchical sensing and actuation of mirror position is required. Concerning the operation of hierarchical control during the standard operation of the interferometer, the task is achieved by performing the large corrections at low frequency upstream the mechanical filters. In this way the control noise introduced is filtered out and does not reach the mirror. Intermediate amplitude corrections at intermediate frequency are performed at marionette level and only fine corrections are applied at mirror level (Figure 43) [45].
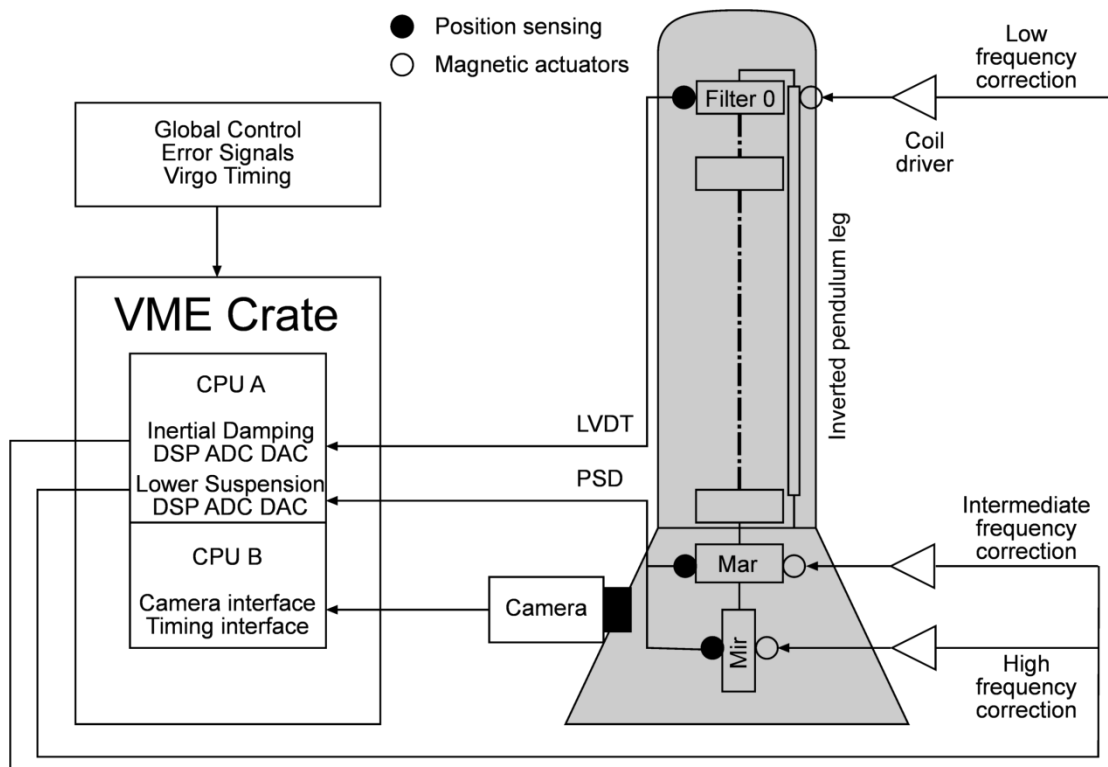
Figure 43. Hierarchical structure of the suspension Control System.

The control system has to handle the following situations:
1   re-alignment of the suspension
2   pre-alignment of the interferometer
3   local angular control and damping of payload normal modes
4   lock acquisition;
5   automatic alignment;
6   locked standard operation

The sensing and actuation devices meant to control the Virgo mirror payload along 4 d.o.f. are integrated to constitute, together with the standard digital chain, the so-called Local Control system (Figures 40, 41, 42) [46], a system replicated over 8 locations, i.e. 6 mirror payloads plus two suspended benches.

In the incoherent state the mirrors are controlled by sensors located close to the suspensions and referred to ground. Hence their relative positions are mechanically correlated by the ground and subject to independent drifts (~1 µrad/h). In the coherent state the control is operated through the beam itself, picked-up in several locations, and the mirror positions are optically correlated by interferometer signals (Global Control). The system has large operation dynamics since it allows to recover the mirror alignment from ± 50 mrad off and to keep it with accuracy < 0.2 µrad rms and also to damp mirror oscillations at the level of the ground seismic figure (10^{-7} µm/Hz$^{1/2}$ at 1 Hz). The system is designed to accomplish a highly automated level of operation. Herein software issues will not be described. The control servo-loops using local and ground-based mirror position read-out have a bandwidth from DC to 2-3 Hz and are meant to be left open once the control is through signals derived from the coherent state of the interferometer (locked). The transition from local to global control of the interferometer has to be accomplished in a smooth way.

6.6.1 Mirror position measurement

Since LC sensors are clamped to the ground their accuracy has to be comparable with the level of the ground seismic noise and is achieved using classical optical means. The overall sensing hardware modified according to the experience acquired with the Central Interferometer [46] is described below (Figures 40, 41, 42).

- Coarse mirror position readout is performed by a CCD-camera EEV-17CAM located in air at 1.2 m from the mirror and at 35° incidence angle. The CCD-chip is a scientific grade 512x512 pixel matrix on a 7x7 mm^2 area. The pixel clock is set at 20 MHz and the device provides a digital signal through an 8-bit ADC. The image is gathered and converted in 16 ms. A dedicated read-out board was designed to use this device in real-time applications in a standard VME environment [47,48].

- Fine mirror position readout is provided by an optical lever measuring the mirror position along three d.o.f.. It is composed by a 1 mW laser diode coupled through a SM-PM optical fibre (OZ Optics), to an anti reflection (2 10^{-3} at 670 nm) coated viewport. After the reflection onto the suspended mirror the beam goes out of the vacuum tank through a symmetrically positioned optical viewport, impinges on a 50% splitter cube and then hits two Position Sensing Devices (PSD Hamamatsu S2044, 4.7x4.7 mm^2) located at the focal and image planes of a lens with 200 mm focal length. The system is rather compact and the laser is injected through the same optical port used for the CCD camera. This two-sensor device provides a measurement in 3 d.o.f., i.e. pitch, yaw and longitudinal motion of the mirror along the optical axis.

- Fine marionette control of angular pitch and yaw (θ_x and θ_y) is provided through a further optical lever impinging at 30° incidence angle on a 1" metal-coated auxiliary mirror attached to the bottom side of the marionette. The sensor used are of the same kind as above.

Coarse and fine position signals are managed by a server running in a dedicated real-time CPU. Suitable error signals and logical flags are built and passed to the DSP (Digital Signal Processor) where digital filters are applied (Figure 43) [46]. According to the hierarchy of the actual architecture, the

marionette-level read-out is the last error signal servoed before passing the angular control to the automatic alignment based upon wave-front sensing.

The optical components of each local control system are located on 30x30 cm^2 removable optical benches clamped to the suspension vacuum chambers inside the tower baking ovens. Each optical element of local control read-out is equipped with fine adjustment stages. This allows to reach optical diagonalization of the readout signal (i.e. separating mirror translations from tilts and pitch from yaw) reducing cross-talk between d.o.f.s to 0.1-0.5 %.

6.6.2 Marionette and Mirror Actuators.

The actuators to control the Virgo payload (see Sec. 6-4) have been designed taking into account several requirements. Some of them are related to the geometrical constraints given by the marionetta and reaction mass shapes and to the force needed during the procedures to control the mirror position. The other requirements are dictated by the need of keeping the injected electromechanical noise below the intrinsic noises of the system and to keep the power dissipated into the coils as low as possible.

To keep the interferometer locked it is necessary to act on the mirrors also in the detection frequency band, above 10 Hz. This modifies the interferometer response therefore the actuators together with their electronics need to be precisely calibrated. Due to the required accuracy the calibration cannot be performed on each suspension separately but one has to use the interferometer itself, controlled as a whole, to determine the mirror actuator transfer function (see Section 10.3).

All the actuators acting at the level of the suspension are coil-magnet pairs. Four coils control the marionette from the last seismic filter of the chain (Filter 7) . In between the coils and the marionette magnets metal-coated Kapton membranes (0.1 mm thick) separate the seismic attenuator vacuum chamber from the lower part where the marionette is suspended. Other six actuators are designed to operate at the mirror level. Four coils are attached to the rear side of the reaction mass and act on the corresponding mirror magnets for position control and damping along the beam axis. Indeed they allow fast damping of mirror motion modes in pitch (θ_x), and yaw (θ_y) d.o.f. as well. The last two actuators are rather compact and act on the sides of the mirrors along the x coordinate to damp transverse motion. A detailed description of the actuators design can be found on reference [49,50].

The following table summarizes the actuators present in the suspension last stage. Cylindrical Samarium-Cobalt UHV compatible permanent magnets (ϕ=11mm, h=4 mm for marionette and ϕ=5mm, h=3 mm for mirror) have been chosen. Copper wires with a cross section of 0.75 mm^2 were used to provide the required actuation current without overheating the payload. The coil-magnet nominal relative position is such that the actuator force response is maximum ($z_{opt}=R_m/2$, where R_m is the mean coil radius). The geometry of the coils was designed compatibly with the mechanical room available in order to widen as much as possible the flatness of this curve around the operation point [49,50].

The number of actuators of each set is shown in column 1. The target object of the actuator is marionette (M) or mirror (m). In column 3 the magnetic moment orientation is provided in the Virgo standard reference system, shown in figure 41. The d.o.f. controlled by the given actuator are shown in column 4. Column 5 gives the magnetic field at the pole surface. Column 8 gives the correspondence between current and applied force.

n	Loc.	axis	d.o.f.	Mag [T]	Coil Turns	R_{coil} [Ω]	α [N/A]
2	M	Y	θ_x, z	1	1092	12	0.025
2	M	Z	θ_y, z	1	1092	12	0.025
4	m	Z	z, θ_x, θ_y	1	256	5	0.010
2	m	X	X	1	40	0.5	0.0053

6.6.3 Suspension control electronics

Each of the 9 Virgo superattenuators has a dedicated suspension control unit made of boards for data conversion, CCD camera image acquisition, processing and communication that are located in a VME crate (Figure 43). Each suspension uses around 60 channels of analog I/O, 4 digital optical links (DOL, Section 8.1.1), a CCD camera and a Timing system interface. Supervision and camera readout software run on two PowerPC-based CPU boards.

Two DSP boards based on the floating-point processors Motorola DSP96002 compute the control signals using digital filters. They are triggered at 10 kHz by the timing distribution system to read error signals from ADC and DOL and to write back to DAC and to DOL the correction signals. The digital filters used have typically 100 poles and require each a sustained rate of about 10 million floating point operations per second (MFlops). The overall computing power for the 9 superattenuators is in the range of 200 MFlops.

The ADC boards contain 8 differential channels that use 16 bits (corresponding to 14.5 effective bits) and are operated at 10 kHz. They are equipped with analog anti-aliasing 7th order Cauer filters with 3.7 kHz cut-off frequency. The maximum signal on the differential inputs is 20 Volts peak-to-peak.

The DAC boards contain 8 channels that use 20 bits (17.5 effective bits) and are also operated at 10 kHz. The analog anti-aliasing filters are the same as those of the ADC boards. Balanced outputs provide a 20 Volts peak-to-peak signal. These components, which were not available commercially with the required specifications (speed and dynamic range), were designed by Virgo.

The coils used for mirror and marionette actuation are fed with a suitable current generated by coil driver circuits. These convert the voltage control signal in to a current flowing in the coil. The coil drivers have two electronic channels in order to allow the use of large control signals during lock acquisition and reduced ones with a low noise level when the lock is acquired. These electronic channels are called High Power (HP) and Low Noise (LN) respectively.

Within a Suspension Control Unit, in addition to the available communication channels between boards, VME and VSB, a private protocol was developed to increase data throughput between DSP and conversion boards.

7. Optics

7.1 Introduction

As outlined in Section 2.1 a complex optical system is used to measure the path difference between the two arms of the Virgo interferometer induced by gravitational waves. The required precision in the measurement is achieved by having a pure TEM00 monochromatic light beam and using the best available optical elements to preserve the beam quality. The error signals and finally the gravitational wave signal are obtained analyzing the light beams at the several output ports of the interferometer (Figure 44).
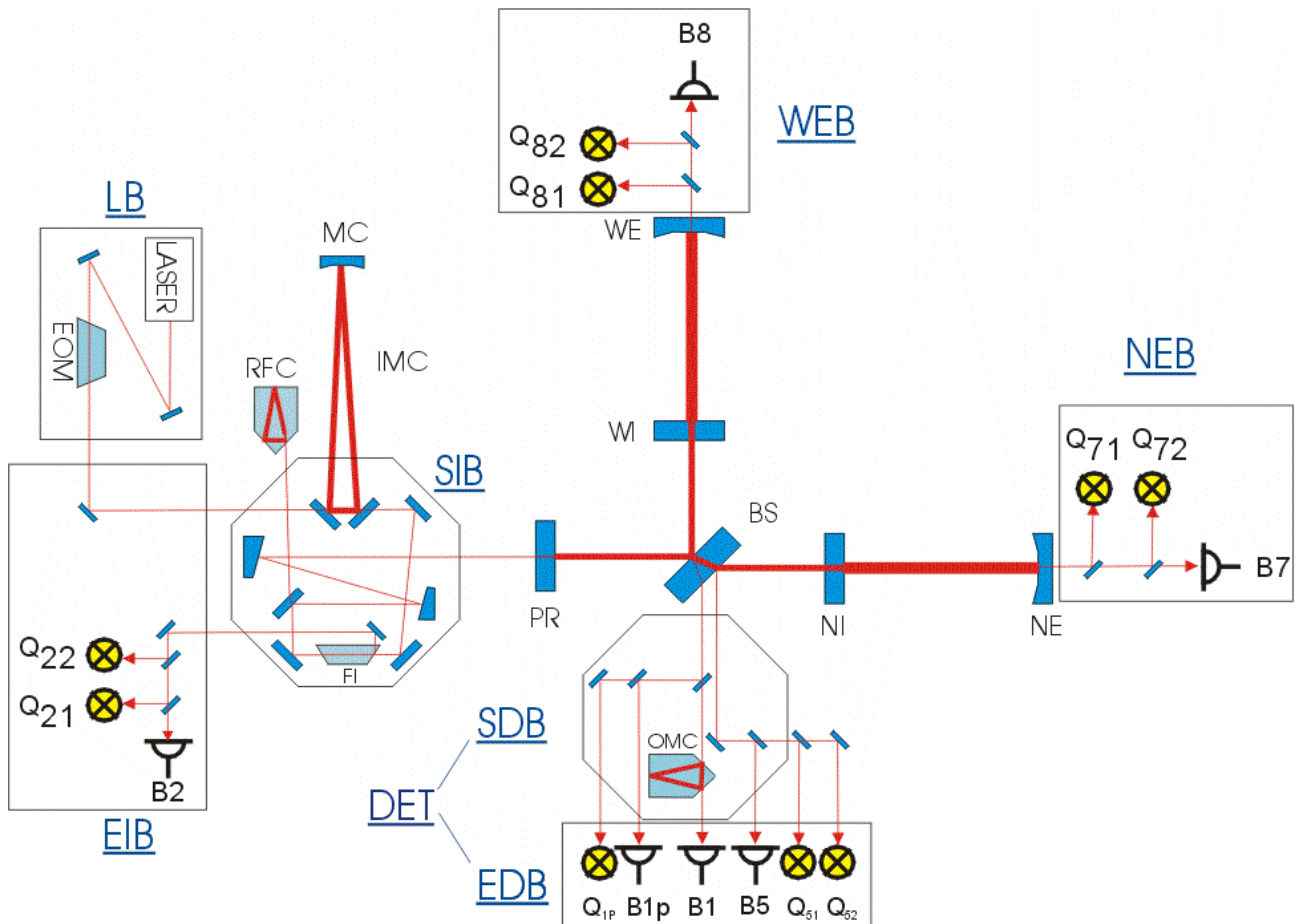
Figure 44. Virgo optical layout. SIB: suspended injection bench, MC: input mode cleaner end mirror, RFC reference cavity, NI,NE,WI,WE: North/West input/end mirror, PR power recycling mirror. B1…B8: interferometer output beams, analyzed by the corresponding photodiodes. EOM: electro-optic modulator.

This section first introduces the full Virgo optical scheme. Then the light source and injection system are described, followed by the Virgo mirrors. Finally the detection system used to measure the output beams and to extract the relevant signals are described to complete the section.

7.1.1 Virgo Optical Scheme

The laser beam used in the interferometer has to be stable in phase, lateral jitter and power [51]. This is realized using first a suspended Input Mode Cleaner (IMC) cavity that performs many functions. The IMC

length is used as a reference in the laser frequency prestabilization circuit. The IMC filters also the input light thus determining the position and angle of the beam that goes to the interferometer, keeping only the TEM00 component. The resulting intensity fluctuations are corrected acting on the laser power by means of a feedback loop.

The beam entering the interferometer is divided by a 50% reflecting Beam Splitter, in two orthogonal beams. The light power in the arms is enhanced by Fabry-Perot cavities with a finesse of 50. A power recycling mirror sends back to the interferometer the light returning towards the laser, forming a power recycling cavity with almost 500 W incident on the beam splitter; the power in the arm cavities becomes 8 kW. The two arm beams recombine on the Beam Splitter. At the output port, looking at the second face of the BS, the interference dark fringe is analyzed by a complex detection optical bench.

The five main beams exiting the interferometer (Figure 44) are analyzed with photodiodes, and give information about the condition of the interferometer. As described later in Chapter 8 this information is used by the locking system for maintaining the resonance in the arm cavities and in the recycling cavity, and keeping the destructive interference at the interferometer output. The correction signals are sent to the actuators controlling the positions of end mirrors, beam splitter and power recycling mirror. The combined error signal of the arm cavities is used for a second level of laser frequency stabilization. Moreover, each output port contains a set of quadrant photodiodes, giving information on the misalignment of the mirrors, which is used in the autoalignment system for correcting mirror angles and the input beam alignment. Mode cleaner and reference cavity have their own system of locking and autoalignment.

7.2 The Injection System

Due to the very stringent requirements on the light source the injection system has a rather complex layout, shown in figure 45.
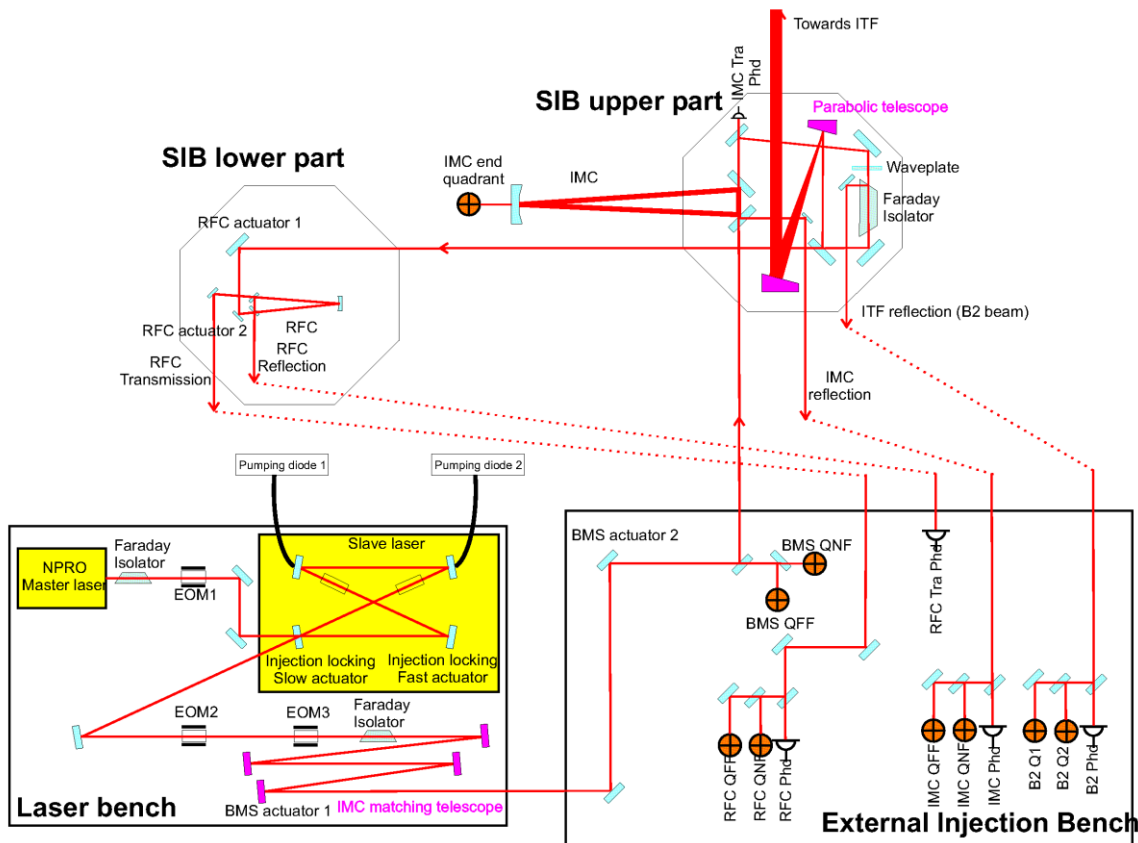
Figure 45. The Virgo Injection System. The Master and Slave Laser bench is on the bottom left. The light goes to the External Injection Bench on the bottom right. The Suspended Injection Bench top and down views are shown on the top right and left respectively.

7.2.1 The 20 W laser

The power laser (slave laser) is a 20 W, solid state, laser: two Nd-YVO4 rods are pumped by two 30W fibered diodes. The cavity is a four mirrors ring cavity in "bow tie" configuration, the cavity support being made of invar, with 2 mirrors glued on piezoelectric actuators. The optical/optical efficiency is about 50%.

The slave laser is injection-locked to a "master" laser (1 W Non Planar Ring Oscillator laser from Innolight Cie). As a result, the slave is phase-locked with the master laser, and therefore, the slave laser frequency can be driven by the master laser frequency [52]. The slave laser pumping diodes are inserted in a feedback loop to control the power being sent to the interferometer.

The injection locking range is about 3 MHz. Both lasers must be kept within this range for the injection process to be effective: this is obtained thanks to piezoelectric actuators driving the slave laser cavity length, the achieved unity gain frequency being about 80 kHz. The associated error signal is based on the Pound-Drever-Hall technique: the master laser beam is phase modulated at 14 MHz and the error signal is extracted from the beat of the sidebands with the carrier at the reflection port of the slave laser.

This setup allows the slave laser to work with full power (about 22 W) on a single longitudinal mode, the frequency fluctuations being those of the master laser itself ($10^4/f$ Hz/Hz$^{1/2}$), plus a residue kept negligible thanks to the slave laser analogue loop and injection process. At the end of 2006 the system had been running continuously for more than 27000 hours.

Two Faraday isolators, one before and one after the Electro Optical Modulator (EOM), provide the attenuation needed by the laser system (more than 40 dB). The beam coming out of the slave laser is passing through a first Faraday isolator (LB_F2 in the figure), then collimated inside another EOM (LB_EOM2), which provides the phase modulations at 22 MHz, 6 MHz and 8 MHz. The first modulation is used for the longitudinal lock of the Input Mode Cleaner (IMC) and the remaining ones for the lock the whole interferometer. After the EOM there is the second Faraday isolator (LB_F3). Downstream an all reflective telescope (LB_M9 – LB_M12) expands the beam from 2 mm diameter to 1 cm as needed to match the IMC cavity.

The whole laser system is accommodated on a dedicated optical bench (Laser Bench, LB), resting on ground within a plexiglas protection and an acoustic isolation enclosure.

7.2.2 External Injection Bench

The beam coming from the Laser Bench passes through an acoustically isolated tube to the External Injection Bench (EIB). The EIB rests on ground in the laser laboratory and is acoustically isolated. It supports the optics to steer the beam to the Suspended Injection Bench. In addition it hosts the photodetectors measuring the light reflected by the injection system and the interferometer itself (beam B2).

Before entering the vacuum chamber of the Suspended Injection Bench, a small fraction of the input beam is sent to a Beam Monitoring System (BMS) based on two DC quadrant photodiodes and related optics. This system aims at correcting beam drifts with respect to a ground based reference (DC readout photodiodes). One quadrant photodiode (BMS_QN) is placed on the image plane of the last mirror of the Laser Bench output telescope (LB_M12) and the other one (BMS_QF) on the focal plane of a telescope, so that beam lateral shifts and angles can be controlled. The signals of these photodiodes are linearly combined in order to allow performing pure angular and translational motions with respect to the IMC input mirror. The actuation is obtained using two mirrors (LB_M11_ABP1 and EIB_M3_ABP2) controlled by piezoelectric crystals.

The beam reflected by the IMC is sampled by a broadband photodiode (IMC_DR) and is used for the IMC longitudinal locking. The same beam is sampled by two broadband quadrant photodiodes (IMC_QF,

IMC_QN) performing the wavefront sensing for the IMC automatic alignment, measuring position and angle respectively. In addition a digital CCD camera images the beam.

In a similar way the signals to monitor and control the Reference Cavity (RFC) are generated using a photodiode (RFC_DR), two quadrants (RFC_QF, RFC_QN) and a camera.

Finally the reflected beam from the interferometer (B2) is sampled for longitudinal locking purposes using three photodiodes (B2_f_6MHz, B2_3f_6MHz and B2_f_8MHz). The signal from these photodiodes is demodulated using the 6 MHz reference signal, its third harmonic and the 8 MHz reference respectively. The beam position is measured using broadband quadrant photodiodes (Q21 and Q22) placed to have on the photodiode planes the required Gouy phase. Finally a digital CCD camera images the interferometer reflected beam.

7.2.3 Suspended Injection Bench and Input Mode Cleaner

The Suspended Injection Bench (SIB) is an octagonal, 900 mm diagonal optical bench suspended in vacuum from a short superattenuator. Its main components are the input optics of the IMC, the RFC, which is placed below the bench, a large aperture Faraday isolator, and the optics to match the beam to the interferometer and the related photodetectors.

Coming from the External Injection Bench, the beam enters the SIB tower through a large antireflection coated (AR) 3° inclined silica window, reaching directly the input mirror of the Input Mode Cleaner. The reflected beam is sent back to the External Injection Bench by means of a plane mirror (SIB_M8) placed on the SIB. The transmitted beam is sent through a Faraday isolator and an off-axis parabolic mirrors telescope to the interferometer through a diaphragm located at the exit of the SIB. The telescope is necessary to widen the beam to the size required by the interferometer equipped with a flat Power Recycling mirror. In the past, this was achieved taking advantage of a flat-concave Power Recycling mirror, with the drawback of being sensitive to transverse displacements. The Faraday isolator turned out to be necessary to prevent light coming back from the interferometer to enter the Input Mode Cleaner. These elements were not present in the first version of the SIB.

A small fraction of beam transmitted by the IMC is monitored by the photodiode (IMC_D1T) used by the laser power stabilization system.

Downstream the Faraday isolator a small fraction of the beam is sent to the Reference Cavity (RFC) by means of a periscope (SIB_M11-SIB_M12). The RFC is a 30 cm long monolithic triangular cavity, attached under the injection bench. The body is made of ULE® [53], an ultra low thermal expansion coefficient ceramic, supporting three optically contacted mirrors. It is used as a frequency reference in the first stages of the lock acquisition, so that the laser frequency line width is lower than the recycling cavity line width. Its finesse with P-polarization is 1000, providing a DC frequency reference better than 10^{-2} Hz/√Hz [54].

The beams transmitted and reflected by the RFC are sent respectively to a photodiode placed on a small external bench at the level of the RFC, and to the RFC photodiodes and quadrants on the EIB. In this configuration the RFC cannot be locked before IMC locking.

The Input Mode Cleaner is an in-vacuum suspended triangular Fabry-Perot cavity with a length of 143.6 m. Its design finesse is 1000. The input mirrors (IMC1 and IMC2) are flat Suprasil substrates 80 mm diameter and 30 mm thick, coated on one side for Nd:YAG at 45° angle of incidence, S polarization, and AR coated on the other side. The two mirrors are rigidly connected, being optically contacted to a pierced Zerodur [55] block forming a dihedron with an aperture angle of slightly less than 90° in order to make the light path closed. The dihedron is resting on a three point support using steel stems mounted on the SIB. The cavity end mirror has a diameter of 80 mm, a radius of curvature of 180 m and is suspended in vacuum from a short SA. The incidence angle on the far end curved mirror is 300 μrad, reducing the astigmatism aberration losses. The beam waist is 5 mm and the light intensity 170 W/mm^2.

The IMC free spectral range is 1.044 MHz. This allows a large choice of modulation frequencies for the main interferometer beam, that have to be a multiple of it. The selected modulation frequency is 6.264 MHz. The achieved matching of the input beam to the IMC is of the order of 98%. However, owing to IMC

internal losses, the transmission at the IMC resonance is of the order of 50%, thus yielding about 10 W maximum power.

Before entering into the interferometer the beam goes through a Faraday isolator (SIB_F) with a quite large aperture (20 mm). Even with this aperture, the beam coming out of the IMC has to be reduced to about half of its size (from 5 to 2.65 mm), in order not to be clipped.

Downstream the Faraday isolator a 8x magnifying optical system is used to match the beam size to the interferometer. This collimating parabolic telescope is formed by one 2" diameter +75 mm focal length mirror (SIB_M5), with a 12.7 mm off-axis, and a 4.5" diameter +600 mm focal length mirror (SIB_M6), with a 101 mm off-axis.

All the optics is adequately dimensioned to deal also with parasitic beams where needed, and to avoid beam clipping. Behind some mirrors PSD detectors (position sensing photodiodes, PSDi on the drawings) have been placed in order to monitor possible beam drifts. Finally several beam steering elements are remotely controlled. The most critical actuators operate in a closed-loop mode to allow controlled and reversible movements.

The alignment of the SIB is performed in two stages: the SIB is locally controlled using a CCD camera looking at a small plate supporting four markers and two mirrors placed in front of the dihedron. The coarse alignment of the SIB is performed using the markers, illuminated by an halogen lamp. The fine control is performed using two HeNe beams coming from outside and reflected by the mirrors into the camera which detects their displacement.

7.2.4 Injection system control

The expected frequency stability given by shot-noise resolution is 10^{-6} Hz/√Hz. With an expected common mode rejection factor of better than 10^{-2} this frequency noise does not limit the interferometer sensitivity. However since the IMC mirror positions determine the light beam parameters and phase, this stability can only be obtained by means of a feedback system acting on the suspended optical elements and on the laser itself (Figure 46).
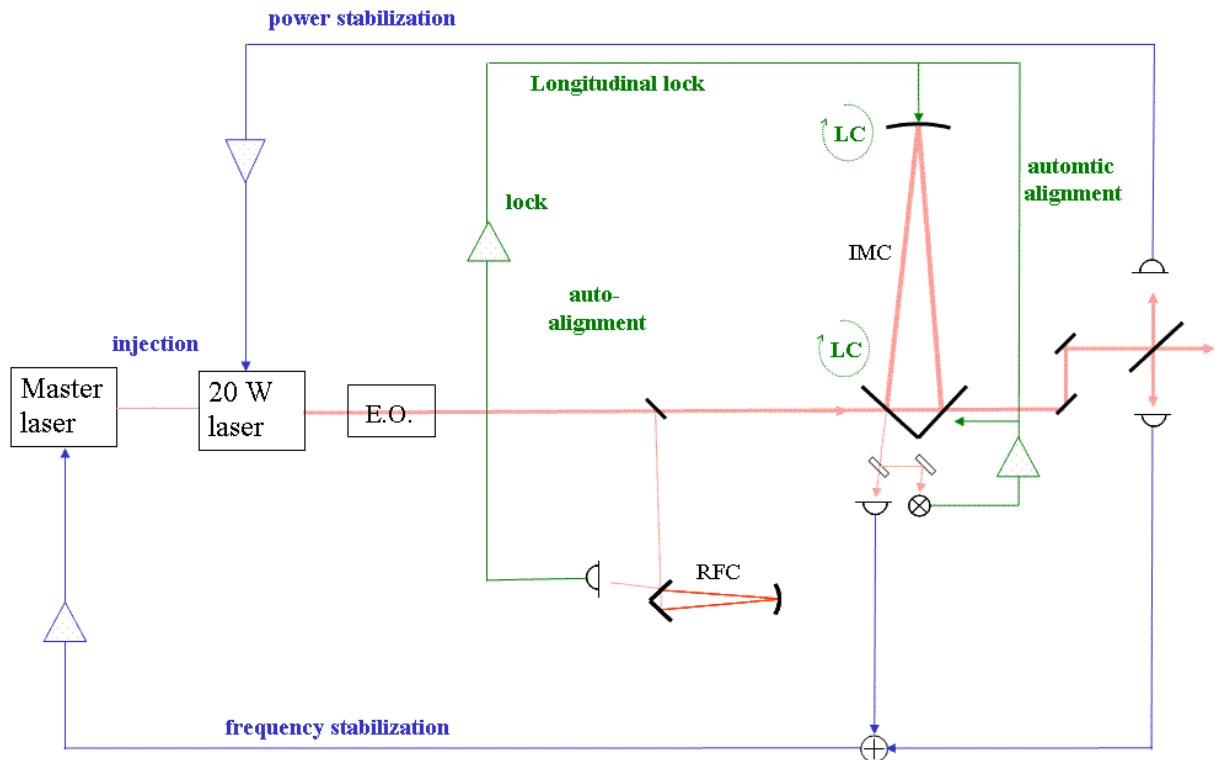

Figure 46. Injection system control scheme.

Due to the large dynamic range required for control, the laser frequency is pre-stabilized on the IMC. A Pound-Drever-Hall scheme with a phase modulation at 22 MHz is used, which analyzes the beam reflected by the IMC. Before the full lock of the interferometer, the IMC length is stabilized on the RFC, with a 100 Hz bandwidth. The error signal is processed in a digital chain, and the correction signal is sent to the coils acting on the IMC end mirror.

The laser frequency is eventually stabilized using the interferometer common mode as a reference, with a relative frequency noise of 10^{-19} $Hz^{-1/2}$. This is called the Second Stage Frequency Stabilization (SSFS). When the full frequency stabilization is active these two signals are added to provide the feedback error signal.

The laser phase is controlled by three different actuators: a corrective EOM device for fast actuation (30 kHz – 300 kHz), a piezoelectric crystal that controls the master laser cavity length at intermediate frequency and the laser crystal temperature control (< 1 Hz).

The mutual alignment of the IMC and of the incoming laser beam is achieved with the Ward technique using two quadrant photodiodes, placed on the EIB. In addition the beam position at the IMC end mirror is measured using a quadrant in transmission. These sensors provide six error signals that include longitudinal and angular information. The corrections are sent to the SIB position control, as well as to the IMC mirror angular control. The IMC alignment correction is engaged first acting only on the end MC mirror, which therefore follows the beam. When the full alignment control of the IMC is switched on, corrections are applied also to the SIB and the Local Control can be switched off.

The power transmitted by the IMC is stabilized with a feedback on the slave laser pumping diodes. The feedback is AC coupled, with cut-off around 30 mHz and unity gain frequency at 40 kHz. The feedback is applied either on the DC current supply of the diodes or on a fast "shunt" connected in parallel with one of the pumping diode (fast actuation). In Figure 47 the measured performance in terms of Relative Intensity Noise (RIN) is shown.
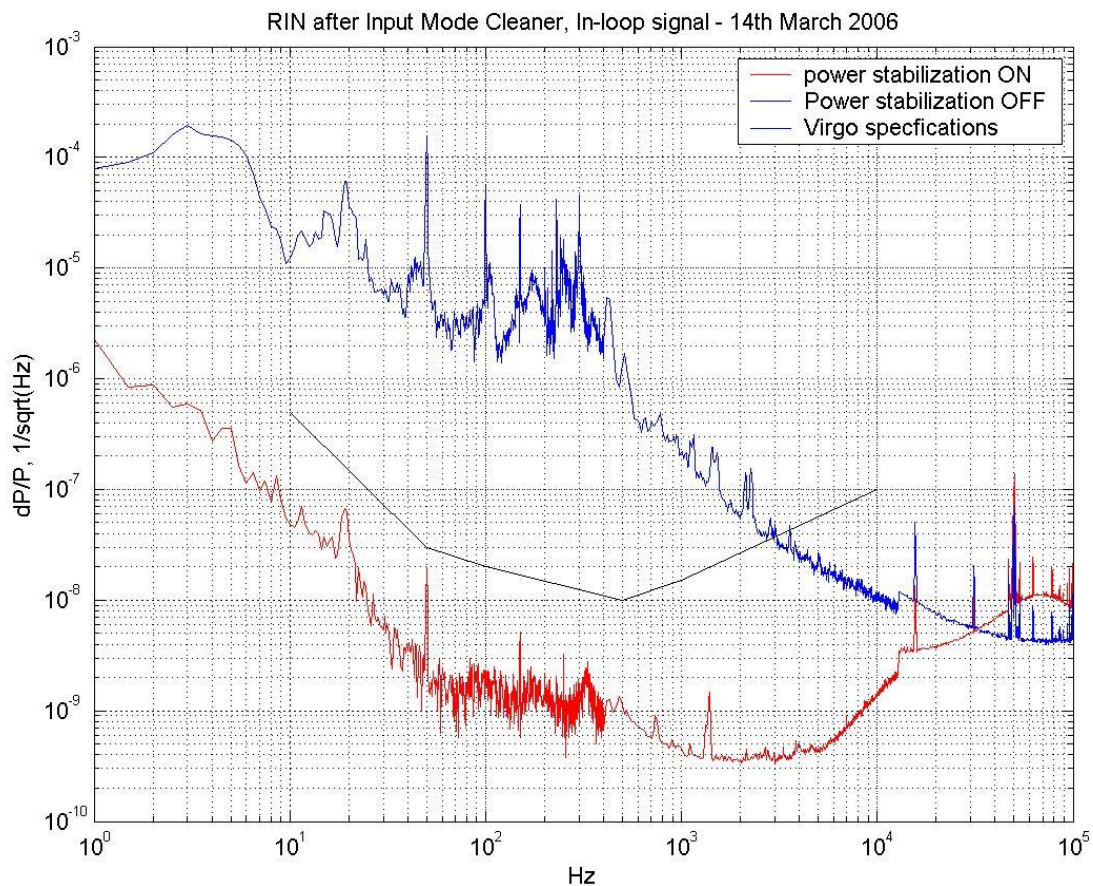
Figure 47. RIN of input mode cleaner transmitted beam, In-loop signal.

7.3 The detection system

7.3.1 The detection system design

The detection system analyzes the beams coming from the output ports of the interferometer as shown in figure 48. The beam B1 provides the gravitational wave signal and is analyzed by the main detection system. This system measures also the beam reflected by the second face of the beam splitter (B5) providing also error signals for the longitudinal and angular control loops. Beams B7 and B8 are analyzed on benches located at the end of each interferometer arm completing the set of control signals and the beam reflected by the interferometer (B2) is analysed on the injection bench.

The main detection system is designed to measure variations of light power of a few 10^{-11} W at the modulation frequency corresponding to changes in interferometer arm length smaller than 10^{-19} m. On the other hand the mirrors residual motion at low frequency, of the order of 10^{-12} m causes large fluctuations of the light intensity. This puts severe constraints on the dynamic range and residual noise of the photodiodes and their read-out system. Additional high quality optics is required to handle the various beams and to adapt their size to the photodetectors. The different components of the detection system are suspended in vacuum or located on an optical bench in air depending on their sensitivity to seismic and acoustic noise.

Due to various defects such as mirror surface deformation and interferometer misalignments higher order transversal modes are present in the B1 beam. This increases the contrast defect and can spoil the sensitivity by a factor 2-3. An output mode cleaner in vacuum is used to improve this contrast defect.

The read-out photodiodes are located on a second bench placed outside the vacuum chamber and the produced signal is demodulated according to the Pound-Drever-Hall technique. A principle scheme of the main detection system is shown in figure 48. Other similar benches are also located at the transmission port of the Fabry-Perot cavities and at the reflection port.
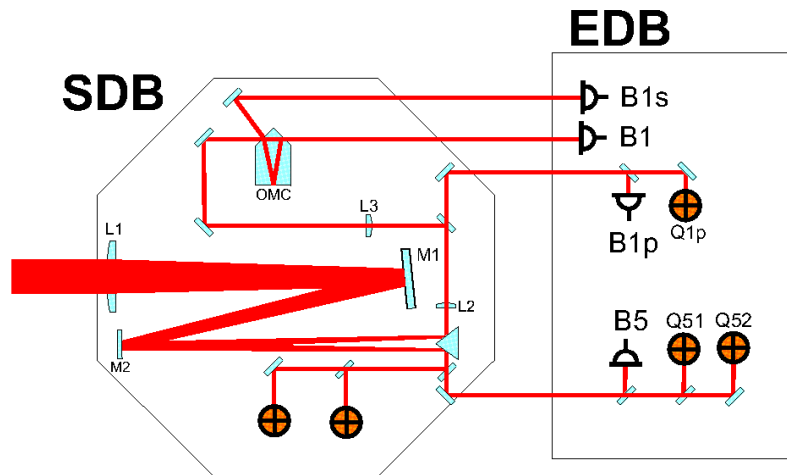
Figure 48. Schematic view of the detection system. B1 is the dark fringe beam and B5 is the beam reflected by the second face of the Beam Splitter mirror. B1p is a small fraction of B1 extracted before the output mode cleaner (OMC) and B1s is the beam reflected by the OMC.

7.3.2 The output mode cleaner

The output mode cleaner (denoted OMC on figure 48) is a short triangular monolithic cavity (2.5 cm long) made out of silica with a finesse of 50 [56]. The large cavity bandwidth (75 MHz) allows the transmission of both the carrier and the sidebands in the same Airy peak. Due to this choice a small change in the mode cleaner length induces a change in the relative phase of the carrier and the side-bands and simulates a gravitational wave signal. Therefore its length has to be controlled with a precision of about $3x10^{-10}$ m. To reduce the effect of external disturbance the cavity is suspended to a seismic isolator inside a vacuum chamber.

The cavity length is controlled by varying the OMC temperature using Peltier cells. A temperature scan allows to identify the fundamental mode TEM_{00} looking at the shape of the transmitted beam. The OMC is kept on resonance by modulating the cavity length at 28 kHz with a piezoelectric device and detecting the error signal synchronously. The achieved length precision is about 10^{-10} m (rms).

7.3.3 The suspended detection bench

The output mode cleaner is located on an optical bench suspended in vacuum to a seismic isolator. This bench contains also a telescope whose purpose is to adapt the interferometer output beam (B1) to the output mode cleaner cavity: the waist of the beam is reduced from 2 cm to 140 μm. The positions of the 3 lenses (L1, L2 and L3 on figure 48) forming this telescope can be remotely adjusted in order to tune the waist of the beam and its location. The alignment of the beam on the mode cleaner is performed using the signals from two quadrant photodiodes (DQ1 and DQ2) and acting via pico-motors on the orientation of mirrors M1 and M2 located inside the telescope. Downstream the output mode cleaner a Faraday isolator avoids that the small fraction of light back scattered by the photodiodes recombines with the interferometer beam.

In order to keep the output mode cleaner aligned with the interferometer output beam the suspended bench position should be controlled in all degrees of freedom with a precision of the order of 1 μm in translation and few tenths of μrad in angle. The control system [57] is based on a CCD camera placed

outside the vacuum chamber. The camera looks at the image of four different clusters of LEDs, attached to the vacuum chamber and reflected by four mirrors attached to the bench. Using the image positions of the four clusters the bench position in all its six degrees of freedom is deduced. Each cluster is composed by 10x10 LEDs to increase the measurement sensitivity. The camera noise allows the measurement of displacements of a few 10^{-8} m/Hz$^{1/2}$ and misalignments of a few 10^{-7} rad/Hz$^{1/2}$. The bench position measured by the camera is used as error signal for a feedback performed using a DSP board and DAC channels driving eight electro-magnetic actuators. Once the feedback is closed all the mechanical resonances are damped and the bench is controlled with the required precision.

7.3.4 The external detection bench

The external detection bench (Figure 48), located inside an acoustically isolated enclosure, supports the photodiodes used to detect the gravitational wave signal (B1) and to provide the longitudinal and alignment error signals. It is equipped with CCD cameras to image the beams and monitor their position. The typical beam detection layout includes two photodiodes and, depending on the beam, quadrant photodiodes, CCD cameras and photodiodes demodulated at twice the modulation frequency. To avoid burning the photodiodes in case of large intensity fluctuations a fast shutter is positioned on the B1 path.

7.3.5 The end benches

Acoustically isolated benches are located in the end buildings to detect the beams B7 and B8 transmitted by the Fabry-Perot cavities. Similarly to the external detection bench, each bench supports the photodiodes, quadrant photodiodes and CCD cameras. The photodiodes provide a low sensitivity length error signal while the quadrants are used to control the alignment. The size of the beam coming out of the end mirror is adapted to the bench optics using a large lens doublet (see figure 49).
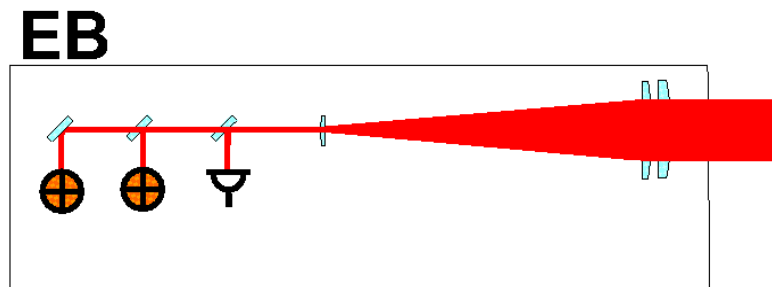

Figure 49. Schematic layout of the North and West End benches.

7.4 The photodiodes and readout electronics

7.4.1 Photodiodes for the dark fringe and the longitudinal control

Once the dark fringe is filtered by the output mode cleaner the light is detected by photodiodes. Since the shot noise limit decreases as the square root of the detection efficiency, very high quantum

efficiency photodiodes have been selected [58,59]: these are 3mm diameter InGaAs photodiodes that, thanks to anti-reflective coating, have an efficiency larger than 90%. The diameter is the maximum imposed by the junction capacitance, in order not to limit the electronic bandwidth. These photodiodes are also used for the detection of the other beams used to control longitudinally the interferometer. Two photodiodes are used for each beam for redundancy. In case of bad contrast defect up to 16 photodiodes are available for the dark fringe.

In order to detect the large signals at low frequency and the tiny signals at high frequency the electronics should have a dynamic range of at least 10^8 and a noise equivalent to few 10^{-11}W/ Hz$^{1/2}$. The photodiode RF current is pre-amplified (with a typical gain of 400 V/A) using a filter which selects the signal at the modulation frequency. The noise of the preamplifier is 4 nV/Hz$^{1/2}$. Then the RF signal is demodulated yielding two output signals, the in-phase and in-quadrature signals, which are digitized with 18 bits ADCs sampled at 20 kHz. With these ADCs it is possible to achieve a dynamic range of 10^7 Hz$^{-1/2}$ (10 V peak over a noise of 1μV/Hz$^{1/2}$). In order to fit the ADC range the signal low frequency component is attenuated by a low noise analog filter before digitization. This increases the dynamic range of the detection system up to 2×10^8. Digital processing recovers the original signal.

For longitudinal control or interferometer characterization purposes the signals at 2 or 3 times the modulation frequency are also measured with photodiodes and electronics chains similar to those described above. The wrong polarization beams are also extracted using polarizing prisms and measured with dedicated photodiodes.

7.4.2 Photodiodes for the alignment control

The photodetectors used for the alignment control [60] are silicon quadrant photodiodes (EG&G YAG-444) with 11.4 mm diameter. The circular sensitive area is divided by two 125 μm gaps in 4 quadrants of 25 mm^2 each. The vertical/horizontal alignment error signals are obtained by building the intensity difference on the two halves of the detector (inside the front-end electronics box), followed by an off-board demodulation. The error signals are shot noise limited for an incident light power of 0.3 mW or more, the maximum allowed light power being 3 mW. The phase and quadrature signals contain information about angle and position of the wavefront of the carrier with respect to the modulation sidebands, from which the mirror misalignment can be deduced by using a suitably computed reconstruction matrix. This matrix can also include the additional information from the non-demodulated difference signals.

7.5 Mirrors

7.5.1 Introduction

The Virgo mirrors must meet very stringent specifications to allow the interferometer to reach the required sensitivity. The Virgo interferometer design imposes very large (350 mm diameter) and heavy optics (20 kg). The total losses of substrate and coatings at 1064 nm (including absorption, scattering and large-scale wavefront distortion) should not exceed 100 parts per million (ppm). There are specific constraints on the absorption ($<$ 5 ppm) due to thermal lensing, that is mirror heating and deformation due to power absorption, which causes wavefront distortion. The large angle scattering level has to be less than 5 ppm to minimize noise due to the scattered light which might recombine with the output beam.

These specifications can only be met with very stringent requirements on substrate composition and high quality polishing. The detailed requirements on substrates and coatings are presented in the tables.

Mirror Substrate specifications			
Component	Fabry-Perot End Mirrors	Fabry-Perot Input Mirrors	Power Recycling Mirror 2006	Beam Splitter Mirror

Material	Herasil 1 Top	Suprasil 312 SV	Suprasil 312 SV	Suprasil 311 SV
Diameter (mm)	350 - 0, +0.5	350 – 0, +0.5	350 – 0, +0.5	230 – 0, +0.5
Thickness (mm)	96 – 0.5, +0	96 – 0, +0.5	96 – 0, +0.5	55 – 0, +0.5
Shape Side B	Concave $R = -3450+/-100$ m	Flat	Flat	Flat
Shape Side A	Flat	Flat	Flat	Flat
Wedge (mrad)	1.1 +/-0.1	no wedge (<< 1µrad)	no wedge (<< 1µrad)	1.1 +/-0.075
Roughness Side A	1-1.5 Å RMS	< 0.5 Å RMS	< 0.5 Å RMS	< 0.5 Å RMS
Roughness Side B	< 0.5 Å RMS	< 0.5 Å RMS	< 0.5 Å RMS	< 0.5 Å RMS
Flatness Side B	8 nm RMS $\varnothing = 150$ mm	8 nm RMS $\varnothing = 60$ mm	8 nm RMS $\varnothing = 60$ mm	13 nm RMS $\varnothing = 120$ mm
Flatness Side A	50 nm RMS $\varnothing = 200$ mm	8 nm RMS $\varnothing = 60$ mm	8 nm RMS $\varnothing = 60$ mm	13 nm RMS $\varnothing = 100$ mm

Mirror Coating Specifications				
Component	Fabry-Perot End Mirrors	Fabry-Perot Input Mirrors	Power Recycling Mirror 2006	Beam Splitter Mirror
Incident angle	0°	0°	0°	45°
Coating diameter (mm)	330	200	200	210
Coating Side B (S polarization)	H.R. $R>0.99995$	AR $R < 5.10^{-4}$	H.R. $R = 95\%$	$T = R = 0.5$ +/- 0.005
Coating Side A (S polarization)		$R = 0.88$	AR $R < 5.10^{-4}$	AR $R<10^{-3}$
Losses (absorption = scatttering)	< 5 ppm $\varnothing = 150$ mm	< 5 ppm $\varnothing = 60$ mm	< 5 ppm $\varnothing = 60$ mm	< 5 ppm $\varnothing = 120$ mm
Flatness Side B	8 nm RMS $\varnothing = 150$ mm	8 nm RMS $\varnothing = 60$ mm	8 nm RMS $\varnothing = 60$ mm	13 nm RMS $\varnothing = 120$ mm
Flatness Side A	50 nm RMS $\varnothing = 200$ mm	8 nm RMS $\varnothing = 60$ mm	8 nm RMS $\varnothing = 60$ mm	13 nm RMS $\varnothing = 100$ mm

A new type of silica was developed specially by the German company HERAEUS in collaboration with Virgo.

For the coatings it was essential to build new equipment in LMA. New tools were also developed to manipulate the mirrors between every production step of the process (cleaning, coating, metrology) in clean conditions with a total safety. These tools are also used on the Virgo site in Cascina.

7.5.2 Mirror substrates

In order to have a very low bulk absorption level (< 1ppm/cm), a very high refractive index uniformity and a low birefringence the substrates were made out of a new type of fused silica (Suprasil 311 SV, Suprasil 312 SV). The OH content is very low (<<50 ppm), the refractive index is homogeneous in all directions and the birefringence is very low (< 5.10^{-4} rad/cm). The result obtained was satisfactory with an achieved absorption = 0.7 ppm/cm for both Suprasil 311 SV and 312 SV.

An American company (General Optics) polished the bulk parts. This company was the only one able to polish very large substrates having at the same time a low micro-roughness (< 0.5 Å RMS), a good flatness (< 8 nm RMS on Ø150 mm) and few punctual defects. All the polished components, that were delivered, complied with the Virgo specifications.

The design coating (quarter-wave stacks) of each mirror depends on its function. For example, the end mirrors have a very high reflectivity level while the input mirrors have only 88% of reflectance; in order to obtain a finesse of the Fabry-Perot cavities close to 50.

7.5.3 Mirror coatings

For the coating process it was decided to use SiO_2 for the low index layer and Ta_2O_5 for the high index one, which have the best optical properties in the mid-infrared region. The extinction coefficient at 1064 nm is:

- for SiO_2: $k = 4.0 \ 10^{-7}$ +/- $0.5 \ .10^{-7}$
- for Ta_2O_5: $k = 4.5 \ 10^{-7}$ +/- $0.5 \ .10^{-7}$

The quarter-wave multilayer mirrors realized by this deposition system have an absorption of 0.6 ppm at 1064 nm. This value is lower than the Virgo requirement (5 ppm).

The SiO_2 layer is the restrictive factor regarding the layer thickness uniformity. Indeed, the uniformity is worse by a factor 3 than that of the Ta_2O_5 layer (the emission of the sputtered particles is different for the two materials). The single layer thickness uniformity is shown in figure 50. Nevertheless, the uniformity obtained on a multilayer mirror was good enough for Virgo: 0.6 % on Ø300 mm.
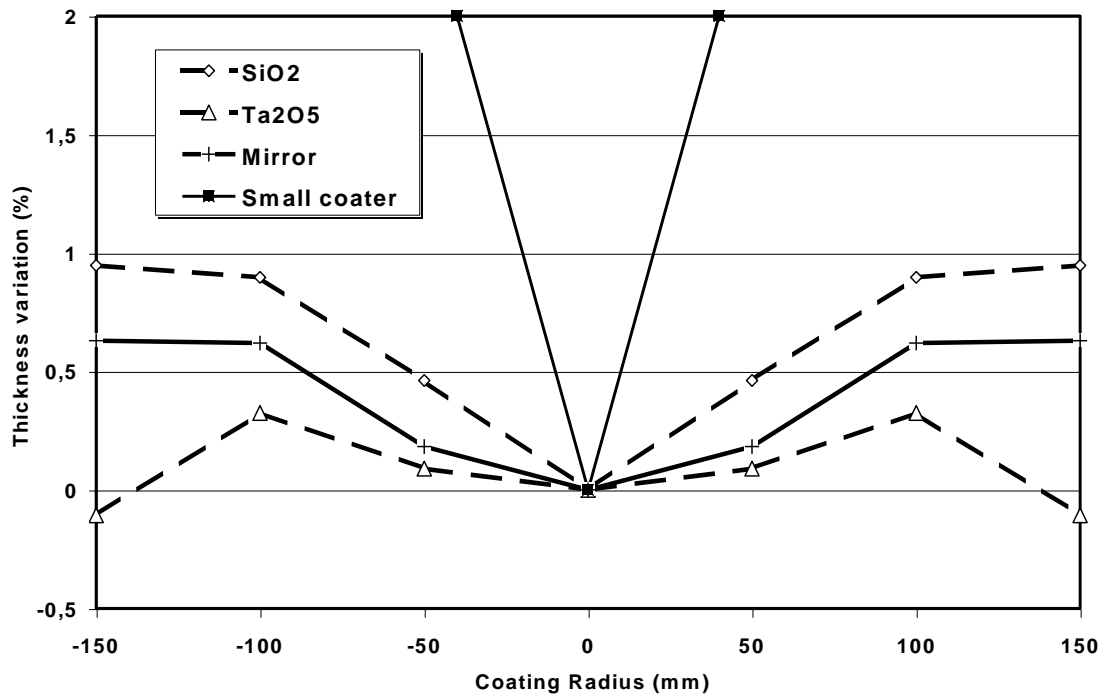
Figure 50. Thickness variation, with respect to the centre, as a function of the coating radius.

The only deposition technique able to produce components with the required optical performances is the Ion Beam Sputtering (IBS). LMA-Lyon already demonstrated that this technique allows to reach very low-loss levels (< 5 ppm) [61, 62]. This was obtained on high reflectivity mirrors up to a diameter of 100 mm.

To reach the severe Virgo requirements on ∅350 mm, a new Ion Beam Sputtering (IBS) coater was designed and manufactured. In order to obtain the lowest coating absorption one had to optimize the deposition conditions (beam current, target angles, gas flows). This was done by working first on single layers.

At the same time LMA developed metrology tools able to characterize the optical performance of the coatings on a large area: wavefront, scattering, absorption and roughness measurements, as well as point defect detection. All these devices were installed in a new building in a class 1 clean room (Figure 51).

Figure 51. General view of the class 1 clean room (surface: 150 m^2).

This environment is necessary to avoid any contamination (particles) of the substrate before or after coating, which may increase the scattering and the absorption level.

7.5.3.1 Ion Beam Sputtering (IBS) coater

The new IBS system design was defined and optimized with a on purpose developed simulation software [63], which describes precisely the sputtering phenomenon in the IBS process. This software takes into account all the geometrical and electrical parameters.

The mirror dimension required to have a vacuum chamber of 2.4*2.4*2.2 m^3 (Figure 52):
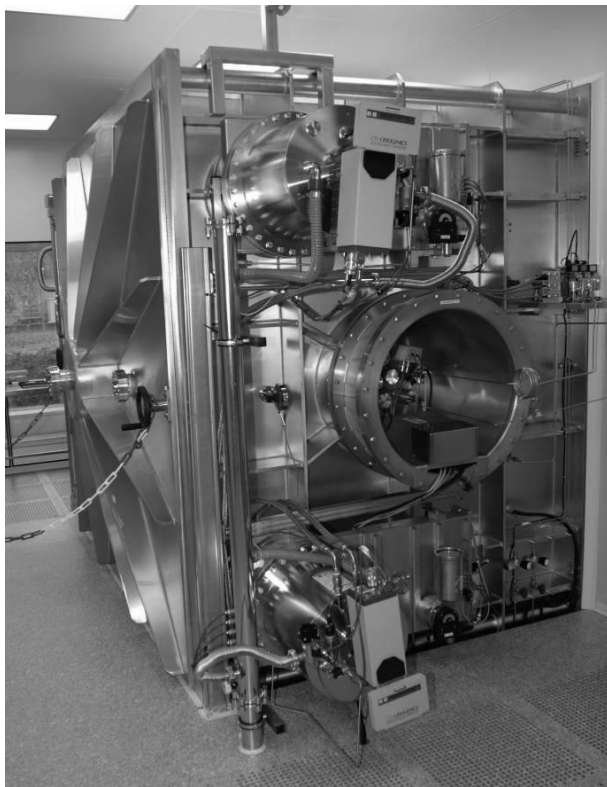

Figure 52. IBS deposition system.

this is the largest IBS coater in Europe. The sample holder (robot), operating under vacuum, allows every movement of the substrate inside a circle of 1 m. The coater was installed in a 150 m^2 class 1 clean room in 1999. .

Primary pumping reduces the pressure to 8.10^{-3} mbar in 30 minutes while the secondary pumping performed by four CTI cryopumps allows to reach a base pressure of 4.10^{-8} mbar in 3 hours. This pumping configuration guarantees a very clean vacuum without hydrocarbon contamination controlled in real time with a residual gas analyzer (RGA).

Radio frequency ion sources are used to sputter the coating materials out of ultra-pure targets (Ta_2O_5, SiO_2). Several reasons have justified this choice instead of classical Kaufman ion sources. On one hand the possible layer contamination due to the tungsten filament, which degrades the layer absorption, is avoided. Furthermore, since the deposition time is very long (40-50 hours) and the filament lifetime is comparable, the choice of filamentless sources was imperative.

The layer thickness is monitored by four quartz balances which allow a very efficient in-situ control. Another component developed by LMA is the automatic control of the coater. It manages the pumping and venting procedure (done with ultra pure dry air) and every step of the deposition process (control of the ion sources, the gas flows, the targets movements).

7.5.3.2 The optical metrology devices

The optical metrology of the coatings is fully part of the mirror production process. Indeed, it allows to improve rapidly the coating performance and to reach a very high quality level. To avoid contamination of the mirrors, all the metrology tools are installed in the class 1 clean room, close to the IBS coater.

All the metrology benches are able to characterize the entire surface of the large Virgo components (400x400 mm^2) and to handle heavy samples (20 kg). In this paragraph, we report only the main performances of the optical benches. More details can be found in [66].

- Scattering and Transmission measurements:

The scatterometer is a commercial CASI type instrument able to measure scattering levels lower than 1 ppm (Bi-directional Reflectance Distribution Function noise floor of 10^{-9} sr^{-1}). The absolute BRDF as a function of the scattering angle θ_s is measured with a beam size of 1 mm over the whole sample. This system can also be used as a very sensitive wattmeter to determine very low transmission or reflectivity values (T < 1 ppm).

- Absorption measurements:

A new absorption bench was developed to measure surface and bulk absorption on large samples. It is based on the photothermal deflection technique whose capability to determine very low absorption levels has already been demonstrated [61]. The sensitivity of this bench at 1064 nm is remarkable: 20 parts per billion (ppb) for surface absorption and 30 ppb/cm for bulk absorption have been achieved, allowing to verify the high quality of the mirrors.

- Wavefront measurements:

A commercial interferometer from ADE Phase Shift (minifiz type interferometer, pupil $\varnothing$150 mm, wavelength 1064 nm) is used. To measure large wavefronts ($\varnothing$400 mm), a numerical method called "Stitching Interferometry" [64, 65] was developed in collaboration with a French company (MB Optique). The reproducibility of this rather complex method based on the difference between two successive measurements is 0.4 nm RMS on $\varnothing$400 mm. Without stitching the reproducibility is 0.04 nm RMS on $\varnothing$150 mm.

- Roughness measurement and defect detection:

A commercial profilometer MICROMAP, modified to characterize large optics, is used. The sensitivity is 0.2 Å RMS. The roughness of all the Virgo substrates, polished by the American company General Optics, was found to comply to the requirement (< 0.5 Å RMS).

The scattering level depends not only on the Rayleigh diffraction, which is linked to the surface roughness, but also on the number and the size of the point defects on the surface. To detect small defects (detection threshold $\varnothing 0.3$ µm) a prototype based on the profilometer was developed. It is possible to check the substrate surface quality (maps on $\varnothing 400$ mm) and also the substrate cleaning procedure, which is a crucial part of the deposition process. Small defects (between 0.3 and 1 µm), larger defects (> 1µm) and scratches are distinguished.

7.5.4 The Virgo large mirrors

The Virgo interferometer uses six large mirrors, as shown in figure 44. The substrate and coating specifications are listed in the previous tables. The first set of Virgo mirrors was ready in June 2002. Figure 53 shows a Virgo mirror in its characterization mounting.
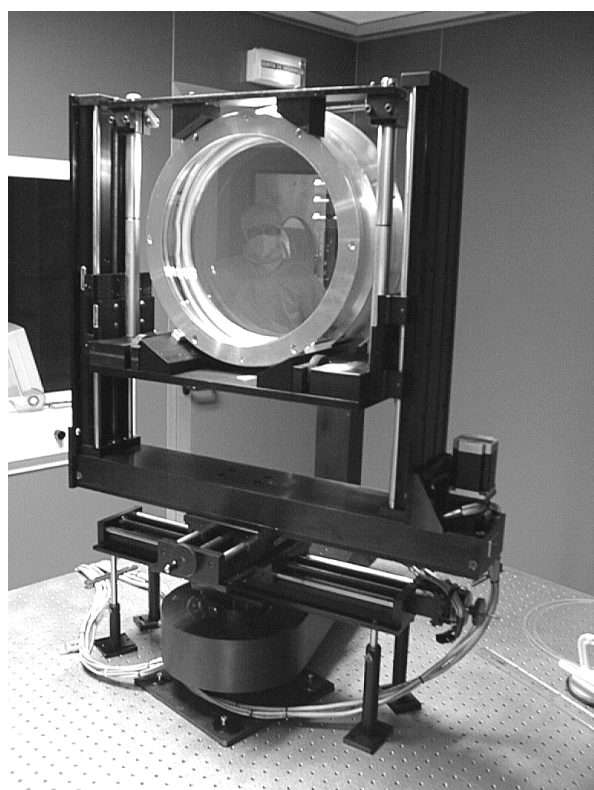

Figure 53. First Virgo End Mirror during the scattering measurement.

Measured optical performances of the large mirrors							
	Coating Nature and Clear aperture (mm)		RMS Wavefront (nm)		Average Absorption (ppm)	Average Scattering (ppm)	Transmission
	Side A	Side B	Side A	Side B			

North End Mirror	-	HR ∅330 mm	3.9 ∅150 mm	3.8 ∅150 mm	0.67 ∅150 mm	4 ∅150 mm	42.9 ppm
West End Mirror	-	HR ∅330 mm	2.8 ∅150 mm	3.4 ∅150 mm	0.69 ∅150 mm	6.5 ∅150 mm	38.3 ppm
North Input Mirror	HR ∅200 mm	AR ∅200 mm	2.6 ∅60 mm	3.8 ∅60 mm	1.25 ∅60 mm	5 ∅60 mm	11.80 %
West Input Mirror	AR ∅200 mm	HR ∅200 mm	2.6 ∅60 mm	2.5 ∅60 mm	1.20 ∅60 mm	8 ∅60 mm	11.66 %
Recycling Mirror 2006	HR ∅200 mm	AR ∅200 mm	1.4 ∅60 mm	1.08 ∅60 mm	0.54 ∅100 mm	8 ∅60 mm	5.13 %
Beam Splitter n°1	AR ∅210 mm	HR ∅210 mm	3.9 ∅100 mm	5.4 ∅120 mm	1.35 center	5.5 ∅100 mm	49.8 %

The absorption and scattering requirements (< 5 ppm) are satisfied for each component. The dispersion in the absorption values comes from the coating design: the higher the reflectivity the lower the absorption. Some scattering values are higher than 5 ppm, however inside most of the central area where the beam is more intense scattering was measured to be within the Virgo specifications.

Another remarkable result concerns the wavefront flatness of these large components. The "8 nm RMS on ∅150 mm" requirement on the wavefront is always satisfied. The limiting factor to reach the specifications is the substrate. Indeed, the RMS flatness value is the same with or without coating (3.37 nm RMS and 25.2 nm PV, 3.38 nm RMS and 25.5 nm PV respectively). The coatings reproduce exactly the substrate surface.

8. Overall Interferometer Control

8.1 Overall control

An apparatus like Virgo requires several control loops to reach and stay on its working point. Initially the various systems (mainly the injection system, the mirror suspensions and the detection system) are running and are being controlled in an autonomous way (see dedicated sections for details). In order to reach the interferometer working point the state of the various components will have to be steered in a global way. In its nominal running, two main feedback loops are active. The longitudinal control of the mirror positions (z degree of freedom as shown on figure 41) is achieved with the locking feedback loop. The alignment loop controls the transverse degrees of freedom (θ_x and θ_y on figure 41).

Figure 54 presents a schematic view of the different systems which are involved in the overall control of the interferometer:

- timing system (Section 8.1.2) which distributes a time reference over the site.
- DAQ system which collects all interferometer measurements. It is involved in the control loops as data provider for the Automatic Locking Procedure (ALP), Section 8.3.
- photodiode and quadrant readout (Section 7.4, figures 55, 56) which collects the photodiode and quadrant signals.
- suspension control (Section 6.6) in charge of the actuation on the mirror.
- laser and injection control (Section 7.2.4),
- Global Control (Section 8.2) which computes locking and alignment corrections
- ALP, which provides a set of high level commands to couple the different systems (see Section 8.3 for details).
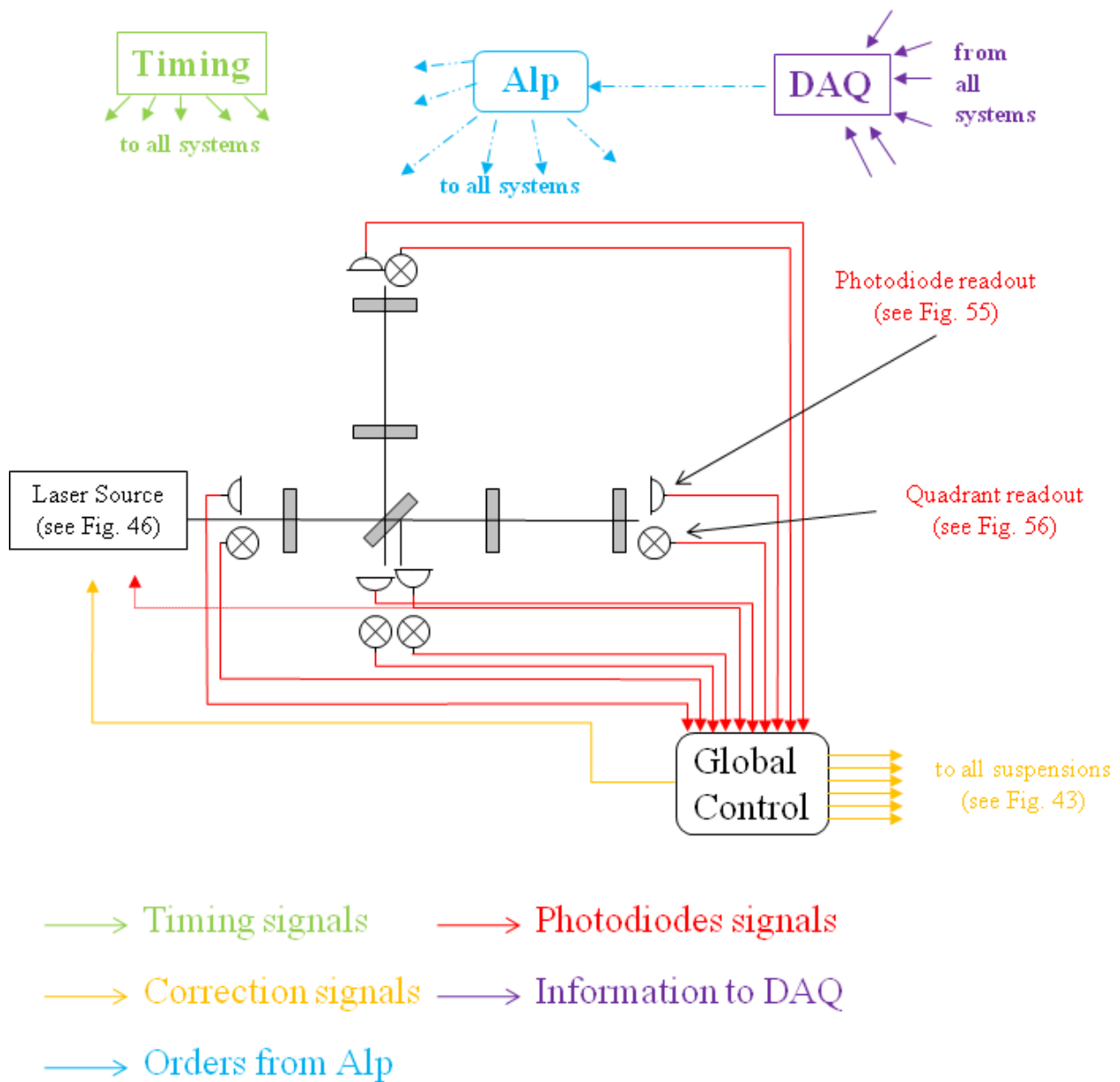
Figure 54. Overview of the systems involved in the overall control of the interferometer.

Photodiode

Preamplifier
2 Ω Decimation

DC   AC

Demodulation

Phase   Quadrature

Dynamics Reduction

Anti Aliasing

ADC   Digitisation

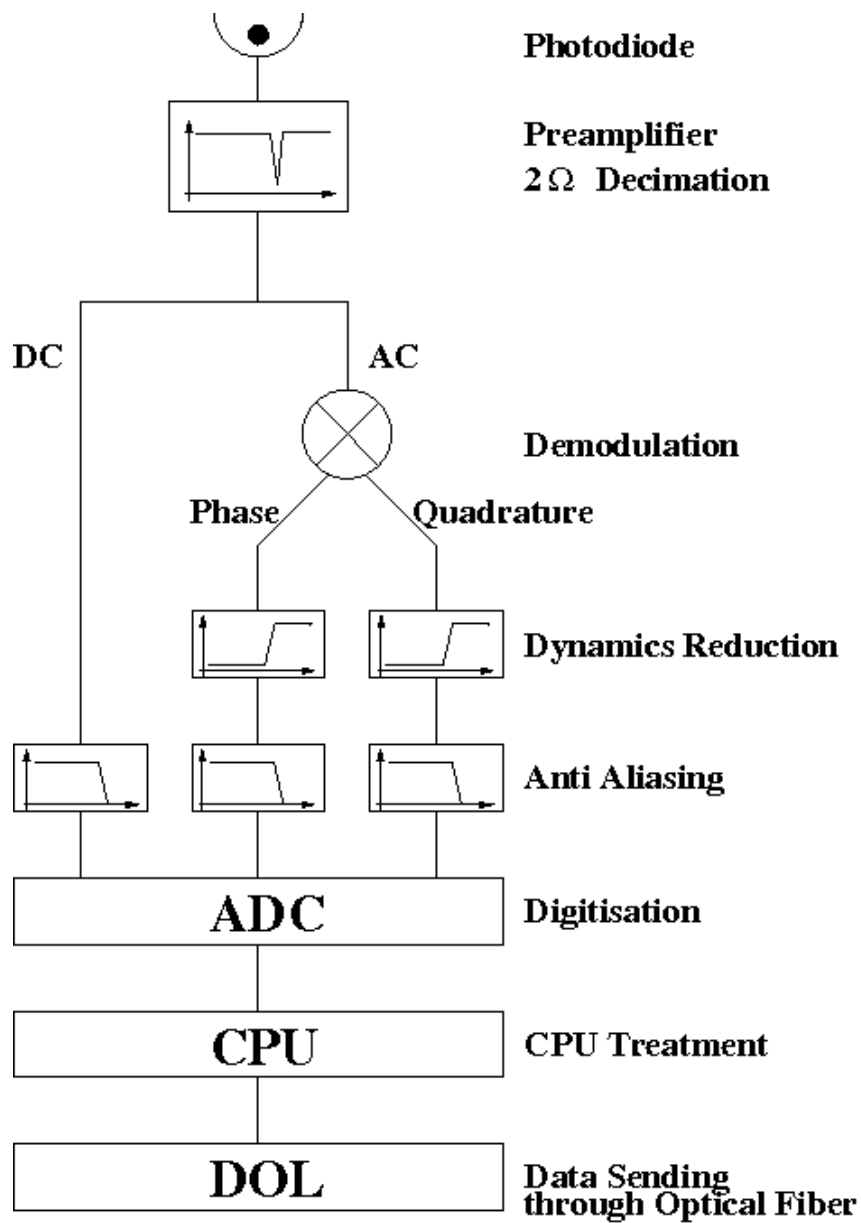CPU   CPU Treatment

DOL   Data Sending
through Optical Fiber

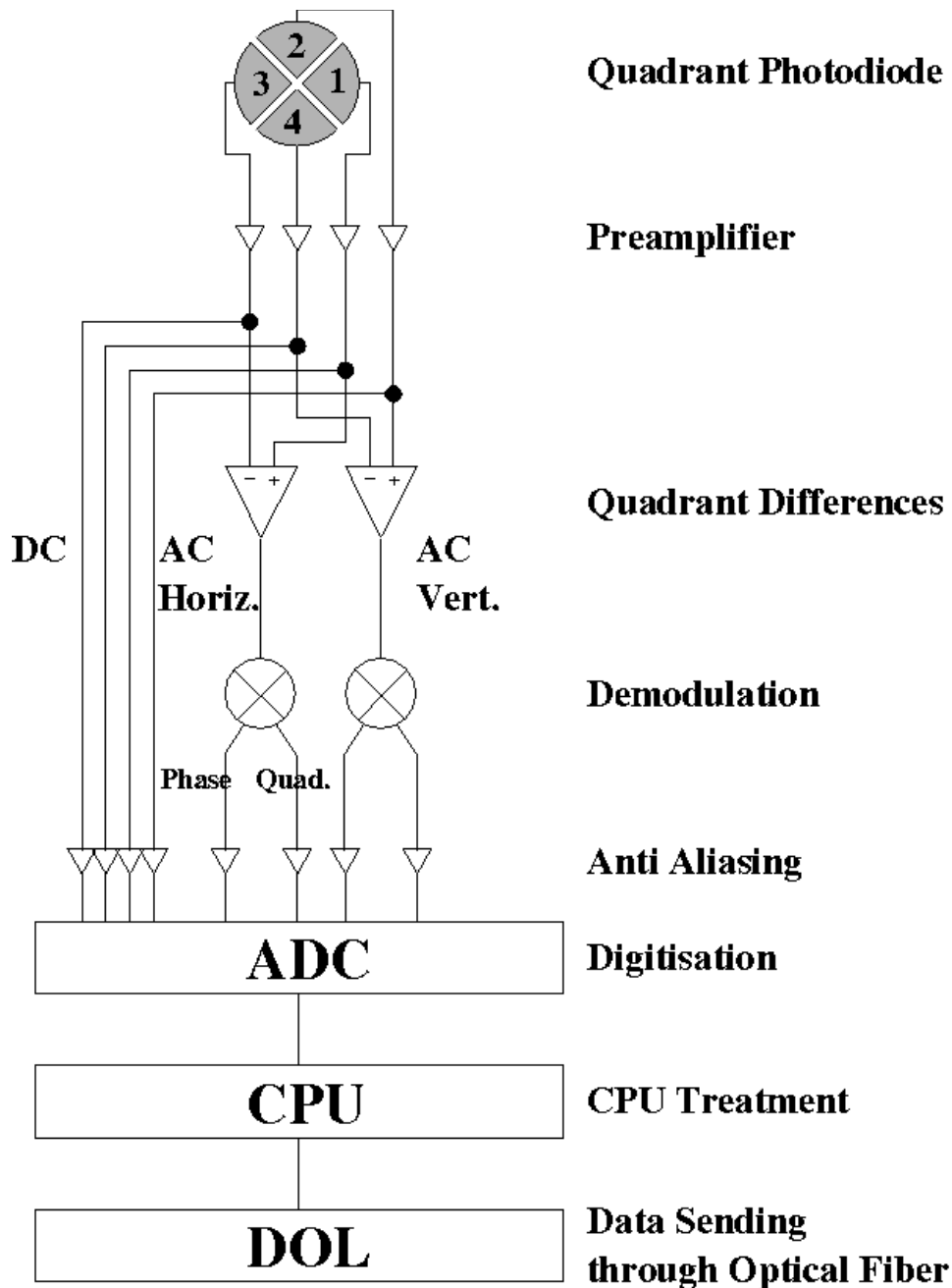Figure 55. Photodiode readout electronics.

Figure 56. Quadrant readout electronics.

The control system is implemented using digital servo loops. The locking loop runs at 10 kHz and the alignment one at 500 Hz. The overall synchronization is insured by the timing system described in Section 8.1.2 and the communication between systems is performed using Digital Optical Links (DOL) [70] (Section 8.1.1). Locking and alignment loops behave in a similar way. The photodiode signals (both DC and AC, Figure 44) are acquired by the photodiode and the quadrant readouts (for locking and alignment respectively) which send them to the Global Control. Using these signals, the Global Control computes the four lengths and the fourteen angles to be controlled. After appropriate filtering the Global Control sends to each mirror suspension the correction signal to be applied. At this level, depending on the state of the lock acquisition procedure, the corrections can be mixed with those coming from the local control system. This complex procedure is driven by the ALP which has access to the data collected by the DAQ system, allowing the determination of the interferometer status. When the science mode is reached, all mirrors are controlled in a global way and almost all the local control loops are switched off as they are noisier than the global ones.

8.1.1 The hardware environment

Virgo decided to use the VME and VSB standard for the boards dedicated to the online system. The standard CPU for Virgo is the RIO8062 from CES [67], based on the PowerPC 604 chip from Motorola. This board has been chosen for its good interrupt time response and its block transfer capabilities on VME and VSB [68]. The Virgo operating system is LynxOS [69], a UNIX-compatible real-time operating system for embedded applications. The version used is v2.5.1.

The various sub-systems of Virgo (Photodiode Readouts, Suspensions, Frame Builder, Global Control) exchange only digital data through optical fibres connected to a DOL dedicated board. The DOL board is a VME/VSB slave module which is able to send a small number of data (some kBytes) in point to point mode, over long distances (up to 3.2 km), with no latency. Moreover, powering off of the receiver DOL will not affect the transmitter DOL which allows a decoupling between the sub-systems. It is designed with 2 channels: one to send data, one to receive data which are completely independent. On each channel, a FIFO buffer takes care of the asynchronous operation between the optical link and the local bus of the board. The chosen FIFO buffer depth is 512 32-bit words for the transmitter channel and 512 or 16K words for the receiver channel.

8.1.2 The Timing System

In order to perform the feedback loops, to insure the coherence between acquired data all over the site, a central timing is needed to synchronize all Virgo sub-systems. This is achieved with a master clock driving a set of timing boards. The master clock is derived from a GPS system located in the control building [71]. Clock signals are distributed by optical fibre links to the different buildings (up to 3.2km away) where a local timing board converts them to TTL signals and VME bus interrupts for local use. The data, sampled at a frequency of up to 20 kHz, receive from these signals a time stamp with an accuracy of 1μs [72].

8.2 Global interferometer control

Virgo needs an active control of the positions of the suspended optical components, keeping the detector on its working point. The constraints are about 10^{-12} m RMS for the longitudinal control ("Locking") and 10^{-9} rad RMS for the angular degrees of freedom ("Alignment"). The dedicated hardware and software system named Global Control [73] is in charge of the locking and the alignment feedback loops. This system has been designed to provide a flexible tool for the integration of the various algorithms needed for the control of Virgo.

The locking feedback loop runs at 10 kHz and one of its major constraints is to be perfectly synchronized at this frequency. Any uncontrolled jitter or delay can introduce instability in the feedback loop. The Global Control receives through the DOLs the digitized photodiode signals and computes the mirror position deviation from their optimal working point. The associated corrections are sent to each suspension control system to bring the mirrors back to the right position. The alignment feedback loop runs at 500 Hz and is similar to the Locking one.

In order to fulfill the timing constraints and insure a perfect synchronization, two dedicated boards have been built. The first one, the Transparent Memory Board (TMB), allows a fast access to the optical fiber boards in write and read mode. It also avoids the use of interrupts for the synchronization, which are a source of uncontrolled delays. The second board, the Spy Data Board (SDB), is dedicated to the supervision of the processor running at 10 kHz. It gets a copy of all data exchanged at 10 kHz and delivers them to the monitoring machine.

The Global Control hardware is divided in three parts as shown in figure 57:
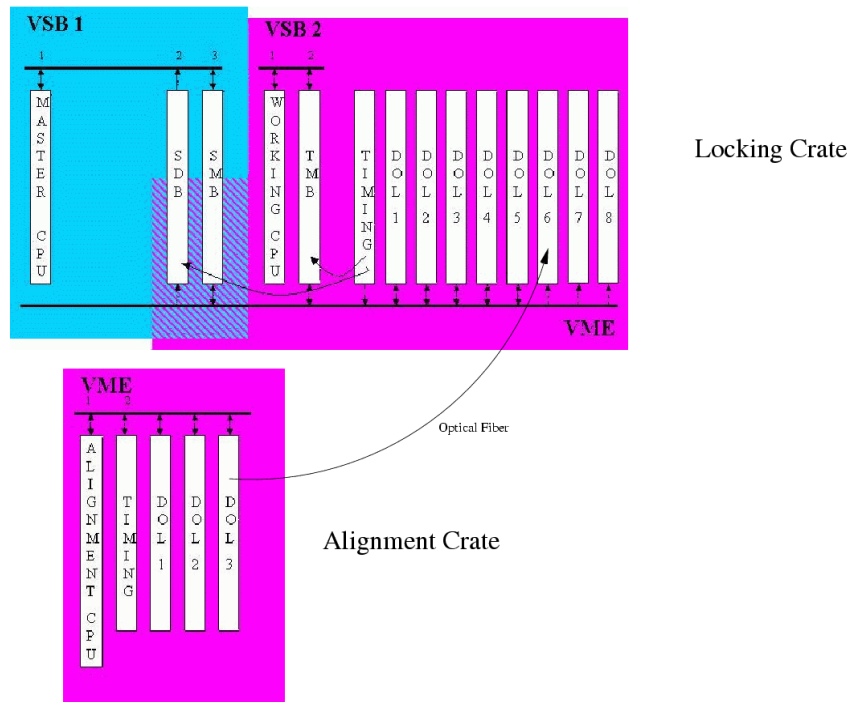
Figure 57. Schematic view of the Global Control crates.

a crate housing the hardware dedicated to the locking feedback loops, a second crate for the alignment control loop and a workstation monitoring the system.

The first crate is dedicated to the locking activities and the distribution of the correction signals. The second crate handles the alignment loop. In order to send the Alignment corrections to the suspensions, a DOL connects the locking and alignment crate. The two components of the locking part are the ''working'' CPU synchronized at the locking frequency and the ''Master''. The latter steers the working part and transfers data for monitoring purposes. When synchronized at 10 kHz, the CPU housing the locking process is isolated from the network and communications go through a dual port VME/VSB Shared Memory Board (SMB).

The alignment CPU uses the VME bus to access the DOL boards. The synchronization is performed using a VME interrupt generated by the timing board.

A general purpose CPU has been chosen for the implementation of the control algorithms: this solution gives the best flexibility for the design of the feedback loops. In particular, the length reconstruction needs powerful algorithms requiring many mathematical operations that change during the lock acquisition process. The algorithms are split in three parts: sensing, filtering and driving. The Sensing part converts the photodiode signals in lengths and angles, the filtering part applies in the time domain the correction filters to the quantities computed by the sensing. In the driving part for locking, the various feedback signals are distributed to the relevant mirrors according to the driving matrix given by the user. This algorithm division has been chosen to allow switches between different versions of a given task without modifying the others. For example, it allows to change on the fly the length reconstruction procedure (from a lock acquisition to a lock maintaining algorithm for example) while keeping the same filtering.

All free parameters of the algorithms (optical gains, filter characteristics, trigger thresholds, etc.) are stored in the Virgo on-line data base. This allows the user to easily change the behaviour of the algorithms without modifying the C++ code. In addition, the full history of parameter changes is stored in the data base leading to an efficient recovery of previous configurations. Some parameters can also be modified on the fly without stopping the 10 kHz loop.

For both locking and alignment, the algorithm part of the code has been isolated in dedicated libraries which can also be used offline on recorded data or connected to SIESTA [74], the simulation program in the time domain developed for Virgo. This feature allows the complete development and test of

an algorithm on an offline workstation without perturbing the current version running in the online chain. In this case, the developer is not limited by real-time constraints and can use powerful tools to debug its code. It should be underlined that the connection with SIESTA is a major improvement of the algorithm reliability as the algorithm runs offline in conditions as close as possible to the real ones. This feature really improved the efficiency of the locking activities.

8.3 The Automatic Locking Procedure

The working point of the detector is reached and maintained using elaborate procedures, built on two levels:
- a real time and fast automation layer directly implemented at sub-system level, involving local and global control, with a bandwidth up to 10 kHz;
- a control and monitoring automation layer using the data coming from the DAQ channels to drive the different phases of the locking procedure.

The interaction between the two levels is implemented via the Virgo inter-process communication protocol Cm using DAQ channels.

The software developed for the control and monitoring level has a server architecture.

The basic concept is to use the data acquired by the DAQ and to compute on a standard workstation the state of any subsystem by processing the data from the relevant channels. According to the subsystem state, actions can be performed using system calls or directly with messages in Cm format (Figure 58).
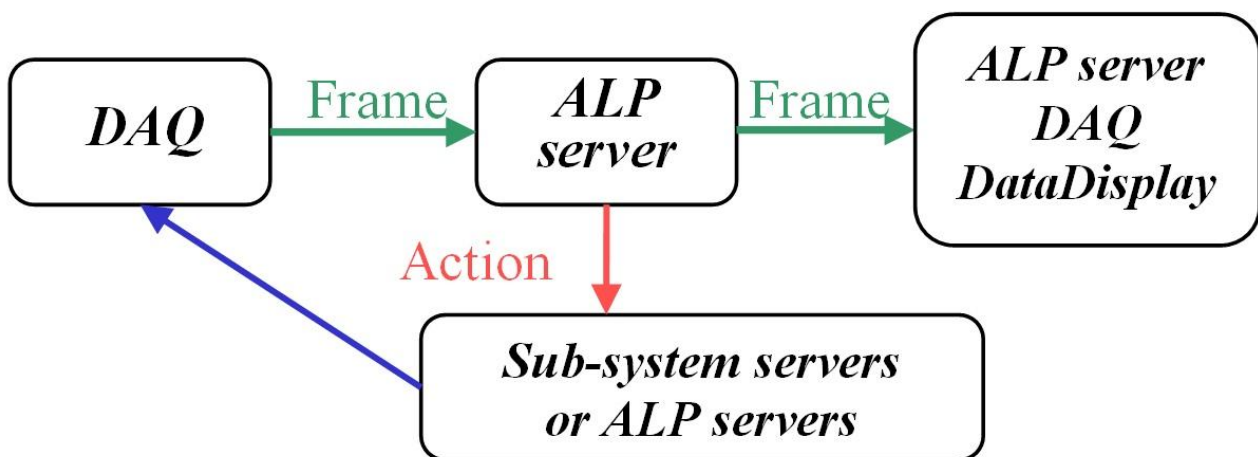

Figure 58. ALP simplified architecture

The ALP server uses the DAQ framework to access the data and to report on the performed actions. It uses a script programming language. It is possible for example to create internal variables, compute signal statistical properties in the time domain (mean, min, max, rms, range) or in frequency domain (FFT, RMS in a frequency band, coherence, …) to perform the lock acquisition.

In order to better distribute the computational load and to provide a clean hierarchical organization (subsystem-linked) to the different automation tasks, an automation architecture based on a Master and several ALP servers has been developed.

The overall automated procedure consists of two main sequences:
- *Pre-alignment sequence*. In this procedure the alignment of the beam in the N and W cavities is performed and the long optical cavities are tuned to resonance
- *Alignment/Locking/Noise Reduction sequence*. This procedure allows to fully lock the interferometer along the longitudinal degree of freedom and introduces all controls for low noise operations.

After having applied the main lock acquisition algorithm (called Variable Finesse [75]) it activates the angular drift control and the alignment control loop. It then tunes the Output Mode Cleaner. Next it undertakes actions aimed at lowering the control noise and finally it adds permanent sinusoidal signals to the different mirror corrections for calibration.

During the sequence execution and after its completion, a special macro, working in background, watches for any unlock event. In case of unlock, it brings the ITF to the lock acquisition pre-conditions, while avoiding further excitation of suspension motion.

This automation effort has been an important element in achieving a duty-cycle higher than 80 % during data taking. A typical locking sequence is shown in figures 59 a, b.
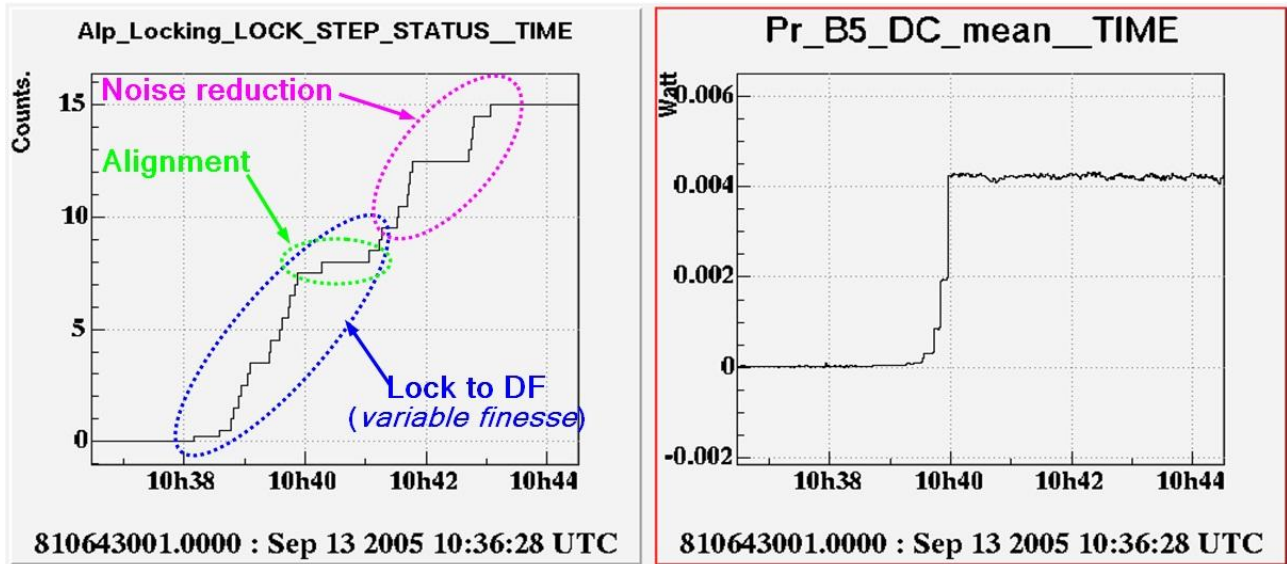

Figure 59. Left: locking status value transitions during the full sequence. Values correspond to the sequence step numbers. Right: power into the recycling cavity during the sequence evolution.

The risk of human error has been considerably reduced and the daily commissioning activities, where unlocking/relocking the ITF is often required, have been greatly simplified.

9. Environmental Monitoring

The environmental monitoring system of Virgo records all the physical parameters that can contribute or alter the response of the interferometer. In fact, due to the high sensitivity of the antenna and to the weakness of the expected signals, many external perturbations can influence the performances of the interferometer. The purpose of the environmental monitoring system is to generate vetoes against false gravitational wave signals in the data analysis phase. Such vetoes are based on the understanding of the noise generated by environmental factors.

The environmental monitoring system is composed by two main subsystems: the slow monitoring, also called Building Control, and the Fast Monitoring. The first one [76, 77] records slowly changing parameters with a sampling frequency of 1 Hz. The second subsystem [77] records physical quantities with a sampling frequencies of the order of some kHz. The actual sampling frequency depends on the characteristics of the probe being used. Actually the slow control subsystem manages the acquisition of several outdoor and indoor parameters: weather conditions, lightning events, rain, temperature, pressure and humidity.

The meteorological conditions are monitored using a commercial station, model Vantage Pro by Davis, equipped with an anemometer, a rain rate probe, a thermometer, an hygrometer and a barometer. These sensors are integrated in a single box placed on the roof of the central building of Virgo. The lightning detector is a commercial radio frequency detector, model LD-250 from Boltek, that is able to detect events and recognize them as strikes up to a distance of 400 Km. This device is also positioned on the roof of the central building. Both the weather station and the lightning detector are connected, using a standard RS-232 link, to the VME based master Building Control CPU.

The monitoring inside the Virgo buildings of the slow varying parameters, temperature, pressure and humidity, is performed using a highly modular and distributed acquisition system. The base element of this system consists of a commercial remote acquisition board, model TRS-56 from Tecnint, equipped with 16 12-bits ADC channels. Conditioning electronic circuits adapt the signal range to the ADC input range. The standard transmission protocol used, RS485, allows to connect in cascade several boards over a distance of 300 meters. The master board is a TVM-932A VME board from Tecnint which resides in a crate together with a main CPU collecting all the data and sending them to the acquisition system. Due to the slow acquisition frequency (1 Hz), no special synchronization is required to manage these processes. There is one such system serving the central and mode cleaner buildings and two other systems for each end building. The total number of slow monitoring probes, actually operational in Virgo is: 244 temperature, 11 pressure and 11 humidity probes, 1 weather monitoring station and 1 lightning detector station.

The Fast Monitoring subsystem, records physical quantities with a broader frequency band. The system is composed by mechanical vibration sensors, acoustic sensors and magnetic field sensors as listed in the table.

Environmental sensors			
Model	Physical quantity	Number of axes	Frequency band (Hz)
Kinemetrics MFS-06	Acceleration	3	0.1 – 200
Brüel and Kjaer 4378	Acceleration	1	0.1 – 3000
Güralp CMG-40T	Velocity	3	0.03 - 50
Brüel and Kjaer 4190	Pressure (Acoustic)	1	0.1 - 3000
Metronics MFS-06	Magnetic Field	1	4 - 10000

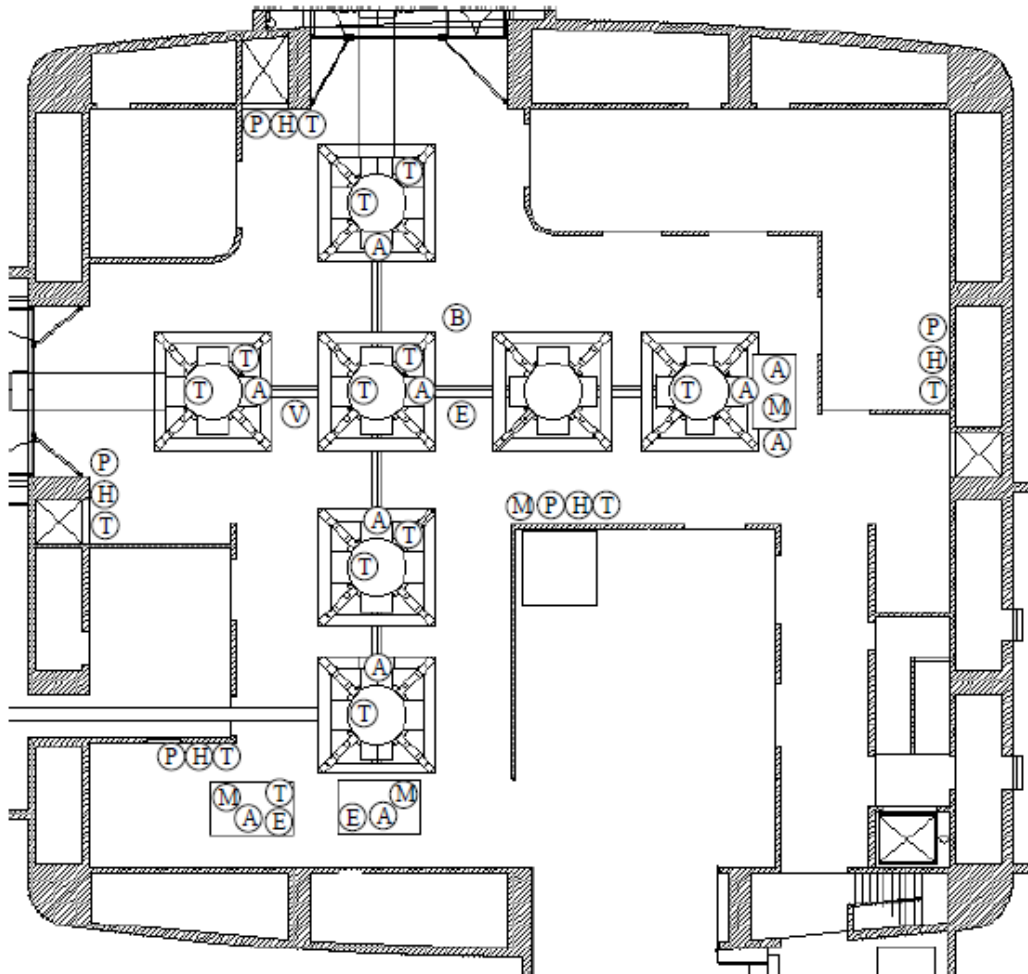The location of the various sensors is shown in figures 60 and 61.

Figure 60. Location of the various sensors in the Central Building. M: Microphone, B: Magnetometer, E: Episensor, V: Velocimeter, A: Accelerometer, T: Temperature probe, P: Pressure probe, H: Humidity probe.
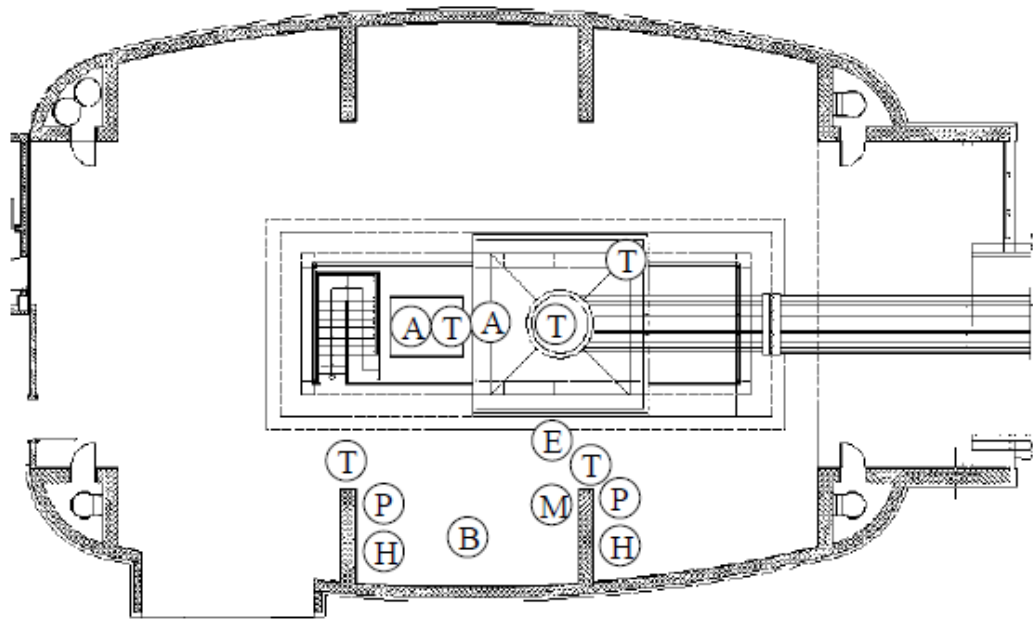
Figure 61. Location of the various sensors in the End Buildings. Same labels as in figure 57.

In particular vibration and acoustic sensors are located near the superattenuator base and on the optical benches. The mechanical vibration sensors are of three kinds. The first one consists of single axis accelerometers, model 4378 from Brüel and Kjaer, with a frequency band spanning from 1 Hz to 3 kHz. The second kind includes tri-axial accelerometers, working in the frequency range 0.1 to 200 Hz, model FBA ES-T from Kinemetrics. The last one is a tri-axial broadband velocimeter, model CMG-40T from Güralp, whose frequency band spans from 30 mHz up to 50 Hz. The acoustic sensors are microphones, model 4190 from Brüel and Kjaer, with a frequency band 0.1 to 3 kHz. Finally the magnetic sensors are broadband induction coil magnetometers, model MFS-06 from Metronix, with a frequency band from 4 Hz to 10 kHz.

All the fast monitoring probes are connected to the ADC's of the data acquisition system of Virgo [Section 10]. For microphones and single axis accelerometers a commercial amplifier, model Nexus from Brüel and Kjaer, is used, while home-made conditioning amplifiers are used for the remaining sensors.

The large number of probes used for the monitoring and their optimal positioning allows to understand several properties of the environmental noise on the site and to study its coupling with the Virgo interferometer [78,79].

10. Data acquisition and storage

10.1 Data Acquisition (DAQ)

The task of the data acquisition system [80] is to collect in a coherent way all the information needed for the validation of detector.data and gravitational wave signal extraction. Therefore it requires a site wide timing system to produce and record synchronously all the data, different dedicated readout systems or interfaces to the control servos distributed over the site, tools to format, transport and write the data on files and online monitoring tools to display the data or to analyse in real time the state of the detector.

The DAQ is a fundamental component of the Virgo control system, which is digital for a very large fraction. The timing system is the same as the one used to drive the controls (section 8). The digitized signals used by the servo loops are collected by the DAQ. This is achieved without introducing any disturbance or delay in the control loops.

One important requirement on the DAQ system is to be flexible and scalable in order to accommodate the evolution of the interferometer during the commissioning phase. In addition reliable continuous operation must be ensured during the whole lifetime of the experiment, while following technology progress.

10.1.1 Data acquisition choices

The high number of channels to be read out in Virgo requires a DAQ system able to sustain several MByte/s of data flux and a high data storage capacity with fast random access to the data. Further requirements are imposed by the distribution of the DAQ over the two 3 km arms. In addition, online control constraints require a latency of at most a few seconds between ADC readout and availability of data for display in control room. Finally, the production of several monitoring and trend data streams is needed to follow the state of the detector and to monitor the performance of the data acquisition system.

The number of channels has evolved according to the comprehension of the detector behaviour and the phases of the commissioning. The necessary flexibility has been achieved using modular hardware and software building blocks. Standard Unix-like workstations with a set of libraries and "plug-and-play-like" software tools compose the data acquisition system. Shared memories and Ethernet connections are used for communication. Some Virgo home-made basic libraries [81] are used to easily handle in a uniform way the configuration management, the online monitoring, the data transfer or the online access to the data. The same data format, called "frame" format [82], is used for data acquisition and online processing. It provides an easy way to store data as time slices of various lengths and to produce different data streams. This frame format has been adopted for data exchange between the various gravitational wave detectors around the world.

This modular data acquisition system has a three level structure: the front-end readout, the frame builder and the frame collector.

10.1.2 The front-end readout

The front-end readout processes are synchronized over the whole site using a timing system (Section 8) based on GPS signal with microsecond precision. Real time processors (RIO 8062 PowerPC) running under LynxOS manage the exchange of data with the electronics modules hosted in VME crates. These include ADCs, timing boards, DSPs, DACs, digital camera readout. Time critical data transmission is achieved using Digital Optical Links (DOLs) while other data are exchanged with an Ethernet connection.

10.1.3 The frame builders

These elements collect the data from the front-end readout and put them in frame format:
- *The Slow Frame Builder:* It collects the data sent through Ethernet by the Slow Monitoring Stations which provide data at a rate less than or equal to 1 Hz. Periodically, the timing system sends a message to the slow frame builder, Then the slow frames builder requests data to the various Slow

Monitoring Stations through Ethernet. Data are sent back as an ASCII string and are put in frame format. The slow frame builder sends periodically those frames to the frame collector.

- *The Fast Frame Builder:* It collects data sent through optical links by the front-end processors for photodiodes and suspensions sensors. The data are stored in the buffer of the reception DOL. The packets collected from various DOL's and stamped with the same frame number are merged in one second frames. A data compression algorithm reduces the size of those frames by a factor of about 2.5 in stable interferometer conditions.

- *Specific Frame Builders:* Some processes, in charge of specific actions (detection bench control, output mode-cleaner control, camera readout or the environment monitoring) read ADCs when receiving an interrupt signal provided by the timing system. Then they format the data in frames and send them directly to a frame collector.
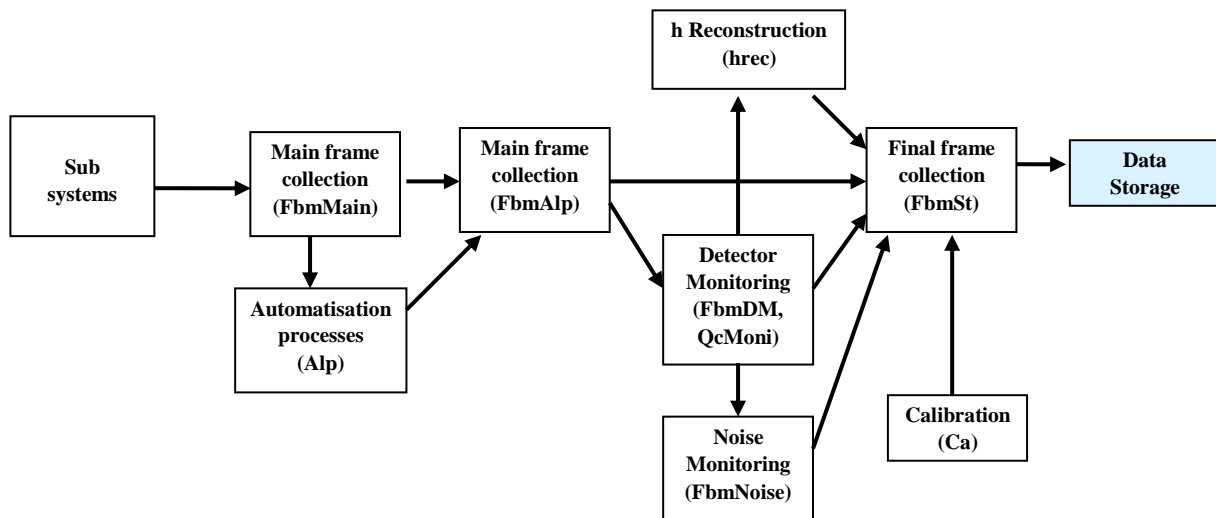
The Frame Builder architecture is shown in figure 62.

Figure 62. Frame builder architecture.

10.1.4 The frame collectors

Also named Main Frame Builders, they collect asynchronously the frames sent by the various frame builders and merge them into a single frame containing all the data acquired. Those data are then dispatched to the next stage of the DAQ pipeline using a shared memory. This mechanism allows for a fast and easy online access to the data. Several "consumer" processes can read this shared memory, each with its own channels selection, its own processing and its own output destination. All the frame collectors run on standard workstations under a Unix-like operating system.

Each main Virgo sub-system (suspensions, detection, injection and environment monitoring) has its own data acquisition line with the three data acquisition levels described above. This allows, when needed, an independent online access to the data of each sub-system through its frame collector. It also allows to distribute first level online processing tasks that consume much CPU power. At the output of the four data acquisition lines a final frame collector sends frames to the raw data storage and to the online workstations.

10.1.5 Raw data flow and latency

At the output of raw data collection, each frame (one second of data) contains about 7 MBytes of compressed data (about 18 MBytes per second if uncompressed). Fast Ethernet and Gigabit Ethernet networks with TCP/IP protocol are used to transmit these data down to the online displays programs, to monitoring processes and to the data storage. At this level, the data are available with a delay lower than 2 seconds.

10.1.6 Data streams

To complement the raw data stream as well as to provide summary information over long time segments, trend data with various sampling frequencies are produced. These are the streams of the 50Hz re-sampled data and one second and one minute trend data that contain also results of simple statistical analyses. These streams are produced online and stored on disk, providing information that now spans several years.

An additional data stream containing spectra of selected channels is produced to have fast access to information in the frequency domain (for instance to perform time-frequency plots over hours or days).

10.1.7 DAQ system monitoring

A graphical interface has been developed to control all DAQ processes. This graphical interface uses the Ethernet network and the Virgo basic libraries to provide both in the control room and on a web page the status of the DAQ processes (started or stopped, memory consumption, etc...). In addition to this interface, some trend data are produced within the DAQ chain to perform a statistical analysis of the DAQ system performance.

10.1.8 DAQ system performance

The main characteristics and performance of the DAQ system are the following:

Overall mean latency: 1.8 sec
Mean data flux: 30 MB/s (uncompressed)   8-9 MB/s (compressed)
Mean number of raw data channels: 1350
Mean number of trend data channels: 7600
Frame length: 1 s
Trend frame length: 1800 s
GPS time stamp precision: 1 µs

The channel sampling rate varies from 20 kHz to less than 1 Hz depending on the bandwidth of the measured physical quantity.

10.2 Online Monitoring

10.2.1 Data quality and Detector Monitoring

A set of monitoring programs provides information (mainly quality flags) tagging the time epochs when data are not usable for analysis. This information is also provided online in the control room and on web pages that show the status of the complete interferometer and its sub-systems, and possible operator action. A summary quality flag represents the overall detector status and can be used to prevent analysis in inappropriate conditions. In addition, a "Science Mode" flag is generated upon operator's request, when a

basic set of quality checks are fulfilled. These flags are recorded in the data frames so that they can be used in the data analysis as a first level veto.

10.2.2 Data Display

The Data Display is a program developed on purpose to provide an easy way to display data online or offline and perform some minimal data analysis. It acts as a digital oscilloscope and spectrum analyzer for the signals present in the interferometer. Histograms of signal amplitudes and basic statistical analysis are available. Channels can be combined to study coherence, correlation or to measure transfer functions. The Data Display can also be run remotely or on offline data and is a tool widely used for interferometer studies.

10.2.3 Web Monitoring

Relevant trend data are displayed on web pages using a tool that provides periodically updated plots for the main channels of each detector's subsystems, for the data acquisition or for online processing and data analysis: [http://wwwcascina.virgo.infn.it/MonitoringWeb]

10.3 Storage and data management system

The data storage has to comply with a continuous data flow of 8-9 MB/s, while being highly reliable to guarantee recording of rare astronomical events. In addition, due to the continuous tuning work on the detector, the most recent whole set of raw data (about 5 months) needs to be available for analysis on site. This results in the need for a total of 200TB disk storage farm, 146 of them reserved for the raw data circular buffer. The data storage must allow writing of data by the DAQ system, simultaneous access by users and continuous transfer to the computing centers (CNAF-Bologna and CCIN2P3-Lyon) which act as external data repositories. For archive and safety data are also replicated on tapes.

Data are written using dedicated systems of workstations and on-line buffers, while main user access is through the storage farm (off-line storage). The on-line and off-line storage systems are connected by a dedicated LAN and data are migrated asynchronously from the on-line buffers to the storage farm. From the storage farm data are then sent to the external computing centers where most of the analysis is performed. Figure 63 shows the general storage architecture.
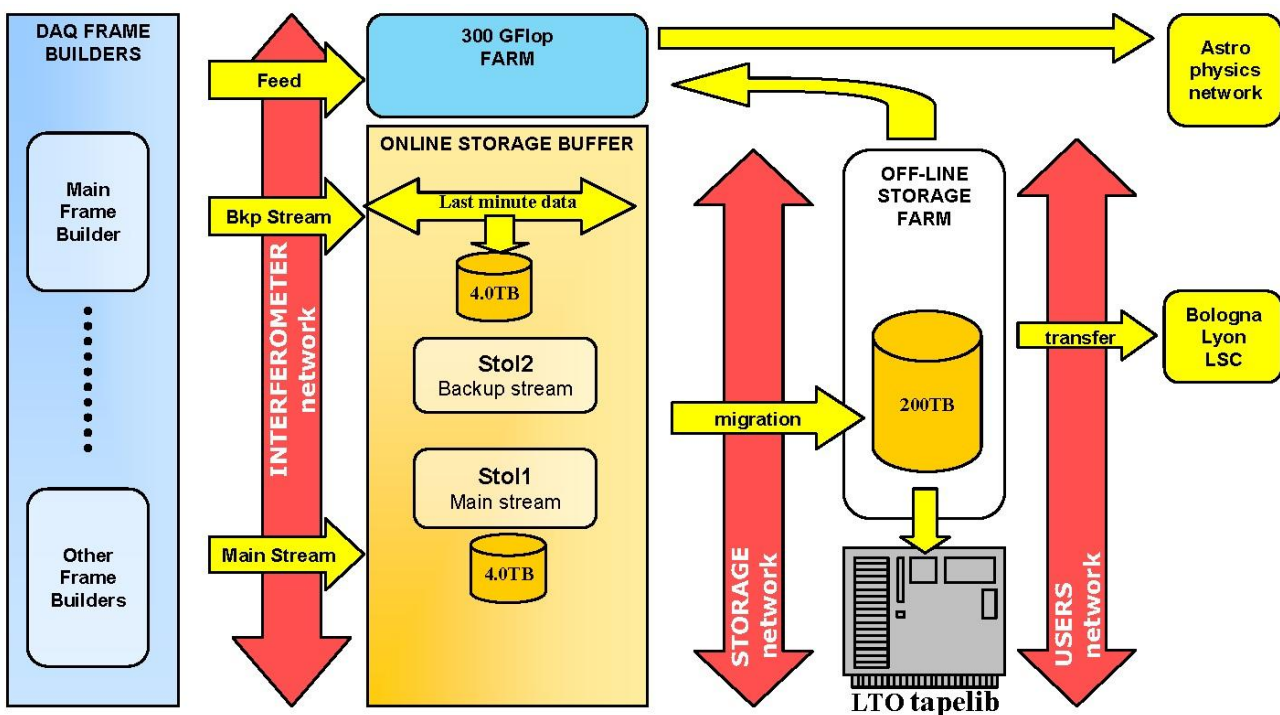
Figure 63. Storage Architecture.

10.3.1 On-line storage

For the raw data, i.e. nearly the total of the produced data, two identical streams are spilled from the Main Frame Builder and sent to two on-line buffers (*stol1* and *stol2*) over Ethernet connections. The buffers are two independent Linux servers where the DAQ clients write on directly connected storage arrays.

Stol1 is considered as the reference stream, therefore the storage is a fully redundant 4 TB FC-to-FC RAID5 high performance array with hot spare disks. It guarantees data buffering for about 1 week in case of failure of the downstream storage.

Data in *stol1* are not directly accessible by users. They become available once they have been migrated to the storage farm.

Stol2 is an identical server but with a FC-to-SCSI array of 4TB, its main purpose being to provide a redundant copy of the data in case *stol1* has some faults.

The *stol2* server exports data directly to user's network via NFS, giving a direct access to the last minute data.

Data sampled at 50Hz and trend data are written on another non redundant server (*stol3)* with 2TB of local disk space. That kind of data is replicated to a dedicated off-line storage area for archiving. These archives are also sent to the remote repositories. .

10.3.2 Off-Line Storage

The storage farm is composed of 10 Linux servers connected to a 200 TB Storage Area Network with a mixed technology with a maximum read/write speed of 2 GB/s. The disk area is seen by the local users as NFS volumes of 1 TB each that can be accessed at the speed of 40 MB/s.

A pool of backup clients run directly on the storage farm's servers and save the raw data files to a 200TB tape library with LTO Ultrium2 tapes. The tapes are vaulted at a rate of 10 tapes per week and put on shelves for crash recovery of the storage farm volumes.

The tape library uses 3 tape drives even if 1 drive is nominally capable to sustain a data transfer rate of 80MB/s.

10.3.3 Computing Farm

The in-time Data Analysis algorithms for triggers and noise monitoring run on a 96 nodes computing farm with a total of 320 CPU cores with aggregated capacity of more than 300 GFlops. The nodes are based on the AMD Opteron processor architecture which proved effective in the SIMD (single instruction, multiple data) computation common to many GW data analyses [83].

The architecture has been optimized for direct on-the-fly feeding from the frame builders via TCP connections and distribution on the internal gigabit interconnect network, but data on the storage farm can be accessed too, allowing computations over longer time windows.

All the nodes are functionally independent to allow different analysis pipelines to run without a centralized batch scheduling system, only the Scientific Linux base platform configuration is managed centrally

10.3.4 Data Management

The absence of a single virtual file system where data can be placed irrespectively of the physical storage and the possibility of hardware failures requires a special software to move the data in a safe way from the on-line buffers to the storage farm (where most recent data are stored in a circular buffer) keeping track of the files position and replicas.

The storage nodes keep track of local files while a global placement map of migration status and volumes availability is maintained. The information about files location and frames content is written in a Frames File List (FFL), which is the common format used by the software applications to locate the data.

The software also selects the best replica available on the on-line storage comparing the two raw data flows, then moves the data to the offline buffers (deleting the oldest files when needed) and schedules them for the tape archiving and for the data transfer to the remote repositories.

The data archive (the entire off-line storage) is exported to user's network via an NFS directory structure handled by an automounter daemon.

10.3.5 Data Transfer

The data transfer architecture involves two dedicated servers (*datagw* and *dataldr*) that see the off-line storage farm as a set of NFS volumes.

The *dataldr* machine is remotely controlled and handles the exchange of data with the LIGO Scientific Collaboration using the LDR software, reading files directly from the off-line storage and saving the incoming data into a dedicated buffer (7TB).

The *datagw* machine takes care of the replica to the remote repositories in the national computing centres of Lyon and Bologna, it hosts some software procedures, integrated with the data management software, that handle the replica to process by means of two different engines (*bbftp* for Bologna and *SRB* for Lyon) that match the different architectures available locally at repositories [84].

It also produces a detailed log for all operations performed and the metadata file (the Frame File List) for both destinations, based upon information stored in a local mySQL database.

11. The Virgo Effective Sensitivity and On-Line Strain Computation

This last chapter shows how the Virgo spectral sensitivity to gravitational wave signals is obtained from the apparatus described in this paper; this needs a precise calibration of the detector considered as a whole, once each specific subsystem has been characterized.

Using the important on line computing power and data storage available on site, this sensitivity can be computed nearly in real time during the running periods, allowing to check the noise status of the instrument and to act quickly if problems are detected.

The instantaneous strain output of the detector, called "h reconstructed" is computed from the dark fringe signal and the calibration. This is the main output of Virgo; it is computed and written on each frame before final storage.

11.1 Detector calibration

The precise recording of a gravitational wave signal based on the relative elongation of the arms requires an accurate calibration of the interferometer response to mirror motion.

Since the ITF is controlled, the mirror motion is reduced compared to the one that should have been induced by the gravitational wave. It is thus necessary to take into account the mirror displacement due to the control signals also. Therefore the calibration consists of two tasks:

- To measure the mirror displacement due to a given control signal in order to obtain the transfer function for each mirror actuator.
- To measure the effect of a differential arm elongation on the dark fringe signal to compute the detector response to gravitational waves.

11.1.1 Mirror actuator transfer function

The procedure to measure the mirror actuator transfer function (TF) is based on the distance between interferometer fringes, determined by the laser wavelength. Due to the high force required this can only be performed using coil drivers in High Power mode (HP). The Low Noise (LN) channel of the coil driver is then calibrated electronically.

First, data are taken with the ITF in free swinging Michelson configurations. Sinusoidal signals (zCorr) are sent to the mirror actuators with the coil driver set in HP mode. In such configuration, it is possible to extract the mirror movement ΔL from the uncalibrated dark fringe signal directly. The ratio $\Delta L/\text{zCorr}$ is the mirror actuator TF in HP mode at each line frequency measured in m/V. Such measurements are done from 5 Hz to 1 kHz on the beam splitter and arm mirrors.

To convert the actuator TF from HP to LN mode white noise is sent to actuator. The current flowing in the actuator coil is measured as a voltage across a resistor with the coil driver in HP and LN mode. This allows to compute the mirror actuator TF in LN mode.

Since the mirror position is partially controlled by the marionette a measurement of the related TF is required. Measurements in the free swinging Michelson configurations are not sensitive enough above a few Hz. The measurement is thus done with the fully locked ITF. The ITF response to an unknown differential arm elongation (10Hz – 100Hz band) sent through the marionette actuation is compared to the response to a known differential arm elongation sent through the calibrated mirror actuation [85].

11.1.2 Virgo transfer function and sensitivity

The Virgo transfer function describes the effect of a differential arm elongation in meters onto the dark fringe intensity in Watt, in the range 10 Hz to 10 kHz. It is measured by injecting white noise from 10

Hz to 1 kHz on the NE or WE mirror actuator and measuring the dark fringe signal. From the mirror actuator transfer function the injected white noise in Volt can be converted into a mirror displacement in meters ΔL. The ratio between dark fringe intensity variation and ΔL is a measurement of the Virgo TF up to 1 kHz. Above that frequency the Virgo TF shape is determined by the 3 km cavity pole behaviour. The pole frequencies have been measured to be at 500 Hz within a few percent.

The displacement sensitivity in m/Hz$^{1/2}$ is obtained multiplying the dark fringe noise linear power spectrum in W/Hz$^{1/2}$ by the Virgo TF in m/W. The strain is obtained dividing the result by the arm length. The best sensitivity, obtained during November and December 2009 is shown in figure 64, together with the design sensitivity.
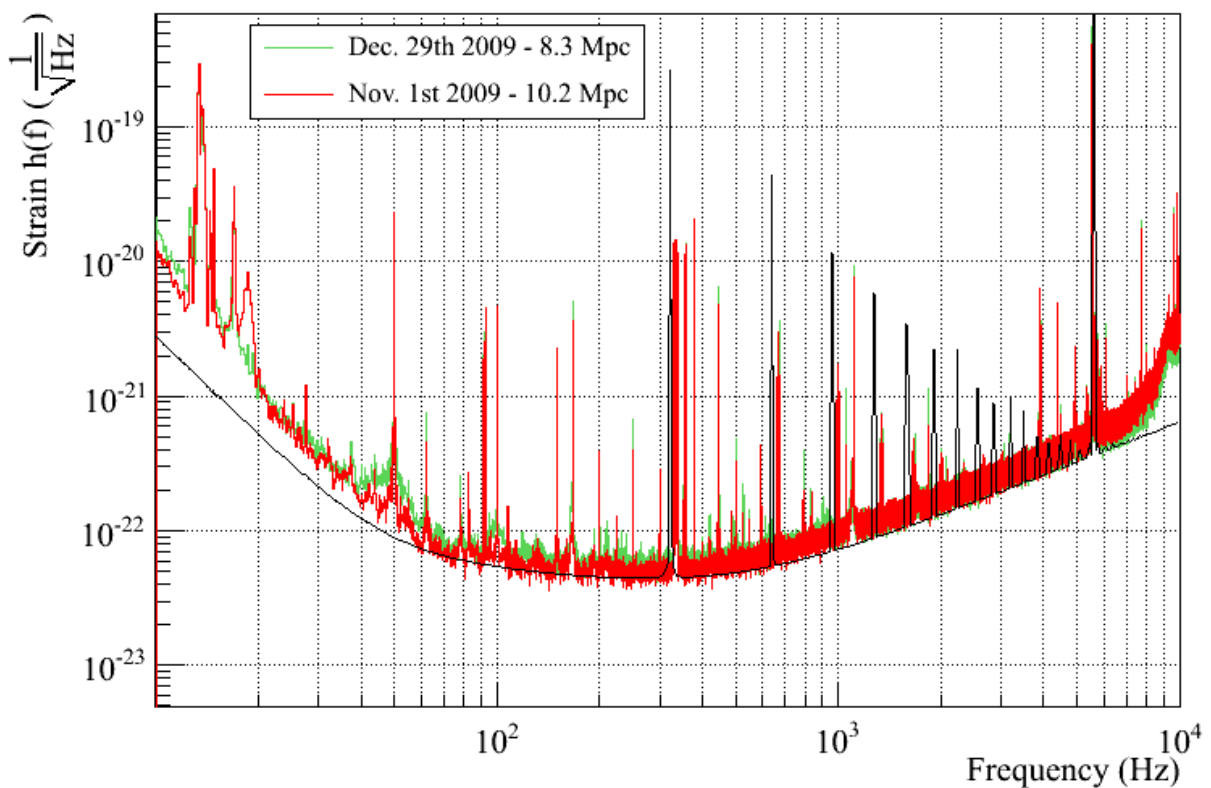

Figure 64. Virgo sensitivity in November 2009 (red), December 2009 (green) and design curve (black).

11.2 On Line Preliminary Analysis

The on-line computing capability on site has been designed for several tasks to be performed on the data as soon as these are acquired. Different algorithms have been written, some of them for data conditioning, such as down sampling. The crucial task of h-reconstruction is also performed, allowing to check immediately the instrument sensitivity and to identify anomalous noise. To monitor the time stability of the detector sensitivity for frequencies between 70 Hz and 1300 Hz (frequency of the last stable orbit for inspiralling neutron stars) the "horizon" is computed online. This quantity is defined as the largest distance at

which a typical binary neutron star inspiral event can be detected by Virgo with a signal to noise ratio equal to 8. Average is taken over all possible orbit orientations and source positions in the sky. The inputs for this calculation are the noise spectrum and the expected waveform [86]. Figure 65 shows this averaged horizon (range) during the second part of 2009 (August to December).
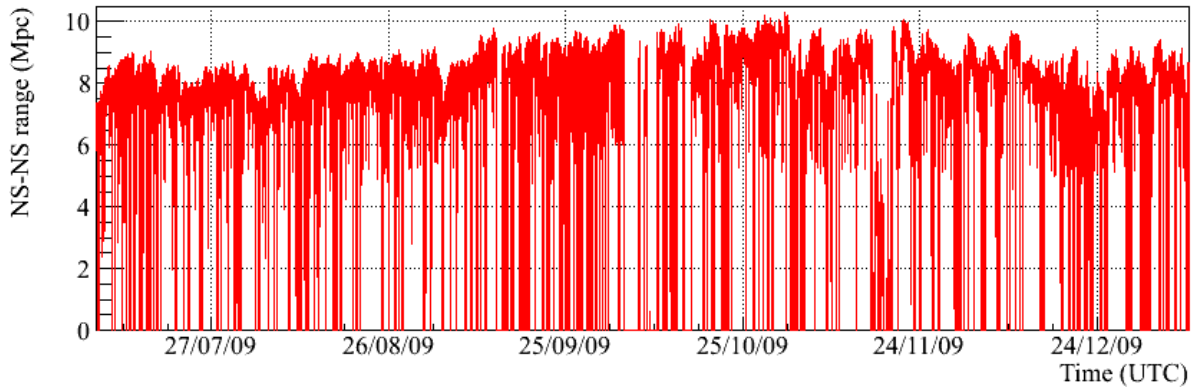

Figure 65. Binary neutron star averaged horizon (range) from August to December 2009. The variations are mainly due to weather conditions and control noises.

Finally algorithms are being designed to detect on line hints of possible event candidates by looking for transient signals from expected sources such as inspiralling binary systems and stellar core collapses (details of possible methods can be found in [87,88]). It is planned to send these signals as triggers to the astrophysic network of detectors.

The final data analyses, that require a huge computing power, are performed offline in the large computing centres.

12. Conclusion

Given the very stringent and mandatory technical constraints, the realization of the Virgo interferometer was a real challenge. Nevertheless, all these difficult constraints have been met. The longest and most difficult task was to control the long cavity length to better than 10^{-15} meter (rms), mirror angles to better than 10^{-9} radian, while achieving a mirror position noise of $2\ 10^{-19}$ m Hz$^{-1/2}$ at 150 Hz.

The present achievement of the Virgo detector leads to a sensitivity very close to the design for frequencies above 100 Hz, putting Virgo among the best GW detectors. Below 40 Hz, Virgo is by far the most sensitive detector, almost at its design sensitivity. Reliability has also been demonstrated and several months of data for GW searches have already been collected.

Nevertheless even if the present sensitivity represents an enormous progress with respect to previous detectors, the latest astrophysical predictions for the detection rate are still low. However measuring wave amplitude rather than energy, the former decreasing as *1/R* , allows to profit of even the smallest improvement in sensitivity. A reduction of a factor 2 in the noise floor allows exploring a volume of universe 8 times larger, increasing the detectable source population by about the same factor. An upgrade program is the obvious consequence of these considerations.

The commissioning of the Virgo detector has shown that the physical principles underlying it are well understood and that after removing remaining technical noises, the sensitivity is going to be determined by the fundamental noise sources: shot noise, thermal and seismic noise. By having chosen to use superattenuators Virgo will be able to decrease seismic noise down to the limit imposed by fluctuations of the gravity gradient at low frequency. Further improvements in that direction require probably to locate the detector underground. On the other hand upgrades of the detector can reduce shot noise, by increasing the power of the light source, and thermal noise, by using different materials, like silica, for the mirror suspensions.

The first Virgo upgrade (called Virgo+) includes the increase of the laser power up to above 50 Watts, coupled with the introduction of a system of thermal compensation to homogenise the temperature distribution on the large input mirrors; this is completed with an infrared radiation curvature correction system. The second improvement is the use of silica fibres to suspend the mirrors. This first step seems to be quite efficient for reducing the thermal noise, improving the sensitivity especially at low frequency (20-60 Hz). Finally, increasing the Finesse of the cavities from 50 to 150 completes these improvements. The detector has been run with these modifications during the last months, and a forthcoming paper will detail all of them, together with the analysis of results.

The second step of upgrade, called Advanced Virgo, will include major changes, mainly in the optical scheme, introducing a signal recycling mirror and increasing the laser power up to 200 W. The foreseen changes would result in an increase of the sensitivity of one order of magnitude in the whole detection band. The accessible universe volume should then be increased by a factor of 1000, as compared to the Virgo design. We would then expect a detection rate of at least a few events per year.

References

[1] A. Einstein, *Näherungsweise Integration der Feldgleichungen der Gravitation, Sitzungsberichte der Preußische Akademie der Wissenschaften* (1916) part 1, 688

[2] R.A. Hulse and J.H. Taylor, *Discovery of a pulsar in a binary system, The Astrophysical Journal* **195** (1975) 51

[3] J. Weber, *Detection and generation of gravitational waves*, *Phys. Rev*. **117** (1960) 306

[4] E. Amaldi. et al., *First gravity wave coincidence experiment between resonant cryogenic detectors - Louisiana-Rome-Stanford, Astron. Astrophys.*, **216** (1989) 325

I. S. Heng, D. G. Blair, E. N. Ivanov, M. E. Tobar, *Long term operation of a niobium resonant bar gravitational wave antenna, Phys. Lett*. A **218** (1996) 190

L. Baggio et al., *3-Mode Detection for Widening the Bandwidth of Resonant Gravitational Wave Detectors*. *Phys. Rev. Lett.* **94** (2005) 241101

[5] C. Bradaschia et al.: *VIRGO: proposal for the construction of a large interferometric detector of Gravitational waves*, CNRS-INFN, unpublished (1989)

[6] B. Abbott, et al., *Detector description and performance for the first coincidence observations between LIGO and GEO*, *Nucl. Instr. Meth. Phys. Res.* A, **517** (2004) 154

[7] B. Willke, et al., *GEO600: status and plans*, *Class. Quantum Grav.* **24** (2007) S389

[8] R. Takahashi et al., *Operational status of TAMA300 with the seismic attenuation system (SAS) Class. Quantum Grav.* **25** (2008) 114036

[9] D.G. Blair et al., *The Science benefits and preliminary design of the southern hemisphere gravitational wave detector AIGO*, *J. Phys.: Conf. Ser.* **122** (2008) 012001

[10] H. Araújo et al., *LISA and LISA PathFinder, the endeavour to detect low frequency GWs*, *J. Phys.: Conf. Ser*. **66** (2007) 012003

[11] R.W.P. Drever, *Gravitational Radiation,* Les Houches Summer Institute (1982)

[12] G. Rupschus, R. Niepraschk, K. Jousten, and M. Kühne, *Detection of small pressure pulses in an ion pumped ultrahigh vacuum system, J. Vac. Sci. Technol*., **A12** (1994) 1686

[13] S. Braccini et al., *Test of Virgo prototype vacuum system*, *Vuoto,* **23** (1994) 41

[14] P. Marin, M. Dialinas, G. Lissillour, A. Marraud, A. Reboux, *Outgassing performances of an industrial prototype tube for the Virgo antenna*, *Vacuum,* **49** (1998) 309

[15] V. Brisson, J. Hoang, G. Lissilour, P. Marin, A. Reboux, M. Bernardini, A. Pasqualetti, *Ultra-high vacuum qualification of the prototype module for the 2×3 km arms of the VIRGO interferometer*, *Vacuum*, **60** (2001) 9

[16] M. Bernardini et al., *Air bake-out to reduce hydrogen outgassing from stainless steel*, *J. Vac. Sci. Technol*., **A16** (1998) 188

[17] M. Dialinas, Virgo Note, unpublished, VIR-NOT-LAL-1390-083, (1997)

[18] M. Bernardini et al., Virgo Note, unpublished, VIR-SPE-PIS-3100-106 (1998)

[19] A. Reboux, Virgo Note, unpublished, VIR-MEM-LAL-3100-166, (1999)

[20] V. Dattilo, Virgo Note, unpublished, VIR-TRE-PIS-4600-145 (1998)

[21] J.L. Beney et al., Virgo Note, unpublished, VIR-TRE-PIS-3400-159 (2000)

[22] K.S. Thorne, *Light scattering and proposed baffle configuration for the LIGO, Caltech Theoretical Astrophysics Preprint* N. GRP-200 (1989)

[23] J-Y.Vinet et al., *Scattered light noise in gravitational wave interferometric detectors: A statistical approach Phys.Rev*. D **56** (1997) 6085

[24] Y.Vinet, Violette Brisson, and Stefano Braccini, *Scattered light noise in gravitational wave interferometric detectors: Coherent effectsPhys Rev* D **54** (1996) 1276

[25] S. Braccini, *Seismic Isolation in VIRGO*, PhD thesis, Scuola Normale Superiore, Pisa, (1996) unpublished

[26] G. Ballardin et al., *Measurement of the Virgo superattenuator performance for seismic noise suppression, Rev. Sci. Instr.,* **72** (2001) 3643

[27] The Virgo Collaboration, *Virgo Final Design*, E.T.S., Pisa, Italy (1995)

[28] G. Losurdo et al., *An inverted pendulum pre-isolator stage for the Virgo suspension system, Rev. Sci. Instr.* **70** (1999) 2507

[29] G. Losurdo et al., *Inertial control of the mirror suspensions of the Virgo interferometer for gravitational wave detection, Rev. Sci. Instr.* **72** (2001) 3653

[30] M. Beccaria et al., *Extending the Virgo gravitational wave detection band down to a few Hz: metal blade springs and magnetic antisprings*, *Nucl. Instr. Meth. Phys. Res.* **A 394** (1997) 397

[31] M. Beccaria et al., *The creep problem in the Virgo suspensions: a possible solution using Maraging steel, Nucl. Instr. Meth. Phys. Res.* **A 404** (1998) 455

[32] S. Braccini et al., *The maraging-steel blades of the Virgo super attenuator*, *Meas. Sci. Technol.* **11** (2000) 467

[33] A. Delapierre and F. Frasconi, *Stress distribution on the suspension wires of the Virgo superattenuator*, Virgo Internal Report VIR-TRE-PIS-4600-137, (1997)

[34] S. Braccini et al., *An improvement in the Virgo Super Attenuator for interferometric detection of gravitational waves: The use of a magnetic antispring*, *Rev. Sci. Instr.* **64** (1993) 310

[35] G. Ballardin et al., *Measurement of the transfer function of the steering filter of the Virgo super attenuator suspension*, *Rev. Sci. Instr.,* **72** (2001) 3635

[36] G. Cagnoli, L. Gammaitoni, J. Kovalik, F. Marchesoni, M. Punturo, *Full scale prototype of high Q pendulum for interferometric gravitational wave detectors, Rev. Sci. Instr.* **71** (2000) 2206

[37] P. R. Saulson, *Thermal noise in mechanical experiments*, *Phys. Rev.* **D 42** (1990) 2437
S. Rowan, S. M. Twyford, R. Hutchins, J. Kovalik, J. E. Logan, A. C. McLaren, N. A. Robertson, J. Hough, *Q factor measurements on prototype fused quartz pendulum suspensions for use in gravitational wave detectors*, *Phys. Lett.* **A 233** (1997) 303

[38] M. Punturo, *The Virgo sensitivity curve*, Virgo Internal Report No. VIR–NOT–PER–1390–51, (2003)

[39] H. B. Callen and T. A. Welton, *Irreversibility and generalized noise*, *Phys. Rev.* **83** (1951) 34

[40] P. Amico, L. Bosi, L. Carbone, L. Gammaitoni, F. Marchesoni, M. Punturo, F. Travasso, H. Vocca, *Monolithic fused silica suspension for the Virgo gravitational waves detector, Rev. Sci. Instr.* **73** (2002) 3318

[41] G. Cagnoli, L. Gammaitoni, J. Kovalik, F. Marchesoni, M. Punturo, *Low-frequency internal friction in clamped-free thin wires*, *Phys. Lett.* **A 255** (1999) 230

[42] G.Cagnoli, L. Gammaitoni, J. Kovalik, F. Marchesoni, M. Punturo, S. Braccini, R. De Salvo, F. Fidecaro, G. Losurdo, *Mechanical shot noise induced by creep in suspension devices, Phys. Lett.* **A 237** (1997) 21

[43] G. Cagnoli, L. Gammaitoni, J. Kovalik, F. Marchesoni, M. Punturo, *Suspension losses in low-frequency mechanical pendulums*, *Phys. Lett.* **A 213** (1996) 245

[44] S. Buchman et al., *The Gravity Probe B Relativity Mission*, *Adv. Space Res.* **25** (2000) 1177

[45] F. Acernese et al., *First locking of the Virgo central area interferometer with suspension hierarchical control, Astroparticle Phys.,* **20** (2004) 629

[46] F. Acernese et al., *A local control system for the test masses of the Virgo gravitational wave detector, Astroparticle Phys.,* **20**(2004) 617

[47] F. Bellacchia et al., *A VME/VSB board for real-time positioning and image analysis*, LAPP Internal Report (1995)

[48] F. Bellacchia et al., *A VME based CCD imaging system for the Virgo interferometer control, Nucl. Instr. & Meth. Phys. Res.* A **413** (1998) 151

[49] A. Bernardini, E. Majorana, P. Puppo, P. Rapagnani, F. Ricci, G. Testi, *Suspension last stages for the mirrors of the Virgo interferometric gravitational wave antenna*, *Rev. Sci. Instr.,* **70** (1999) 3463

[50] P. Puppo and P. Rapagnani, *The electromagnetic actuators of the mirror reaction masses*, Virgo Internal Report VIR-NOT-ROM-1390-311 (2005)

[51] F. Bondu et al., *The Virgo injection system*, *Class. Quantum Grav*. **19** (2002) 1829

[52] R. Barillet, A. Brillet, R. Chiche, F. Cleva, L. Latrach, and C.N. Man, *An injection-locked Nd:YAG laser for the interferometric detection of gravitational waves*, *Meas. Sci. technol*. ISSN 0957-0233

[53] http://www.corning.com/specialtymaterials/products_capabilities/ULE.aspx

[54] F. Bondu, P. Fritschel, C. N. Man, and A. Brillet, *Ultrahigh-spectral purity laser for the VIRGO experiment*, *Opt. Lett.* **21** (1996) 582

K. Numata, A. Kemery, and J. Camp, *Thermal-noise limit in the frequency stabilization of lasers with rigid cavities*, *Phys. Rev. Lett*. **93** (2004) 25

[55] http://www.schott.com/advanced_optics/english/our_products/zerodur/index.html

[56] F Beauville et al., *Improvement in the shot noise of a laser interferometer gravitational wave detector by means of an output mode-cleaner*, *Class. Quantum Grav*. **23** (2006) 3235

[57] F. Beauville et al., *A camera based position control of a suspended optical bench used in a gravitational wave detector*, *Rev. Sci. Instr.* **74** (2003) 2564

[58] B. Caron et al., *Photodiodes selection for the VIRGO detector the first step*, *Nucl. Instr. Meth. Phys. Res.* A **360** (1995) 379

[59] R. Flaminio et al., *The signal detection system for the VIRGO interferometer*, *Nucl. Instr. Meth*. A **409** (1998) 477

The Virgo Collaboration, *Interferometer signal detection system for the VIRGO experiment*, *Class. Quantum Grav*. **19** (2002) 1857

[60] F. Acernese et al., *The Virgo automatic alignment system*, *Class. Quantum Grav*. **23** (2006) S91

[61] L. Pinard et al., *95'Optical interference coatings*, *Tucson, Technical Digest* **17** (1995) 200

[62] J.M. Mackowski et al., *98'Optical interference coatings*, *Tucson,* USA, *Technical Digest* **9** (1998) 18

[63] L. Dognin, *PhD dissertation*, Université Claude Bernard Lyon I France, (1997)

[64] M. Bray, *Stitching interferometry: how and why it works*, SPIE **3739** (1999) 259

[65] M. Bray, *Stitching interferometry and absolute surface shape metrology*, SPIE **4451** (2001) 333

[66] B. Cimma et al., *Original optical metrologies of large components*, SPIE **5252** (2004) 322

[67] *RIO2 8062 User Manual* PowerPC based RISC I/O Boards, DOC 8062/UM, CES (1998)

[68] F. Bellachia, *Virgo Note* VIR-TRE-LAP-5200-101 (1996)

[69] http://www.lynxos.com

[70] D. Boget et al., *Virgo Note* VIR-SPE-LAP-5200-105 (1998)

[71] D. Boget et al., *Virgo Note* VIR-SPE-LAP-5200-103 (1997)

[72] F. Acernese et al., *The Virgo data acquisition system, XIII IEEE-NPSS Conference on Real Time Systems*, (2003)

[73] Arnaud. N. et al., *The global control of the Virgo experiment, Nucl. Instr. Meth. A* **550** (2005) 467

[74] B. Caron, et al., *SIESTA, a time domain, general purpose simulation program for the VIRGO experiment, Astropart. Phys.* **10/4 (1999)** 369

[75] Acernese, F. et al., *The variable finesse locking technique, Class. Quant. Grav.* **23** (2006) S85

[76] A. Anastasio, F. Barone, A. Eleuteri, F. Garufi, L. Milano, *The Environment Monitoring of the Virgo Antenna for gravitational wave detection", in "Gravitational Waves*, Proceedings of the 3rd Amaldi Conference, S.Meshkov editor, AIP Conference Proceedings **523**, Pasadena, California, (USA), 17-19 July, (1999) 463

[77] F. Barone, R. De Rosa, A. Eleuteri, L. Milano, K. Qipiani, *The Environmental Monitoring System of Virgo Antenna for Gravitational Waves Detection*, *IEEE Trans. Nucl. Sci.* **49** (2002) 405

[78] F. Acernese et al., *Properties of Seismic Noise at Virgo Site*, *Class. Quant. Grav.* **21** (2004) S433.

[79] F. Acernese et al., *A First Study of Environmental Noise Coupling to the Virgo Interferometer*, *Class. Quant. Grav.* **22** (2005) S1069

[80] F. Acernese, *Data Acquisition system of the Virgo gravitational waves interferometric detector, IEEE Trans. Nucl. Sci.* **55**, (2008) 225

[81] http://www.lapp.in2p3.fr/virgo/FrameL

[82] B. Mours, Virgo Note VIR-SPE-LAP-5400-102

[83] S. Cortese, EGO Computing Center site report, *INFN Computing Workshop 2004, http://www.infn.it/CCR/workshop/ws2004/doc/II_giornata/cortese_ufficiale.ppt*

[84] A. Bozzi, L. Salconi, VSR2 / S6 Data Transfer report, *https://tds.ego-gw.it/itf/tds/file.php?callFile=VIR-0106B-10.ppt*

[85] T. Accadia et al., *Calibration and sensitivity of the Virgo detector during its second science run, Class. Quantum Grav*. **28** (2011) 025005 (arXiv:1009.5190v1)

[86] L.Blanchet et al., *Gravitational waveforms from inspiralling compact binaries to second-post-Newtonian order, Class.Quant.Grav.* 13 (1996) 575

A. Buonanno, G. B. Cook, and F. Pretorius, *Inspiral, merger, and ring-down of equal-mass black-hole binaries Phys. Rev. D* **75** (2007) 124018

[87] F. Marion et al., *Multi-band search of coalescing binaries applied to Virgo CITF data, Proc. 'Rencontres deMoriond'* (2003)

[88] P. Amico, L. Bosi, C. Cattuto, L. Gammaitoni, F. Marchesoni, M. Punturo, F. Travasso and H. Vocca, *A parallel Beowulf-based system for the detection of gravitational waves in interferometric detectors, Comput. Phys. Commun.* **153** (2003) 179